Università degli Studi di Padova

Dipartimento di Ingegneria Civile, Edile ed Ambientale

Department of Civil, Environmenal and Architectural Engineering

Corso di Laurea Magistrale in Environmental Engineering

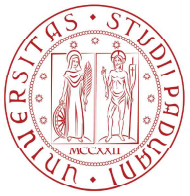

Tesi di Laurea

Streamflow regime characterization in tropical Costa Rica

Relatore: Prof. Gianluca BOTTER

Correlatore: Prof. Christian BIRKEL

.

Laureando: Enrico BONANNO

Anno Accademico 2016-2017

Index

Ai miei genitori,

tutto ciò che ho di buono lo devo a voi,

Grazie.

Abstract

Water fluxes in riverine environments, their variability and sensitivity to external hydroclimatic processes are ruled by spatially heterogeneous, complex and time variable processes. A correct hydrological characterization of a basin strictly depends on quality and availability of field measurements. As a result, a parsimonious theory able to describe streamflow regime is extremely valuable. In this thesis a stochastic analytical model was used in 18 catchments in Costa Rica, following the theoretical framework proposed by Botter et al [2013]. The model, which is able to provide a stochastic description of precipitation events and streamflow regime, was modified in order to deal with the lack of rainfall data and was applied for different seasons in order to rule the distinction between *erratic* and *persistent* flow regimes. In this thesis the absence of rainfall data was compensated by suitable assumptions, and the parameters of the model were deduced entirely from discharge data in order to build the theoretical streamflow pdf and give a characterization of the flow regime. Then the performance of the model was evaluated studying the distance (expressed in terms of *sum of squared difference*) between the empirical pdf and the analytical one. The model was successively amplified with the introduction of different calibration methods in order to look for the pdf parameters able to give the lowest sum of squared difference with the empirical dataset. Contrarily to qualitative difference between *Regular Caribbean Type Streamflow* and *The Irregular Type Streamflow* based on pluvial-streamflow trends proposed by Birkel [2005] the model used in this thesis was able to give an hydrological characterization based on discharge-deduced hydroclimatic parameters and shown permanent regime rivers in catchment previously identified as *Irregular* and erratic catchments on the *Regular* Caribbean side. The developed approach offers a basis for the study and characterization of poorly gauged regions, as developing countries, in order to increase the understanding of hydrologic regimes, human management and floods/droughts in catchments.

Introduction

One of the most relevant research field in modern hydrology is the development of stochastic process based methods which can help to understand the behavior of the hydrologic regime of a river basin thereby improving our ability to better characterize a variety of riverine processes, including flooding potential, hydropower production, habitat availability, transport of solutes, sediment and fluvial hazard. These processes are influenced by a range of physical, chemical and biological variables which are ultimately controlled by the magnitude of streamflows. The variability of streamflow assumes central importance in many ecological and morphological processes shaping river systems as formulated by the *natural flow regime* paradigm [Poff, 1997] which directly links the flow regime to ecological features and morphological changes.

Compared to the metrics compiled by Richter et al. [1996] to supply quantitative assessment of anthropogenic alterations of streamflow dynamics, probabilistic approaches offer an alternative point of view that allows a linkage between the streamflow variability and the ecological and morphological processes along streams. Statistical methods are useful to estimate both frequency and magnitude of streamflow, in this way it's possible to evaluate hazards and potential damages by flooding events and dry periods. These two extreme situations can successively lead to damages to humans and environmental balance of the basin itself. Moreover, the driving processes of the basin (founded on the transformation of rainfall in streamflow) are affected by both natural and human changes to the ecosystem therefore it's possible to individuate a link between modifications in the basin and the underlying streamflow regime [e.g. Bosch and Hewlett 1982; Veldkamp and Fresco, 1996; Lawton et al., 2001; Milly et al., 2005; Ray et al., 2006; Daniels et al., 2011; Birkel et al., 2012; Botter, 2014]. The streamflow regime isn't linked only to geomorphological and climate features of the basin, the availability of river flows is, indeed strictly linked to both physical and chemical attributes of the riverine habitat. Therefore, a temporal modification in magnitude and availability of the streamflow can modify key factors in processes like sediment transport, food mitigation and nutrient release [e.g. Poff, 2007; Ceola et al., 2013].

In this thesis the sight was set on a particular mechanistic and stochastic model developed by Botter et al. [2007] which is able to represent the major physical processes involved in rainfall-runoff transformation depending on catchment-scale soil moisture dynamic. The model enables a formal link among flow dynamics, internal components and external forcing (rainfall). The parameters of the model are deduced using streamflow and rainfall time series and are then used to build the probability density function

associated to daily discharges. This curve, ruled by three parameters able to encapsulate both climatic and geomorphological information, can be compared to empirical frequency distribution of daily discharge. Furthermore, a proper fitting between theoretical and observed pdf helps in a proper classification of the streamflow regime (*erratic* or *persistent*, according to the classification proposed by Botter et al. [2013]) which gives information on the predictability of the streamflow, its sensitivity to external hydroclimatic forcing factors, and the responsiveness of rainfall patterns.

This thesis focuses on the application of the model to Costa Rican basins. Costa Rica can be identified as a humid tropical country [Chang & Lau, 1983] and the tropical regime bears important implications for this region in terms of water management, landscape modification, soil use and potential environmental problems as hydropower production, floods and sediment transport. Hydrological issues are economically and strategically relevant in this country, in which almost 80% of the total national electricity demand is entirely covered by hydropower production. Furthermore, in the last century the development of the county increased pressure on the environment by forest conversion from 67% primary rainforest cover in 1940 to crop and pasture 1983 [Sader & Joyce, 2001] a trend that slowed since 1970 and paused definitively in 1995 leading to a reverse situation with increased reforestation [Veldkamp & Fresco, 1996; Birkel et al., 2012]. Land use, its modification and relative hydrological changes were previously investigated here by several hydrology studies with contrasting results especially in tropical countries [Bruijnzeel, 2004]. Nevertheless, hydrological modelling in Costa Rica recently allowed more precise answers to flow regimes dynamics, identification of dominant rainfall-runoff processes and catchment storage properties [Birkel et al., 2012; Bikel et al., 2015; Birkel et al., 2016] and underlined how a modelling-approach can help in a better understanding of the tropical weather and catchments.

One of the most difficult problem in developing countries, from a hydrological point of view, is the lack of direct measurements of many hydroclimatic variables. In this thesis, which uses a model that characterize river flow regimes from streamflow and rainfall data, the lack of rainfall data had to be handled. This lack ok data was due to three major problems: equipment, their sensitivity and observation time. The country is indeed not sufficiently equipped, which leads to lack of data in terms of pluviographic stations present in the territory. Moreover the intensity of precipitation events, especially in wet season, is so high that even installed instruments are not able to record properly the correct intensity. As a final remark, even when a pluviographic station is available, the datasets are often not sufficiently long in terms of observation time to be useful for a long-term stochastic purposes.

Chapter 1 – The analytical model

1.1 - Probabilistic characterization of streamflow

During the last decades both deterministic and stochastic approaches have been developed in order to characterize, predict and understand the variability of streamflows depending on geomorphological and climatic features [Brutsaert, 2005]. The processes able to characterize the hydrology of a basin can be subdivided in three categories: recharge, losses and storage of water, which are, respectively, rainfall (1), evapotranspiration and discharge (2), and storage variations due to deep percolation (3) [Rodriguez-Iturbe and Rinaldo, 1997; Botter et al., 2009]. The physical processes involved in a basin, even if theoretically simple, are influenced by soil and ecological properties that are heterogeneous both in time and space and poorly characterizable by direct measures. For these reasons deterministic approaches show many difficulties and a parsimonious theory for catchment hydrology remain vague [Kirchner, 2009]. Regardless the kind of the approach used, every model, both deterministic and stochastic, need specific simplification and assumption in order to evaluate in a reasonable way complex processes involved in a basin.

Whit this aim in mind Botter et al [2007a, 2007b, 2008, 2009, 2013] have developed a model in order to link the stochastic fluctuation of a streamflow with the recorded rainfall and soil moisture dynamic at catchment scale. The aim was to use rainfall time series and soil, vegetation and geomorphological features in order to obtain the steady state probability density function of a streamflow (pdf) and its flow duration curve. This way to represent a streamflow regime is able to give information relative to the mean water available, the fluctuation of the discharge and the frequency of extreme events, as extremely high and low flows [Botter et al. 2007a; Botter et al. 2007b].

The temporal evolution of spatially-averaged soil moisture in the root zone can be seen as the consequent of three processes [Rodriguez-Iturbe and Porporato, 2004; Botter et al., 2009]: instantaneous increment from rainfall event, evapotranspiration losses (due to the water hold between the wilting point, s_w, and the field capacity saturation, s_l) and instantaneous deep percolation with the consequence runoff triggering (whenever the saturation passes above a given the threshold, s_1). The analytical model shows how the nature of flow regimes and their sensitivity to climatic, land-coverage and geomorphological changes can be studied through an analysis based on the frequency of the effective flow-producing rainfalls and the time scale of the hydrological response. The

entire sequence of rainfall can be stochastically modelled at daily timescale as a zero dimensional marked Poisson process ruled by its frequency λ_p [T^{-1}] with intensity exponentially distributed with average α [L]. It's important to underline that two implicit hypothesis are assumed: the catchments sizes is considered smaller than the corresponding atmospheric surface interested by the rainfall production and the timescale is greater than the characteristic duration of the rainfall event (daily). In this way it's possible to discard the internal spatial heterogeneity of the rainfall and the temporal one [Botter et al., 2007b].

Precipitation events with a sufficient intensity are able to trigger soil drainage and become effective rainfall. This instance is strictly correlated to the soil-water deficit resulting from evapotranspiration. Being the effective precipitation a subset of the overall precipitation events, it's possible to approximate them by a similar Poisson process which is ruled by the same average intensity α with a reduced frequency $\lambda<\lambda_p$. Consequentially, the ratio λ/λ_p is an indicator able to express the capacity of the soil to store incoming rainfall and it's dependent of transpiration rate, intensity of precipitation and morphological characteristics of the basin. According to Rodriguez-Iturbe et al. [1999] and Rodriguez-Iturbe and Porporato [2004] the effective precipitation frequency can be obtained as:

$$\lambda = \eta \frac{exp(-\beta^{-1})\beta^{-\frac{\lambda_p}{\eta}}}{\Gamma\left(\frac{\lambda_p}{\eta}, \beta^{-1}\right)} \qquad \text{(I. 1)}$$

In which:

- $\Gamma(a,b)$ is a lower incomplete Gamma function of parameters a and b;
- η is the normalized maxim evapotranspiration rate: $\eta = ET/(nZ_r(s_l-s_w))$. Being ET the maximum evapotranspiration rate (deducible via the Penman-Monteith soil-atmosphere interaction model);
- β is the inverse of γ_s, being γ_s the ratio between the soil storage capacity and the mean rainfall depth: $\gamma_s = \gamma_p nZ_r(s_l-s_w)$. The difference between s_l and s_w, depending on the soil and vegetation features, can be reasonably esteemed considering information about soil type and land cover [Rodriguez-Iturbe and Porporato, 2004].

Thus, those precipitations are able to provide available contribution to deep percolation, they recharge subsurface storage of the catchment and consequentially produce streamflow. Note that η and β, (and, therefore, λ) are modeled using basin-averaged properties. The soil moisture is seen as a state-dependent process taking place in the upper part of the soil, assumed constant and homogeneous (i.e. depth Z_r [L], porosity n [-] and soil moisture s [-] are spatially constant).

The modification in the streamflow is due to the effective rainfall events and the capacity of the basin to transform the initial rainfall input into an increase of flow can be

modelled assuming different storage-discharge relationships [Botter. et al., 2009]. These expressions were deduce starting from simple assumptions and lead to a linear and a non-linear laws. It's important to underline how highly engineered basins (where the anthropogenic regulation of the streamflow is not negligible) and snow-affected basins (in which the accumulation and melting process are able to consistently affect the stream dynamic) have to be excluded from the model [Botter et al., 2013].

1.1.1 – The linear case

The postulated linearity in storage-discharge relationship in subsurface state is equivalent to assume that each streamflow pulse triggered by an effective precipitation event is followed by an exponential recession. This point of view has been widely used in the past and was one of the most applied in practical engineering [Chow et al., 1988; Beven, 2001; Brutsaert, 2005].This input could eventually be released to the surface stream network as subsurface/groundwater flow as well. The process can therefore be described [Botter et al., 2009] using a continuity equation for the volume stored in the root zone *W*:

$$\frac{dW(t)}{dt} = -Q + \xi_t'(\lambda; \gamma_w) \tag{I. 2}$$

In which *Q* represents deterministic water losses due by subsurface/groundwater flows and ξ'_t describes the storage increment during deep percolation events, it can be associated to a stochastic noise described by the Dirac delta function δ:

$$\xi_t'(\lambda; \gamma_w) = \sum_{i; t_i < t} \Delta W_i \delta(t - t_i) \tag{I. 3}$$

The arrival times of percolation events, t_i, depending on the stochastic rainfall series, are distributed as Poisson processes as well, with frequency λ, and storage increments due to runoff events, ΔW_i, are assumed to be instantaneous and exponentially distributed with parameter $\gamma_w = a \cdot A$. If the residence time in subsurface is assumed to be exponentially distributed by a random variable it's like to assume that the deeper layers of the soil act as a linear reservoir in which *q* is directly proportional to *W* and therefore $q=kW$. In this point of view *1/k* assumes the role to describe the mean residence time in subsurface/groundwater state.

Thus the linear approach allows the temporal description of the streamflow *Q*, defined as the daily discharge [mm/d], simply multiplying the continuity equation by *k*:

$$\frac{dQ(t)}{dt} = -kQ(t) + \xi_t'(\lambda; \gamma_w) \tag{I. 4}$$

In which k [T^{-1}] is the *hydrograph recession rate* (or *flow decay rate*) and it is the inverse of the time scale of the hydrograph, typically a function of morphological features.

Using another point of view it's possible to observe how, during an effective rainfall event, it's possible to assume the water pulse propagation through the deeper layers of the soil as subsurface and/or groundwater flow. If a pulse released from the root zone at the time t_i has an excess depth h_i [L] it will provide a contribution to the overall specific streamflow (per unit catchment area). Being the system linear, this increment will be directly proportional to the depth h_i and k:

$$Q(t) = h_i k \, exp[-k(t - t_i)] \tag{I.5}$$

And the instantaneous streamflow at the time the pulse is released from the root zone ($t=t_i$):

$$q_i(t = t_i) = h_i k \tag{I.6}$$

If the system is supposed liner the overall streamflow can be seen as the sum of the contribution of different pulses and their temporal superposition don't change the flow decay rate. At daily time scale the dynamic equation of the streamflow is still the I.4 equation.

The associated analytical expression of the steady-states probability distribution function (pdf) is a gamma distribution with shape parameter λ/k and rate parameter αk and reads [Botter G. et al., 2013]:

$$p(Q) = \frac{\Gamma\left(\lambda/k\right)^{-1}}{\alpha k}\left(\frac{Q}{\alpha k}\right)^{\frac{\lambda}{k}-1} exp\left(-\frac{Q}{\alpha k}\right) \tag{I.7}$$

It's important to take in mind that the equation (II.4) used to describe the temporal behavior of the streamflow is valid only for those rainfall events which don't have a fast surface contribution. The effect of intense storms and their related surficial flows is neglected, an approximation which is not too strong, being the slow subsurface components of the streamflow highly superior than the surficial. An observation pretty legit, in absence of extensive waterproof surfaces, for pristine environment. Let's focus on that, according to different authors, it's possible to express the gamma distribution referring to two different couples of parameter. The first generic couple (ξ, θ) and the second one (α, β) are joined together with the following relationships: $\xi = \alpha$ and $\beta = 1/\theta$. The generic gamma function in (α, β) form reads:

$$f(x) = \frac{\beta^{\alpha}}{\Gamma(\alpha)} x^{\alpha-1} exp(-x\beta) \tag{I.8}$$

In this thesis work the pdf is expressed using the couple of parameters in the (ξ, θ) form, which in our case are expressed by the couple (s_1, r_1) = (λ/k, αk). Using this way to write the gamma pdf the mean and the variance read:

$$\mu = \xi\theta = s_1 r_1 \quad \text{(I. 9)}$$

$$Var(X) = \xi\theta^2 = s_1 r_1^2 \quad \text{(I. 10)}$$

1.1.2 – The non-linear case

The non-linear equations are conceptually different from the linear one. Using a non-linear approach implies the use of power-law type recessions. The nonlinearity can be seen as the sum of different factors. According to Van de Griend et al. [2002] they are linked to changes in the connectivity of those regions able to contribute to the runoff processes and to the thickness of the aquifers (both of them can determine an increase of the drainage resistance of the soil after the peakflow) and the increase along the depth of the hydraulic conductivity due to an increased compaction or a decreased fracturing. Since the second half of the XX century the non-linear discharge-storage relations have been used and there are many examples of their use in hydrological models both in the past [Amorocho J.and Orlob G.T., 1961; Amorocho, 1963, 1967; Brutsaert and Nieber, 1977] and in more recent times [Farmer et al., 2003; Kirchner J.W., 2009].

According to Botter et al. [2009] and Ceola et al. [2010] the non-linear temporal description of the streamflow *Q* reads:

$$\frac{dQ(t)}{dQ} = -KQ(t)^a + \xi_2 \quad \text{(I. 11)}$$

Where *K* [L^{1-a} T^{a-2}] and *a* constant and respectively named as *recession coefficient* and *exponent*, being *a* the indicator about the rate of decrease of the flow during the recession; ξ_2 is a time-dependent increment due to percolation events and can be seen as stochastic noise. The general expression of the steady state probability distribution function was deduced by Botter et al. [2009] and reads:

$$p(Q) = C\left\{Q^{-a}\, exp\left[\frac{\lambda Q^{1-a}}{K(1-a)} - \frac{Q^{2-a}}{\alpha K(2-a)}\right] + \frac{k}{\lambda}\delta(Q)H(1-a)\right\} \quad \text{(I. 12)}$$

In which *C* is a normalizing constant, *H* is the Heaviside unit step function.. The term including *H* considers the atom of probability in *Q=0* associated to the Dirac delta function and emerging only when *0<a<1*, which, according to Biswal and Marani [2010] doesn't happen in most cases, being, usually, *a>1*.

The following image summarizes different shapes of the pdf as a function of the non-linear law used to describe the storage-discharge relationships being strictly dependent on the magnitude of the exponent *a* and on the ratio *λ/k* (being this ratio the shape parameter of the pdf and an indicator about the responsiveness of the basin, as explained better

later). A positive value of this ratio refers to “wet conditions”, on the other hand, a negative value stands for “dry conditions”.

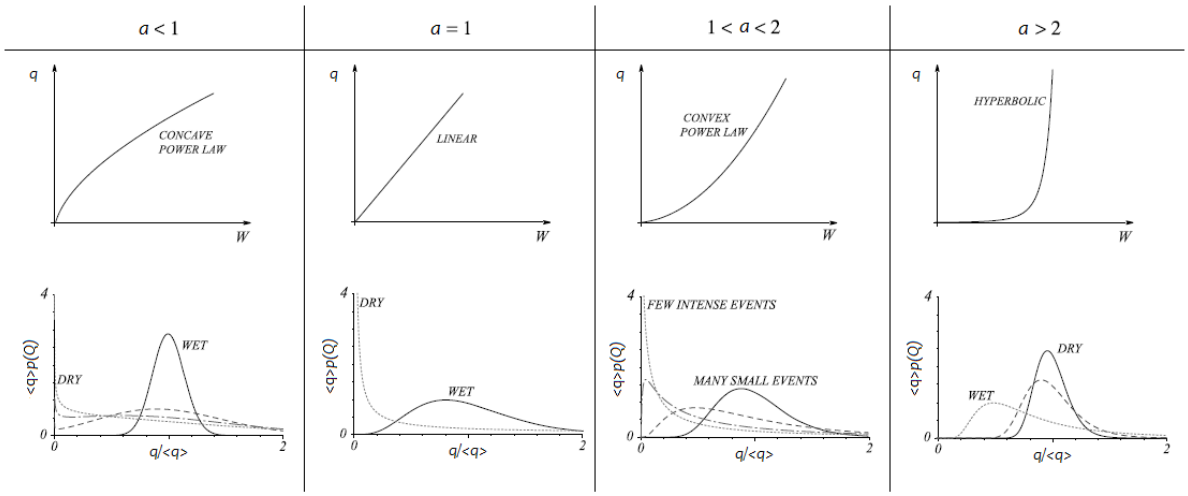

Figure I.1 – Summary of possible non-linear relationships and their related pdf shape depending on a and the λ/k ratio [Botter et al., 2009; Ceola et al., 2010]

If $a<1$ there is an atom of probability for Q=0 and the pdf decreases monotonically without inflection points. A single inflection can be spotted at dry climatic conditions, otherwise the pdf is bell-shaped. The discharge-storage relation is concave power.

If $a=1$ the non-linear model becomes linear. For dry conditions the pdf behaves monotonically, going to infinite for $Q \rightarrow 0$ a decreasing for high values of the discharge. For wet conditions the result is a well-shaped pdf.

When $1<a<2$ the pdf is always bell-shaped for dry and wet conditions. The shape of the bell will modify depending on the weather few intense rainfall events or many smaller one contribute to the climate. In the first case the peak of the bell will shift close to the ordinate axis, in the second one the values will be me more homogeneously arranged around the mean. The discharge-storage relation is convex power.

If $a>2$ the pdf given by the model will be always bell-shaped and in dry conditions will be almost symmetrical with a reduced streamflow variability around the mean (low variance), in wet climates the shape is shown a typical tail on the right (positive skewness) and more dispersed values (higher variance).

Now, the linear model implicitly assumes a single catchment response time, therefore it refers to a specific hydrologic response, the subsurface runoff [Botter et al., 2007b], on the contrary, the non-linear model is able to incorporate different mechanism involved in the flow triggering (deep, subsurface and surface runoff) because the catchment hydrological response can vary in function of different overall water storages.

1.1.3 – The flow duration curve

The flow duration function is an important tool able to express, in mathematical function, the relationship between a certain discharge Q_i and the percentage of time during which this discharge is equaled or exceeded during the time interval considered (usually one year) [Vogel and Fennessey, 1994]. It is analytically given by the integration, in the given reference period, of the streamflow pdf (equation II.7 for the linear case or II.9 for the non-linear one) and it reads:

$$D(Q) = \int_{q}^{+\infty} p(x)dx \qquad \text{(I. 13)}$$

Parameters *k*, for the linear storage relationship, and *K* and *a*, for the non-linear one, are able to describe both the increase of streamflow subsequently an effective rainfall event and the decay of the streamflow between different precipitations. Being λ, α, *k*, *K* and *a* able to describe and summarize the morphological features as well as climatic conditions, they are termed *hydroclimatic parameters* and can be therefore directly evaluated using rainfall, climatic and soil/vegetation information [Botter et al., 2013]. During the application of the model, on the contrary, the flow-producing events are assumed as instantaneous pulses.

1.2 – Flow regimes characterization

The analytical model identifies three major parameters able to characterize the streamflow regime: the mean depth of rainfall events, α; the frequency of streamflow-producing events, λ; the recession coefficient *k* (for the linear model) or *K* and exponent index *a* (for the non-linear formulation). Assuming, for sake simplicity, a characterization based on a linear approach, the flow decay rate *k* can operationally identify the time scale of the hydrological response, being the mean water retention time in the catchment analytically deduced by the inverse of *k* itself. Now, k is able to reassume in an analytical way those attributes that affects basin-scale morphological and hydrological features. If the recession coefficient is a qualitatively high value it means that the mean water retention time is low and the discharge recession after a streamflow pulse follows a temporal rapid decay, the catchment can be assumed as a fast-responding one. On the other hand, a low *k* value implies a high mean water retention time, and the recessions follow a temporal low decay, the catchment can be assumed as a slow-responding one.

The description wrote above is not complete: what does it mean a “high” or a “low” value of the flow decay rate? The answer is given by λ, the mean frequency of the effective rainfall. The parameter according to the formulation in Eq. I.1, embeds both rainfall attributes, soil and vegetation features, and the ratio between λ and the flow decay rate *k* will define the responsiveness of the basin.

If $\lambda/k > 1$ the mean frequency of effective rainfall is higher than the flow decay rate. So, in the considered basin, the precipitation events able to trigger a positive pulse in the streamflow are relatively frequent being their mean interarrival time smaller than the mean duration of the flow pulse. If the precipitation events are relatively frequent it means that there is a continuous water supply to the streamflow. In a stochastically point of view this qualitative observations imply a pdf in which there is not such a wide distribution of values around the mean and the variance is therefore relatively low. This regime is expected in humid climates (high λ) or slow-responding catchment during cold seasons (low k) and the streamflow associated, being quite predictable, is called *Persistent*.

If $\lambda/k < 1$ the mean frequency of effective rainfall is smaller than the flow decay rate. Thus, the mean interarrival between flow-triggering rainfall events is larger than the mean duration of the flow pulse. If the precipitation events are relatively sporadic it means that a wide range of different streamflow can be observed and after an effective rainfall event the soil has the time to dry significantly. In a stochastically point of view this qualitative observations imply a pdf in which the range of observed values of Q is wide around the mean and the variance is relatively high. This regime is expected in fast-responding catchments during dry seasons (low λ and high k) or in hot and humid seasons in which the evapotranspiration assumes an important magnitude (high λ and very high k). The streamflow associated to these characteristics, being less predictable with many streamflow fluctuations, is called *Erratic*.

The linear model is able to give a steady state streamflow pdf described by a gamma function ruled by shape parameter λ/k and rate parameter αk (Eq. I.7). Remembering the general formulation of mean (μ), variance (Var) and coefficient of variation of a pdf with domain Γ (CV) it's possible to find the relationship that links the statistical properties of the observed streamflow pdf with the analytical-deduced *hydroclimatic parameters*. In fact:

$$\mu = \int_{\Gamma} x\, p(x) dx \tag{I.14}$$

$$Var = \int_{\Gamma} (x-\mu)^2\, p(x) dx \tag{I.15}$$

$$CV_x = \sqrt{\frac{Var_x}{\mu_x^2}} \tag{I.16}$$

Using the pdf properties and moments expressed by equations I.9 and I.10 the analytical formulation of the coefficient of variation is equal to:

$$CV_q = \sqrt{\frac{k}{\lambda}} \tag{I.17}$$

This equation totally agrees with the definition of *persistent* and *erratic* regime previously set. A high value of the analytical *CV* (higher than 1) implies, indeed, a relatively high variance respect the mean of the distribution: the streamflow values are widely spread around the mean, the flow is less predictable and the regime is qualitatively *erratic*, according to the ratio of k/λ underlines (*>1*). For a low *CV* (smaller than 1) the variance of the pdf is relatively small and the mean value of the distribution is a more representative value, being the streamflow values mainly spread around the mean itself. The flow is more predictable and the regime is qualitatively *persistent* as the ration of k/λ underlines (*<1*). The characterization of the streamflow proposed is, therefore, coherent both in a qualitative way and in an analytical one. A suitable generalization for the non-linear version of the model is possible as delivered in Basso et al [2016].

1.3 – Parameters estimation

The hydroclimatic parameters of the model can be evaluated based on climate, soil and vegetation information. However, as demonstrated by Botter et al. [2013], their calculation can be done using solely rainfall and streamflow temporal data. The determination of the parameter related to the rainfall events can be directly derived from daily rainfall intensities [mm] collected in a representative meteorological station, which has to be into or nearby the considered basin. Having the data series of rainfall events in a catchment it is possible to estimate the average frequency of rainfall events, λ_p, by comparing the probability distribution of the number of wet days in the overall time period with the corresponding Poisson pdf assumed by the model. In a similar way the inverse of the mean rainfall depths during rainy days, γ_p, can be obtained comparing the observed distribution of spatially-averaged daily depths during wet days with the exponential distribution assumed by the model. As previously explained, α can be obtained from the inverse of the parameter γ_w, ($\gamma_w = \gamma_p/A$). The effective precipitation frequency can be esteemed by using equation I.1 or performing a direct mass balance between mean inflow (described by the ratio λ/γ_p in the subsurface states under the root zone between the mean inflow λ/γ_p. Moreover, for sake simplicity, it's possible to evaluate the effective rainfall frequency studying the mean observed discharge $\langle Q \rangle$ and using the relationship offered by the theoretical mean in a gamma distribution. Making explicit the equation I.9 relative to the mean according to the stochastic model:

$$\lambda = \frac{\langle Q \rangle}{\alpha} \qquad \text{(I. 18)}$$

In this application, due to the lack of rainfall data, the model was modified in order to deduce rainfall parameter starting from solely streamflow data. The main hypothesis simply considers that the streamflow data, with their peaks and their recessions, automatically express the presence of a certain effective precipitation in their dynamical behavior. Every time a peak can be spotted in the time series (whenever $Q_{i+1} > Q_i$) an increase of streamflow triggered by an effective precipitation can be deduced. The

effective rainfall frequency is, therefore, studied considering the frequency of positive jumps observed in the available time sequence. Once the deduction of λ is done the mean effective precipitation frequency can be done using the equation I.18, in order to express α as function of mean streamflow value and mean frequency of effective precipitation.

The recession parameters could be obtained through morphological and pedological features (as dividing the mean channeled paths by scale velocity representing the mean hydraulic conductivity of subsurface environments [Botter et al., 2013]) but the rate or recession can easily be esteemed by plotting the temporal derivate of the streamflow (estimated as the discharge difference in two consecutive days, $-dQ/dt=(Q_{t-\Delta t}-Q_t)/\Delta t$) versus the average Q value of the two days ($(Q_{t-\Delta t}+Q_t)/2$). Due to their high order of magnitude difference their mutual relation is typically shown in log-log plots. The different method used by Ceola et al. [2010] were analyzed and considered with the studies carried on by Basso et al. [2015].

1.3.1 – Regression fitting – Linear cases

For the linear approach different methods were used in order to esteem the value of the flow decay rate. The methods I, II and III are the same expressed in the work done by Ceola et al. [2010] and corresponds to the M1, M3 and M4 introduced by Ceola et al.

1. Method Ia – It's based on the liner regression obtained from the plot of $log(-dQ/dt)$ plotted versus the analogous related value of $log(Q)$. This method has another formulation, called M1b, in which the linear regression is performed individually for every regression, then the final flow decay rate is obtained by the median of all the values obtained. The M1b version has another difference from the mean one: it has to discard recessions shorter than 2 days in order to discard recessions associated to events with fast hydrological response [Basso et al., 2015]. The equation used for the fitting follows the general expression: $y=k+x$;
2. Method II – It's based on a linear regression of binned $<log(Q)>$ on the x-axis plotted versus the corresponding $<log(-dQ/dt)>$. The fitting equation used follows the same mathematical expression for the M1a and M1b methods: $y=k+x$;
3. Method IIIa – It's based on a linear interpolation in graph in which the observed streamflow Q is plotted versus the corresponding $(-dQ/dt)$. The resulting k is obtained with the curve able to fit better the empirical data according to the equation: $y=k \cdot x$; This fitting method, as the first one, has a b-version as well. In MIIIb method only recessions longer than 2 days have to be considered, being shorter recessions associated to events with fast hydrological response [Basso et al., 2015]. Moreover the recession is evaluated individually for every point and the final parameter is esteemed by the median value of all the results.

1.3.2 – Regression fitting – Non-linear case

The parameters estimation was done according to the consequences of the study performed by Basso et al. [2015] which is based on the methods studied by Ceola et al. [2010]. The method can be linked to the Linear I, having, also this time, the plott of *log(−dQ/dt)* versus the analogous related value of *log(Q)* but this time the fitting-type curve is a power-law one with generic formulation: $y=K+A\cdot x$. It's important to underline how this method will discard all the recessions with a length shorter than 5 days and neglecting the first point of each recessions, being associated to fast hydrologic response. Using the power-law curve the parameters were esteemed for each recession. Subsequently the final *a* is esteemed by the median of the obtained *A* values. Than the power-law curve is used again for every recession, keeping fixed the calculated *a* value; finally the final *K* is obtained by the median of all the *K* values deduced in the last step.

1.4 – Performance evaluation

Once the observed pdf was built for every basin and the related hydroclimatic parameters were estimated it is possible to deduce, according to the equations I.7 and I.12, the analytical pdf for both linear and non-linear case. It's then necessary to estimate which method is able to give the best fit with experimental data in order to deduce the performance of the different versions of the model and understand which version is more convenient to calibrate. This aim found answer in the introduction of three different performance-evaluation methods. These three methods evaluate and weight the punctual distance between the experimental pdf and the analytical one, in this way the sum of the differences of *n* intervals is able to give a unique number representative of the performance. Logically the number able to return the smallest value will indicate the most accurate method in which the overall analytical difference between observed pdf and theoretical one is lowest. Being N the number of interval used to deduce both analytical and observed pdf.

Sum of Squared differences – SSD

$$SSD = \sum_{i=1}^{N} [p(Q_i) - p_{obs}(Q_i)]^2 \qquad \text{(I. 19)}$$

Sum of differences – Sdiff

$$Sdiff = \sum_{i=1}^{N} |p(Q_i) - p_{obs}(Q_i)| \qquad \text{(I. 20)}$$

Mean difference – Mdiff

$$Mdiff = Mean|p(Q_i) - p_{obs}(Q_i)| \quad \text{(I. 21)}$$

It's important to note that, being the SSD a method able to weight more (using the squared distance) differences higher than 1 between observed and analytic model, it can happen that the best performing method deduced by the smallest SSD is not the same of the best performing method obtained with the Sum of differences or Mean difference method. Therefore in this thesis work the performances were evaluated considering solely the Sum of squared differences.

1.5 – Calibration methods

The model is a mechanistic and stochastic one, and this consideration leads to numerous advantages: probabilistic models are regular with a well-known trend, they're easily analyzable and their results and properties are well-known as well. These characteristics lead to a useful observation: studying autonomously the analytical pdf in order to find the one that fits better the observed data it's possible to obtain the best-fitting pdf regardless the theoretical model. Than the best-fit pdf can be compared with the best model-deduced one: both of them are gamma distributions and both of them are ruled by shape and rate parameter. The only difference is that the best-fit pdf obtained considering only observed data will have shape and rate parameters which are not expressed in terms of hydroclimatic properties of the basins, they are initially meaningless. However, their comparison with shape and rate parameters obtained by the model will give, on the contrary, meaning in terms of mean effective-precipitation frequency, mean rainfall intensity, flow decay rate and this comparison will be able to fix the values of the model with some correcting-parameters.

How the pdf was evaluated? In the following section five different methods were used and will described: Fit distribution (Matlab code), MLE (Matlab code), hand-made calibration (called Step Calibration), MLE plus a streamflow-removal assumption, method of moments.

Let's image to have the best distribution able to obtain, among all the possible pdf, the best fitting with observed data. This pdf will be defined by a shape parameter, s, and a rate parameter, r. If s_1 and r_1 are, respectively, shape and rate parameter obtained with the analytical model, the difference between s_1 and s, and r_1 and r, will identify the analytical difference between calibrated model and the original one. This observation led to these equations which defines two other parameters able to explicate these relationships:

$$\Delta_1 = \frac{s_1}{s} \quad \& \quad \Delta_2 = \frac{r}{r_1} \tag{I. 22}$$

$$s = \frac{s_1}{\Delta_1} = \frac{\lambda}{k \cdot \Delta_1} \tag{I. 23}$$

$$r = r_1 \Delta_2 = \alpha \cdot k \cdot \Delta_2 \tag{I. 24}$$

The final linear calibrated pdf expressed in function of the model shape and rate parameter of the model and the correction Δ parameters deduced reads:

$$p(Q) = Q^{\left(\frac{\lambda}{\Delta_1 k} - 1\right)} \frac{(\alpha k\, \Delta_2)^{\left(-\frac{\lambda}{\Delta_1 k}\right)}}{\Gamma\left(\frac{\lambda}{\Delta_1 k}\right)} \exp\left(-\frac{Q}{\alpha k\, \Delta_2}\right) \tag{I. 25}$$

The methods described in this section will be able to deduce the best-fitting pdf and, therefore, the best-fit shape and rate parameter.

1.5.1 – Fit distribution & Maximum likelihood estimation

The model was built using Matlab and one of already-written functions in Matlab are FitDist and MLE. These functions are able to fit a distribution on a set of given data. The general rule underlying the MLE estimation is the idea that, choosing a certain probability distribution, the method will determine the theoretical curve able to *better represent* the initial given data. Saying that the obtained distribution is the one able to better represent the data, means that the probability of getting that particular observed data set is greater with the given choice of model parameters, than any other possible choice.

Supposing to maximize the likelihood of a series of data x_1, x_2,…, x_n with a certain pdf *f(x)* having a parameter vector θ. Assuming independence of the data the joint probability of the data, given θ is:

$$f(x_1, x_2, \dots, x_n|\theta) = \prod_i f(x_i|\theta) \tag{I. 26}$$

The aim is to find the value of θ able to maximize the joint probability of x_1, x_2,…, x_n. Now, remembering that θ it the incognito term we can define the likelihood function as:

$$\mathcal{L}(\theta|x_1, x_2, \dots, x_n) = \prod_i f(x_i|\theta) \tag{I. 27}$$

Imagining the likelihood function as an unimodal pdf the peak of the hump will be the point able to maximize the likelihood of the data. This point can be found thanks to the property that the maximum of a function has its first derivative equal to zero:

$$\frac{\partial}{\partial\theta}\mathcal{L}(\theta|x_1, x_2, \dots, x_n) = 0 \qquad \text{(I. 28)}$$

Matlab MLE code acts exactly in this way giving, as result of the best-pdf fitting the shape and the rate parameters associated. The fitdist function uses basically the same principle of the maximum likelihood one with the only exception for lognormal and normal distribution. Therefore the two methods used to fit the data using a gamma distribution will give the same result.

It's interesting to note how, for all the pdf deduced in this way, the correction delta showed the same value both for shape and for the rate parameter. What is the consequence to have a $\Delta_1=\Delta_2$? The first one concerns the next calibration used, the second one has a more theoretical consequence. Considering the equations in I.22, it's possible to write:

$$\frac{s_1}{s} = \frac{r}{r_1}$$

Therefore:

$$s_1 \cdot r_1 = r \cdot s$$

$$\frac{\lambda}{k} \cdot \alpha \cdot k = r \cdot s$$

Which leads to:

$$\langle Q \rangle = r \cdot s \qquad \text{(I.29)}$$

This observation can have two other consequences. The first one has a practical meaning the second one can be useful by a theoretical point of view. In fact if it's possible to obtain a relationship able to link *r* (or *s*) to the mean value of streamflow we can automatically obtain *s* (or *r*) as well. By a qualitative point of view, being *r* proportional to mean rainfall intensity and flow decay rate, two quantities that, for a defined region, have a relatively low scattering, it is the parameter that has been used to define a relationship with <*Q*>. This consequence can help engineers in roughly deducing the analytical pdf of a certain basin knowing only the mean streamflow intensity and having the <*Q*> Vs *r* plot. The other observation is that, if the theoretical model perfectly coincides with the calibrated one (which would mean $r=r1$ and $s=s_1$) the straight line should pass through the axis-origin and II.30 equation would simply be equal to:

$$\langle Q \rangle = r_1 \cdot s_1 \qquad \text{(I. 30)}$$

Regardless the fact we decide to use the theoretical parameters in equation I.30 (r_1 and s_1) or the calibrated values (r and s), it's still possible to plot, for a certain region with the same hydroclimatic and geomorphological features (similar k and α) the bisector (or the best-fitting straight line in the $<Q>$ Vs r plot). The basins analyzed in this thesis showed, indeed, a correlation between the mean streamflow value and the rate parameter of the pdf. If it's possible to deduce a straight line from the $<Q>$ Vs r (or r_1) plot it's possible to use this correlation to deduce the rate parameter of the pdf for streamflows in the same hydroclimatic area with catchments with similar geomorphological features. In many hydrological cases the availability and reliability of data is a central problem, thus, if a certain basin has to be analyzed, thanks to the $<Q>$ Vs r plot it would be possible to deduce the rate parameter of the streamflow pdf knowing solely the mean discharge value. Then, thanks to I.29 equation the estimation of the shape parameter is immediate. These considerations would allow to roughly build the analytical pdf of a streamflow and deduce its moments knowing only the mean discharge value. This method can help in a quick estimation of the streamflow regime in order to give information about the responsiveness of the basin and the probability associated to high and low flows.

1.5.2 – Step calibration

Starting from the observation that the MLE and fitdist functions defined by Matlab gave the same correction delta ($\Delta_1=\Delta_2$) another calibration was performed in order to force the linear pdf distribution to fit better the observed values according the SSD performance method. The idea was pretty simple and the equation I.22 was used in a *for* cycle in which the calibration parameter (Δ) varied between 0.0001 and 25, with a 0.0001 step. The best Δ would be that one able to give a pdf with the lowest SSD. This cycle, involving 250000 iterations, was too slow (more than 4 hours to give the final value of the parameter), and for this reason another algorithm was concerned and implemented:

1. The first one evaluated the best Δ in a range from 0 to 25 with step equal to 1. The best value (we can call it Δa), the one able to give a pdf with the smallest SSD number, will be obtained using 25 iterations of the code;
2. The second cycle evaluated the best Δ in an interval equal to $\Delta a \pm 0.9$ with 0.1 step. The value able to give a pdf with the smallest SSD would be called Δb. 19 iterations of the code;
3. The third cycle evaluated the best Δ in an interval equal to $\Delta b \pm 0.09$ with 0.01 step. The value able to give a pdf with the smallest SSD would be called Δc. 19 iterations of the code;
4. The fourth cycle evaluated the best Δ in an interval equal to $\Delta c \pm 0.009$ with 0.001 step. The value able to give a pdf with the smallest SSD would be called Δd. 19 iterations of the code;

5. The fifth cycle evaluated the best Δ in an interval equal to Δ*d*±0.0009 with 0.0001 step. The value able to give a pdf with the smallest SSD would be called Δ*e*. 19 iterations of the code;

The last value obtained would be the best Δ able to give a corrected-pdf with the less SSD with the observed values. Moreover, this way to write the calibration allows an iteration of the code which is way faster than the previous one (101 code executions instead of 250000).

1.5.3 – Best Q% removal

The SSD estimation between calibrated model and observed values was done for all the dataset, according to the number of intervals used to build both observed and theoretical pdf. The previous calibration showed how even if the calibrated models are able to increase the performances in terms of SSD (or Sum_Diff and Mean_Diff) the peak displayed by the observed bell of value was far away from the theoretical one, which is lower. To fit better the bell-shaped pdf, another calibration was minded in order to obtain an analytical curve able to reproduce more accurately the most frequent events. This purpose led to a rearrangement of the discharge dataset from the lowest value recorded to the highest one, then a certain percentage of the *Q* was used, starting from the lowest value. For example, if 88% of the values of *Q* are considered it means that 12% of the values of the streamflow, the highest (and less frequent) one, are discarded from the calibration. In this way the MLE method can be applied in order to obtain the best analytical curve and the relative values of the correction parameters Δ_1 and Δ_2.

Thus, a *for* cycle was written and considered a removal of a certain percentage of high values of the discharge. This percentage removal varied from 30% (70% of the entire dataset of *Q* in increasing order used for the calibration) to 0% (the entire dataset was accounted) with a 0.1% step. The relative SSD was estimated for every percentage used and the final percentage value of *Q* used was the one able to give the smallest SSD. Successively the relative shape and rate parameter of the pdf were deduced as well as the parameter Δ_1 and Δ_2.

I.5.4 – Method of moments

The parameters which we want to esteem are, basically, shape and rate parameter of the pdf. In order to obtain the best characterization of the basins and to deduce how the parameters change to give a perfect and unique correspondence between *persistent* and *erratic regime* the observed coefficient of variation obtained by data was set as equal the square root of the ratio between the analytical-deduced flow decay rate and effective-

rainfall frequency. Now, considering that the coefficient of variation is function of the mean and variance of the observed pdf as previously written:

$$CV_x = \sqrt{\frac{Var_x}{\mu_x^2}} \tag{I. 13}$$

$$CV_Q = \sqrt{\frac{k}{\lambda}} \tag{I. 14}$$

The CV_Q can be used to directly deduce the lambda in function of k and, using the equation I.18 it's possible to use the first moment of the observed distribution to set it as function of λ and α. Now, the aim is to perfectly calibrate the model, it means to find the shape and rate parameters able to give the same mean and variance of the observed plot. If these parameters are decomposed using λ, k and α another moment should be used in order to have three equations able to solve the system. The skewness was introduced as well as the variance and the mean:

$$\begin{cases} \mu = sr = \alpha\lambda \\ Var = sr^2 = \lambda\alpha^2 k \\ \chi = \dfrac{2}{\sqrt{s}} = \dfrac{2\sqrt{k}}{\sqrt{\lambda}} \end{cases} \tag{I. 31}$$

How it's possible to note it's sufficient to elevate on the square the third equation and divide the second equation with the third one to observe the removal of k. The system, therefore, it's not closed. In another way it's possible to express from the first equation in the system I.31 the proportionality:

$$\alpha \propto C_1 \cdot \lambda^{-1} \tag{I. 32}$$

And, from the third equation of the I.31 system:

$$k \propto C_2 \cdot \lambda \tag{I. 33}$$

Substituting these proportionalities (I.32 and I.33) in the second equation of the I.31 system it's possible to say that:

$$Var \propto \lambda \cdot (C_1 \cdot \lambda^{-1})^2 \cdot C_2 \cdot \lambda = C_3$$

It's evident the impossibility to evaluate λ (or one of the other parameters) and, therefore, the system has one degree of freedom and allows ∞^1 solutions. This problem was bypassed considering, instead of the single hydrocilmatic parameters, only the shape and rate parameter of the gamma pdf. In this way the method can be done regardless the exact values of the parameters:

$$CV_Q = \sqrt{\frac{1}{s}}$$

And

$$\mu = r \cdot s$$

This calibration was then continued in order to deduce, starting from the difference between shape and rate parameters obtained from the model and the moments method, the correction value of Δ_1 and Δ_2.

Chapter 2 – Case study

2.1 – Costa Rican scenario

Costa Rica is a Central America country bordering to Nicaragua in the north and to Panama in the south and with two different coastlines, one in the east (the Caribbean Sea) and one in the west (the Pacific Ocean). Central America is a very heterogeneous land in terms of geological, meteorological and physiographical features and it's set in a region called Isthmus, between North and South America. Costa Rica takes up a surface of 51110km^2 and it is comprised between 8^{o}03' and 11^{o}13' as North latitude and from 82^{o}32' to 85^{o}57' as West longitude (including *Isla de Coco*). The geography of the country has been classified, according to Silva [1991], into four major physiographical regions:

1. The *Cordillera* represents the inner mountain range of Costa Rica, characterized by several volcanoes which are part of the *Pacific Ring of Fire*. Its individuation can help the hydrological subdivision of the state, discerning into a Caribbean side and a Pacific Ocean one, both of them interested by different meteorological features (see Figure II.1).

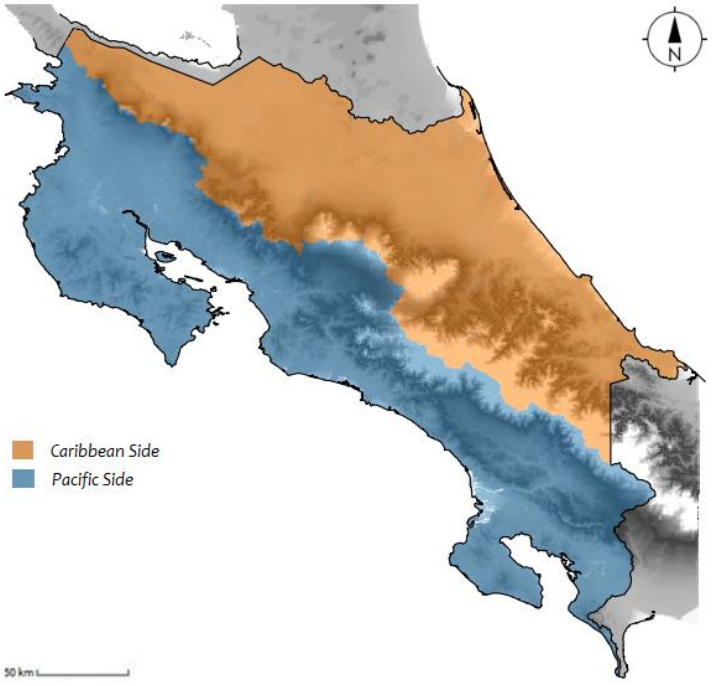

Figure II.1 – Geographical distinction between Caribbean side and Pacific side according to geomorphological features defined by the *Cordillera*.

These two different macro-regions run parallel to the coastlines, from northwest to southeast, following the direction imposed by the cordilleras and show important correlation with the climate (see section 2.2) underling the important role played in the country by elevation in the governing of local rainfall regime [Waylen et al., 1998];

2. The *Central Valley* consists in a northern depression between mountains, it hosts different volcanoes and has roughly extension of 50km from east to west and 20km from north to South with an average height above sea level of 1100m;
3. The *Meridian Valley* is placed between Costa Rica and Panama and it is set between two sets of the Cordillera. It's width is about 20km and the north-to-south extension is roughly 110km and its average height above sea level is 800m. It's the home of *Rio Grande de Terraba*, the Costa Rican river with the most extended catchment with an area of 4771,37km^2;
4. The *Peripheral Plains* represents those flat areas between the mountains of the *Cordillera* and the sea. They are present both on the Pacific and the Caribbean sides, but, even if they are similar in terms of elevation, their climate and morphological composition can be very different [Birkel, 2005].

These four regions can be identified in the figure II.2 in which the mountain range can be spotted in the middle of the country and the *Central Valley*, the *Meridian Valley* and the *Peripheral Plains* are respectively indicated with the squares and the letter A, B and C (C1 for the Pacific side and C2 for the Caribbean one).

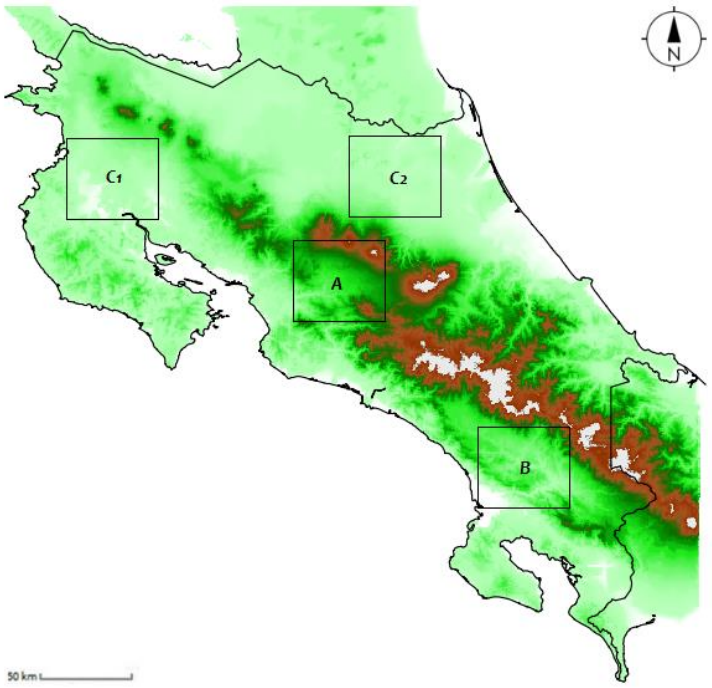

Figure II.2 – Topography of costa Rica according to the Silva characterization.

2.2 – Climate

Costa Rican climate was classified, according to Chang and Lau [1983], as humid tropical, due to high mean annual temperature (> 20^{o}C) and precipitation rates (>1500mm/yr). The variation in terms of temperature, precipitation, pressure and humidity are due to four factors: circulation patterns forming due to the *Inner Tropical Convergence Zone* (ITCZ); the northeast Trades winds, originated from the Bermuda High; the southward infiltration of *northers*, cold air fronts developed over continental North America; the local and unpredictable influences of tropical cyclones and hurricanes [Waylen et al., 1998; Birkel et al., 2012]. The precipitation pattern are strictly linked to the different wind regimes in Caribbean Sea and Pacific Ocean which are separated in the country by the mountain topography that divides the region in the Pacific and Caribbean zone, respectively at west and east, as previously underlined. Even if the country is at the western margin of North Atlantic anti-cyclone, it is mainly dominated by the northeast Trades due to its position in the tropical belt.

The rainfall-shadowing from the Atlantic winds due to the orographic lifting allows the Pacific to be climatically different from the Caribbean side. Moreover, at low levels, the Trades blow and flow through local cols and they pass in the Central America cordillera. One of the main gaps is along the San Juan river, coinciding with the Nicaragua border, and when the Trades reaches the Pacific Ocean the winds coming from the sea through the Gulf of Papagayo deflects to the right producing an upwelling of cool water in the Gulf known as the *Costa Rica Dome*. This characteristic enhances the climatic stability in the Pacific side especially in the Guanacaste peninsula, in the Northwest, during the dry seasons, with precipitations pretty absent during all the period. This dominant aridity is successively interrupted by another northward migration of the Inter-Tropical Convergence Zone. On the other hand, during the wet season, this air movement promotes low-intensity rainfall events. This characteristic implies two slightly different climatic regimes on the Pacific side.

During the boreal summer the seasonal northward migration of the Inter-Tropical Convergence Zone through the eastern equatorial Pacific. From June to September the ITCZ moves up to its northern position at about 10^{o}N carrying with itself unstable air and frequent heavy storm in the western part of the country. This regime is further modified by another factor: the strengthening of the Trades winds in the Caribbean leads to a temporary increase of airflow through the gap of San Juan river which causes a partial interruption in the precipitation events during July known locally as the Veranillos de San Juan due to the related retreat or standstill in the northward progression of the ITCZ. This pause, or decrease of rainfall amount, is associated, contrarily, to an increase of rainfall intensity in the Caribbean side and it is called *little summer*. The residual rainy season days along the Pacific coast following the Veranillos are generally wetter than those preceding it and, on the Caribbean side, this precipitation peak in the western coast corresponds to the season of maximum tropical storm activity in the tropical Atlantic.

During the boreal winter, high pressure cells move over the central US due to meridional pressure gradients forming across the Gulf of Mexico. In December and January active air masses moves south up to 10°N latitude in the Caribbean Sea, due to the movement and the trade winds induced by the movement of the Inner Tropical Convergence Zone. This phenomenon causes a warming of the cool air moving down toward Central America, acquiring moisture from water bodies. When the warmed air hits the Nicaraguan and Costa Rican east coasts several induced convergences and the condensation of the humid air lead to locally heavy precipitations and a generally large quantity of rain throughout all the season. On the Pacific Side, on the contrary, the boreal winter corresponds to dry season. Several studies (Schultz et al., 1998) have recognized two separate types of fronts during this period. The first of them is the most frequent one and occur earlier in the year (November-December), it causes small declines in temperature and it's due to the settlement of high pressure over the central United States after crossing the Rockies from the North Pacific. The second one is less frequent but causes a stronger drop of temperature and the most intense rainfall of the country, due to the descend of cold air masses from Canadian prairies.

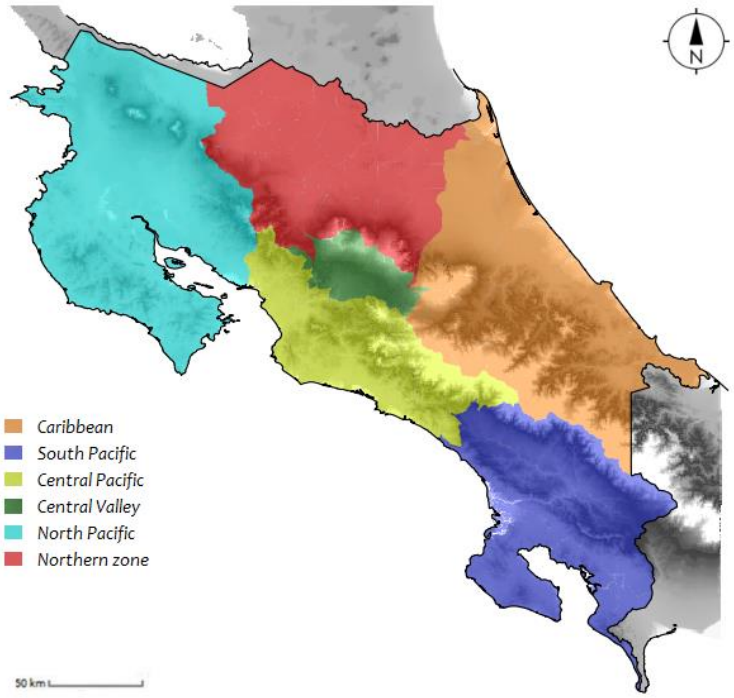

Figure II.3 – Microclimatic areas subdivision according to IMN classification performed using 40years (1950-1990) of precipitation data.

In general it's possible to define two different seasonal patterns in Costa Rica, corresponding to a humid and a dry season. In December and January active air masses moves south up to 10°N latitude in the Caribbean Sea, due to the movement and the trade winds induced by the movement of the Inner Tropical Convergence Zone. This phenomenon causes a condensation of humid air due to wind and topography as soon as this air hit the east coast. On the Pacific Side, on the contrary, the same time period corresponds to dry season. This annual migration of the ITCZ hits the southern Costa

Rican point in February/March. These considerations allow to generally define a dry season during the boreal winter season and a humid one during the summer boreal season [Waylen et al., 1998; Birkel et al., 2012; Hastenrath, 1967; Enfield and Alvaro 1999].

These considerations allow the classification of six different microclimatic zones [National Meteorological Institute (IMN), 2000; Birkel, 2005] which have different features in terms of precipitation patterns, geomorphological assets and streamflow regimes. Figure II.3 shows a generalized representation of this regional distribution of microclimatic regimes.

The Caribbean area have a precipitation all year round, with a weak distinction between dry and wet season. The Northern Zone present relevant intensity in terms of monthly precipitation magnitude but shows a distinct dry period during January, February and March. North Pacific, Central Valley and Central Pacific show a high seasonality with almost no rainfall events during January and February. In normal conditions the typical climatic dry season goes from December to March and the wet one from May to October, November and is balanced by catchment's reservoirs in July and is not characterized by the "little summer" phenomenon of precipitations.

2.3 – Hydrological data

Hydrological studies strictly depends on data availability and their quality; moreover, if a stochastic study is concerned , it relies on the availability of long-term datasets without relevant interruptions. The data used in this thesis came from the *Global Runoff Data Centre* (GRDC) which was founded in order to collect and provide hydrological data for research projects as FRIEND (Flow Regimes from International Experimental and Network Data, CEH, 2001) and its Mesoamerican subdivision, called AMIGO. According to GRDC there are 49 Costa Rican gauging station with recorded daily streamflow data from 1973 to 1993. Unfortunately, as underlined by Birkel [2005], many catchment present gaps of several years.

This database was successively updated by the *Instituto Costarricense de Electricidad* (ICE) and 18 gauging stations where chosen in order to publish partially corrected data series from 1973 to 2003. These 18 stations were selected among all the existing ones in order to choose only pristine catchment without any relevant anthropological activity that could modify the streamflow regime; moreover their distribution in the country allow a good spatial coverage in all the microclimatic conditions present in Costa Rica. The samples of streamflow intensity were collected every day at 17.00h using a pressure transducers (like Onset Hobo U20, [Birkel et al., 2016]). Even if these 18 basins are not affected by long time intervals of data missing it is still possible to have gaps less than one month. In this case they were corrected by Birkel [2005] using a linear interpolation and an approach based on the correlation of other

nearby catchments with similar physiographic and climatic characteristics. The eighteen datasets were therefore completed without gaps in their expression and at the end of the computation it was possible to obtain daily streamflow value for eleven catchment with a full record length of 30 years and other seven with a reduced length.

These 18 basins have a good spatial coverage in Costa Rica for their heterogeneous distribution in the country. Nevertheless it's also important to take in account that catchments with a very large contributing area can be affected by the superposition of different regional climatic zones. However, this observation can be ignored in this case study because all the chosen basins don not cross different climatic zones [Birkel, 2005].

The temporal evolution of Costa Rican streamflow regimes was studied by Dyck & Peschke [1995] and Birkel [2005] and two different patterns were identified and their qualitative behavior mirrors the microclimatic distinction defined by the IMN.

- *The Regular Caribbean Type* is present on the Caribbean flank in which the precipitation pattern present no strong distinction between dry and wet season. This characteristics leads to an equilibrium between rainfall, evapotranspiration and streamflow pretty constant all the year and aquifers capacity is assumed to have a high storage capacity. This features give the streamflow in this area a low variability with a less emphasized maximum and minimum values.
- *The Irregular Type* is present on the Pacific flank and it is due higher difference between dry and wet season. From December to March the streamflow assumes low values and much higher intensity during the dry season. In the Guanacaste region the *little summer* induced by *Veranillos* interrupts (or decrease) partially the rainfall during the wet season and this behavior has consequence on the streamflow regime which shows two peak during the year: the first and weaker one in June, the second and the most important one in October. The Central Valley regime, even if affected mainly by the strong seasonality difference of the Pacific side shows a more balanced behavior due to action of catchment's reservoirs.

These considerations, together with the typical rainfall patterns studied by IMN and the detection of low flow seasons when the streamflow falls below the Q_{95} percentile threshold, allowed a classification between dry and wet seasons for all the catchment studied.

2.4 – Study catchments

In the following figures different maps will be shown in order to underline morphological features of Costa Rica and highlight the catchment analyzed by the model.

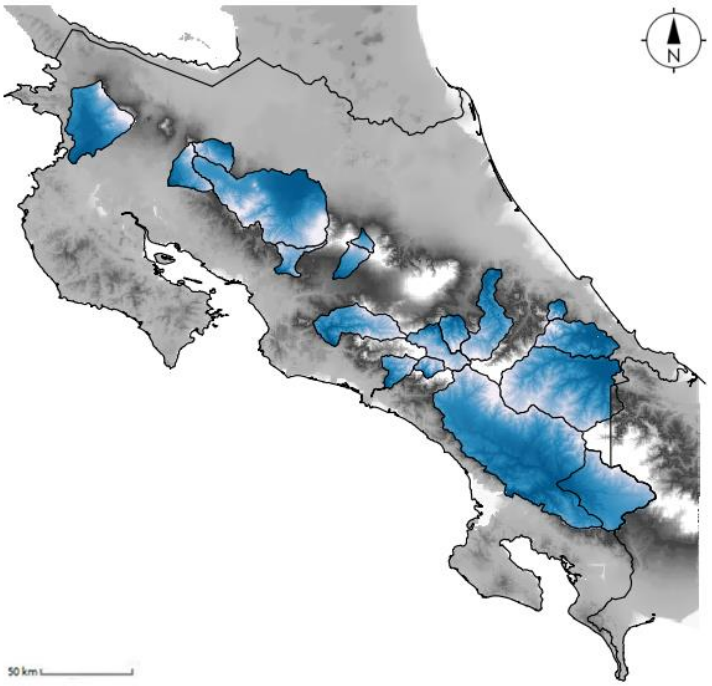

Figure II.4 – Costa Rican map in grey scale and the eighteen catchments studied in white-blue pattern

In the map shown in figure II.5 there is a qualitative representation of basins present in North Pacific and Northern Zone climate areas are showed. The basins are represented using topographic shape file and they've been modified using blue-white color pattern in order to increase the contrast and underline the morphological features of the catchments. White areas represent more elevated zones above the sea level, on the other hand, as the blue becomes darker, the morphology decreases in altitude. The Costa Rican map is, on the contrary, represented in grey scale. It's possible to observe the northern part of the *Cordillera*, in which the highest peaks are white, and the big peripheral plains, on the east (Caribbean) and west (Pacific side), represented in light grey and disposed between the mountains range and the costal lines.

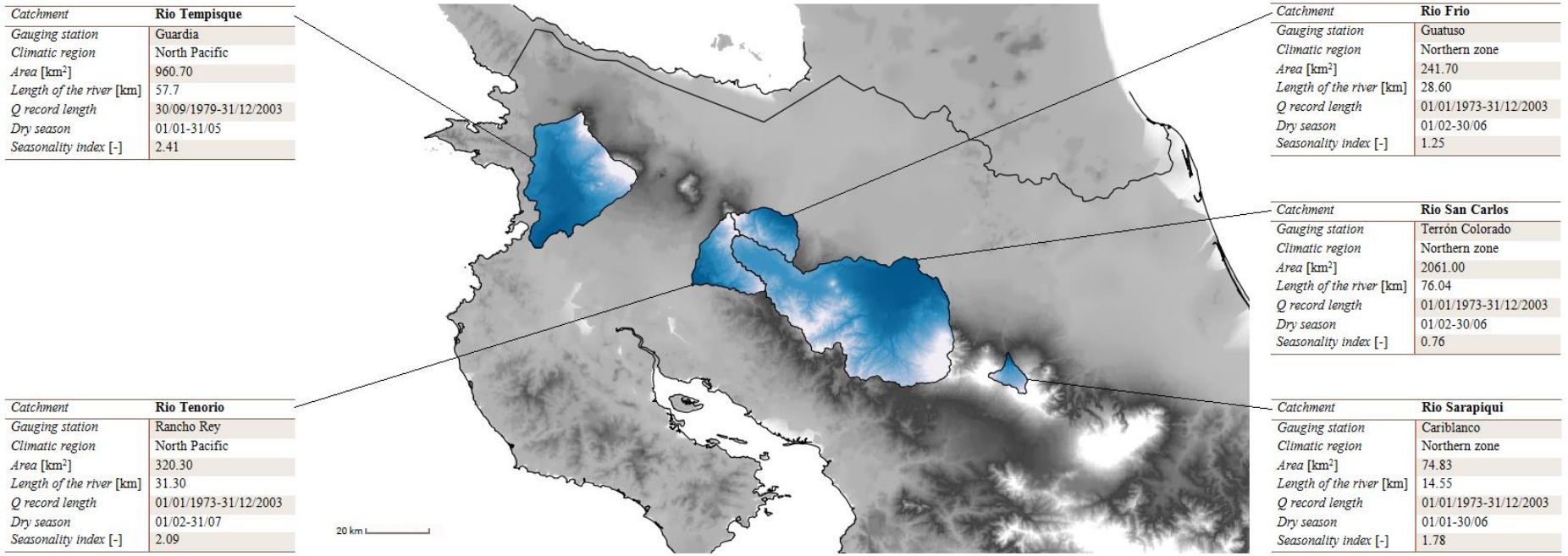

Figure II.5 – Morphological representation in grey-scale of northern zone of Costa Rica, catchment studied are represented in white-blue pattern.

In the map shown in figure II.6 there is qualitative representation of basins present in *Central Valley* and *Central Pacific* climate areas are showed. The basins, as before, were represented using topographic shape file and they've been modified using blue-white color pattern in order to increase the contrast and underline the morphological features of the catchments. White areas represent more elevated zones above the sea level and the darker the blue becomes the more the altitude decreases. In this map it's possible to spot the big development of the *Cordillera* occupying a wide area in the center and south of the country. The highest point of the mountain range are white and, as the slope decreases, the color blends in dark and light grey. It's easy to spot the *Central Valley* area, between the northern part of the *Cordillera* and the central one. Right below the *Central Valley*, the *Central Pacific* area extends in the west part of the country.

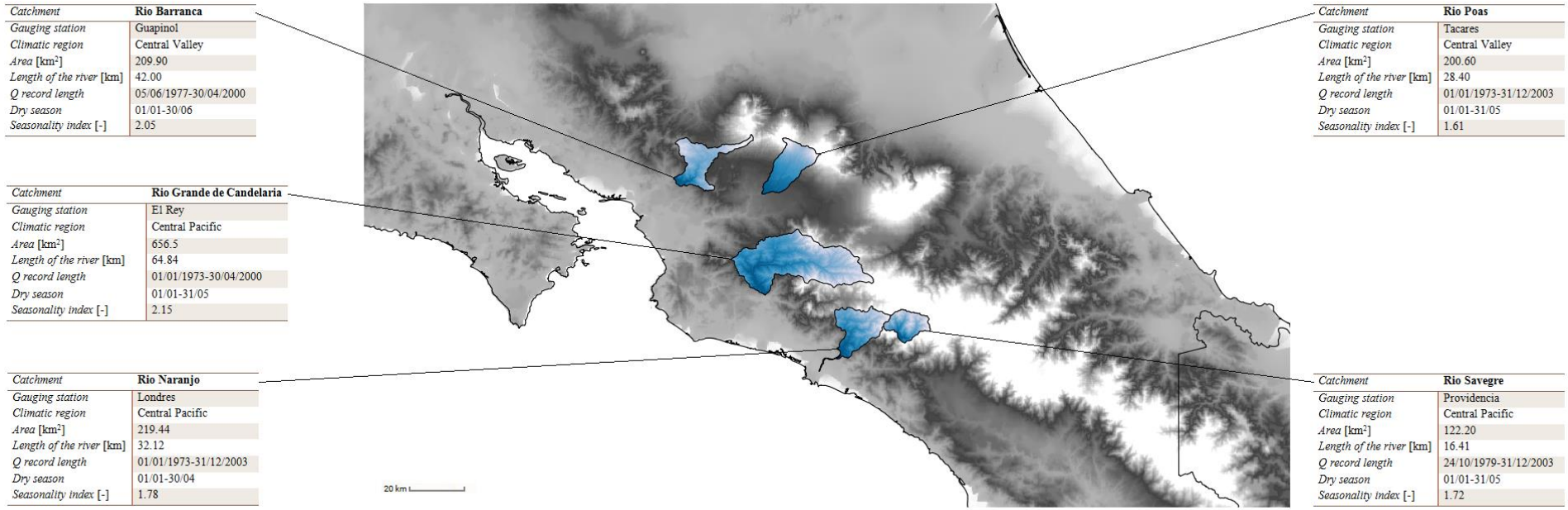

Figure II.6 – Morphological representation in grey-scale of central zone of Costa Rica, catchment studied are represented in white-blue pattern.

In the map shown in figure II.7 there is qualitative representation of basins present in *Caribbean* and *South Pacific* climate areas are showed with the same qualitative color pattern used before for north and central zone maps. It's possible to see how the South Pacific area comprehends two of the most wider catchments (Rio Grande de Terraba and Coto Brus). The Caribbean basins extend themselves from the southern part of the *Cordillera* to more flat areas near the coastline.

Catchment	**Rio Pacuare**
Gauging station	Dos Montanas
Climatic region	Caribbean
Area [km²]	660.40
Length of the river [km]	83.80
Q record length	01/01/1973-31/12/2003
Dry season	01/01-31/05
Seasonality index [-]	1.04

Catchment	**Rio Pejibaye**
Gauging station	Oriente
Climatic region	Caribbean
Area [km²]	229.20
Length of the river [km]	26.55
Q record length	01/01/1973-31/12/2003
Dry season	01/01-31/05
Seasonality index [-]	1.10

Catchment	**Rio Reventazon**
Gauging station	Palomo
Climatic region	Caribbean
Area [km²]	373.00
Length of the river [km]	38.43
Q record length	01/01/1973-31/12/2003
Dry season	01/01-31/05
Seasonality index [-]	1.38

Catchment	**Rio Grande de Terraba**
Gauging station	Palmar
Climatic region	South Pacific
Area [km²]	4771.37
Length of the river [km]	151.92
Q record length	01/01/1973-31/12/2003
Dry season	01/01-31/05
Seasonality index [-]	1.75

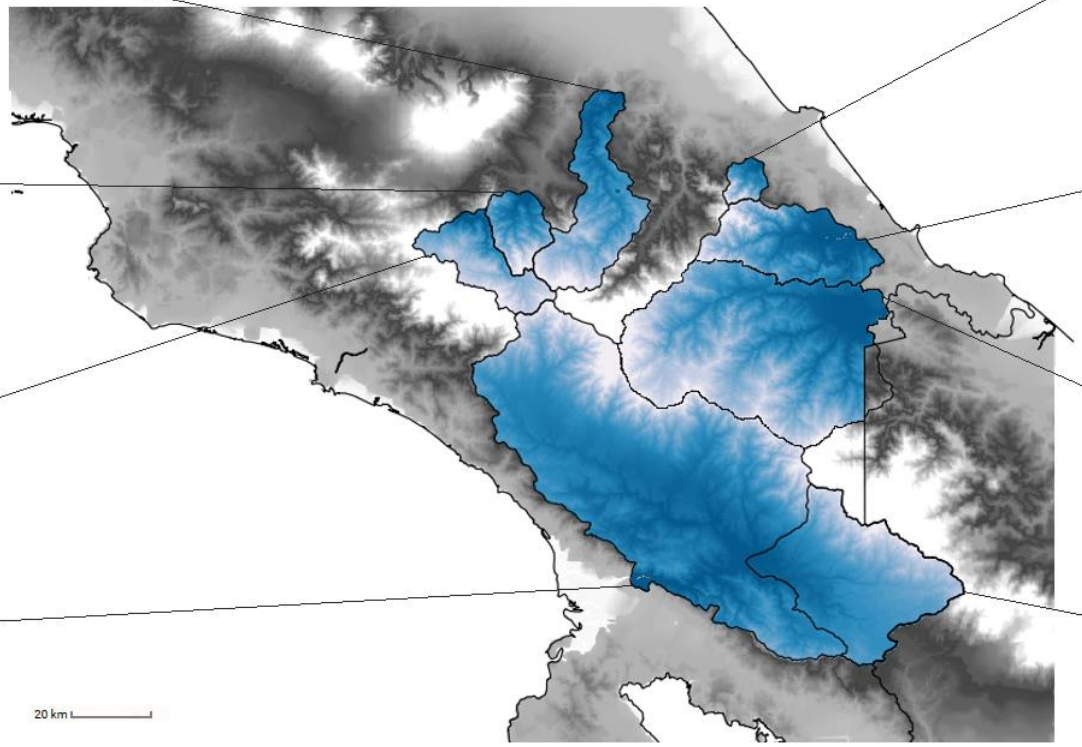

Catchment	**Rio Banano**
Gauging station	Asunción
Climatic region	Caribbean
Area [km²]	89.98
Length of the river [km]	14.78
Q record length	01/01/1973-30/09/1988
Dry season	01/12-31/05
Seasonality index [-]	0.29

Catchment	**Rio Estrella**
Gauging station	Pandora
Climatic region	Caribbean
Area [km²]	637.30
Length of the river [km]	46.74
Q record length	22/06/1973-31/12/2003
Dry season	01/12-31.05
Seasonality index [-]	0.42

Catchment	**Rio Telire**
Gauging station	Bratsi
Climatic region	Caribbean
Area [km²]	2110.00
Length of the river [km]	85.86
Q record length	01/01/1973-30/04/1998
Dry season	01/11-31/05
Seasonality index [-]	0.75

Catchment	**Rio Coto Brus**
Gauging station	Caracucho
Climatic region	South Pacific
Area [km²]	1133.00
Length of the river [km]	60.35
Q record length	01/01/1973-31/12/2003
Dry season	01/01-31/05
Seasonality index [-]	1.8

Figure II.7 – Morphological representation in grey-scale of south zone of Costa Rica, catchment studied are represented in white-blue pattern.

Chapter 3 – Results

3.1 – Outline

In this chapter the results obtained from the model application to 18 Costa Rican basins will be discussed. In order to give a complete summary able to give a good description of the Costa Rica hydrological scenario 6 basins will be shown, one for every microclimatic region. The first following section will display results obtained by the application of the model to the 6 catchments using the annual temporal interval; it will be possible to see how, in many cases, the trend of the pdf showed a double peak. This consideration led the study to continue with a seasonality subdivision of the time series of the daily discharge dataset (dry season and wet season), which will be shown in the successive sections as well. For every basin analyzed the analytical pdfs obtained with the different regression-methods will be shown and the different performances (expressed in *sum of squared difference*, or SSD, with the observed values) will be highlighted. Moreover, being most of the time the regression method II and IIIb ineffective in the estimation of the analytical pdf (the relative recession rate k has an order of magnitude of 10^{-6}, 10^{-7}, 10^{-8}) this chapter will show only the results obtained using the regression methods Ia, Ib, IIIa and with the non-linear application. In the following tables the Roman numbers used previously to indicate the regression methods will be substituted by Arabic numbers.

Name	**Gauging Station**	**Climatic Region**	**Area [km^2]**	**SI [-]**	**Discharge record length**
Rio San Carlos	Terron Colorado	Northern zone	2016.00	0.76	01/01/1973-31/12/2003
Rio Tenorio	Rancho Rey	North Pacific	320.30	2.09	01/01/1973-31/12/2003
Rio Poas	Tacares	Central Valley	200.6	1.61	01/01/1973-31/12/2003
Rio Naranjo	Londres	Central Pacific	219.44	1.78	01/01/1973-31/12/2003
Rio Grande de Terraba	Palmar	South Pacific	4771.37	1.75	01/01/1973-31/12/2003
Rio Pejibaye	Oriente	Caribbean	229.2	1.1	01/01/1973-31/12/2003

Table III.1 – Streamflow studied in this chapter

The sections will be completed showing, for every basin, the results of the calibration, both for the annual pdf and the pdfs of the dry and wet seasons. The direct visualization and analytical comparison between original model and the calibrated one will allow the reader to appreciate the performance increasing of the pdf. For every case further information about the corresponding sum of squared difference and correction parameters values (Δ_1 and Δ_2) will be given as well as consideration about the hydrological characterization of the streamflow regime. The catchment showed in this chapter and their characteristics can be reassumed quickly in table III.1.

3.2 – Characterization of the annual pdf

3.2.1 – Rio San Carlos

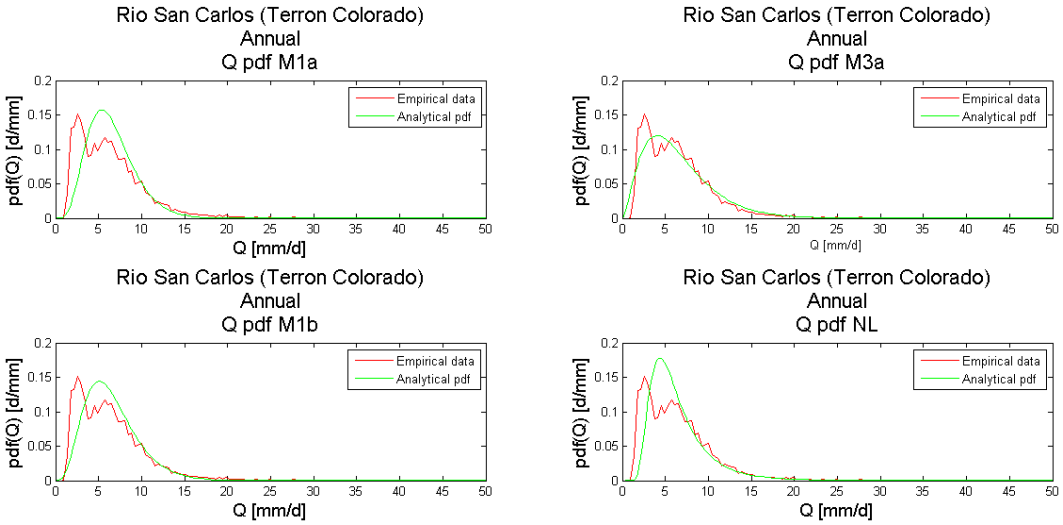

Figure III.1 –Rio San Carlos, Annual pdf with different regression methods.

It's possible to observe how the empirical pdf has a double-bell shape, a typical result for streamflows in which datasets are not divided according to seasons. The duration curve is able to show how the streamflow has always a not-null value of discharge as in permanent rivers. This result is not surprising considering the climate of the region where the catchment is located (Northern Zone). In fact, even though in this zone it's possible to clearly identify a dry period during January, February and March, the storage properties of the soil and/or the rainfall intensity in the area are sufficient to guarantee a minimum streamflow contribution all the year long.

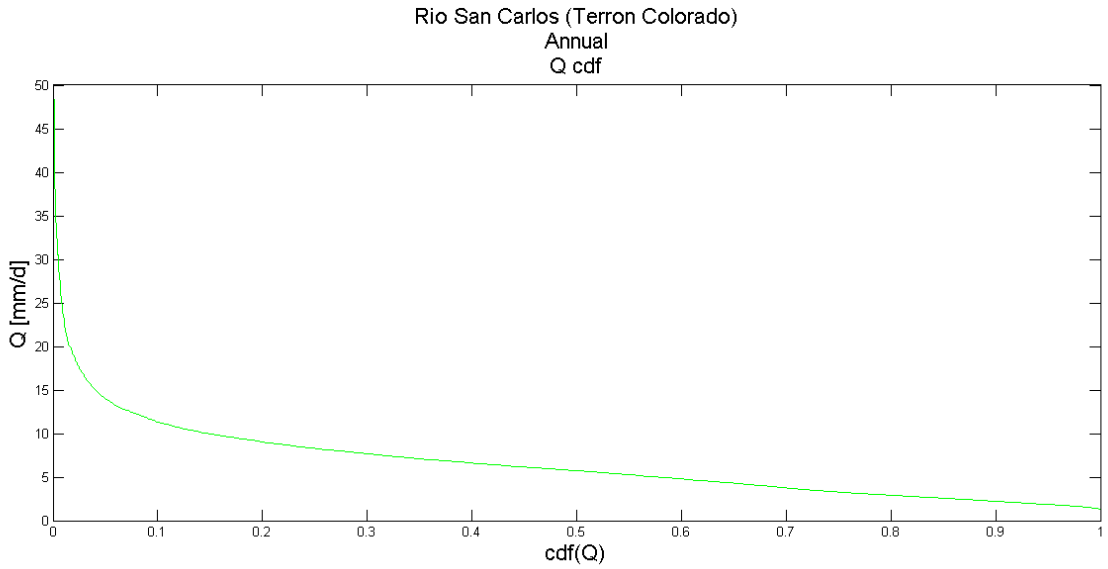

Figure III.2 –Rio San Carlos, flow duration curve.

The analytical pdf are able to fit the empirical distribution in a reasonable way and the performance obtained by different recession methods can be deduced from the table III.2:

<*Q*> [mm/d]	6.5259	M1a SSD performance	0.06283
Var [mm^2/d^2]	21,8756	M1b SSD performance	0.04239
CV_Q [-]	0,7167	M3a SSD performance	**0.01466**
Best recession method	M3a	NL SSD performance	0.07111
α [mm]	18.7273	*Q* min [mm/d]	1.16
λ [1/d]	0.34846	*Q* max [mm/d]	98.1
k (M3a)	0.13228	*Q* dataset length	11322

Table III.2 – Rio San Carlos. Annual pdf pre-calibration results

The MLE calibrated model gives the results shown in figure III.3:

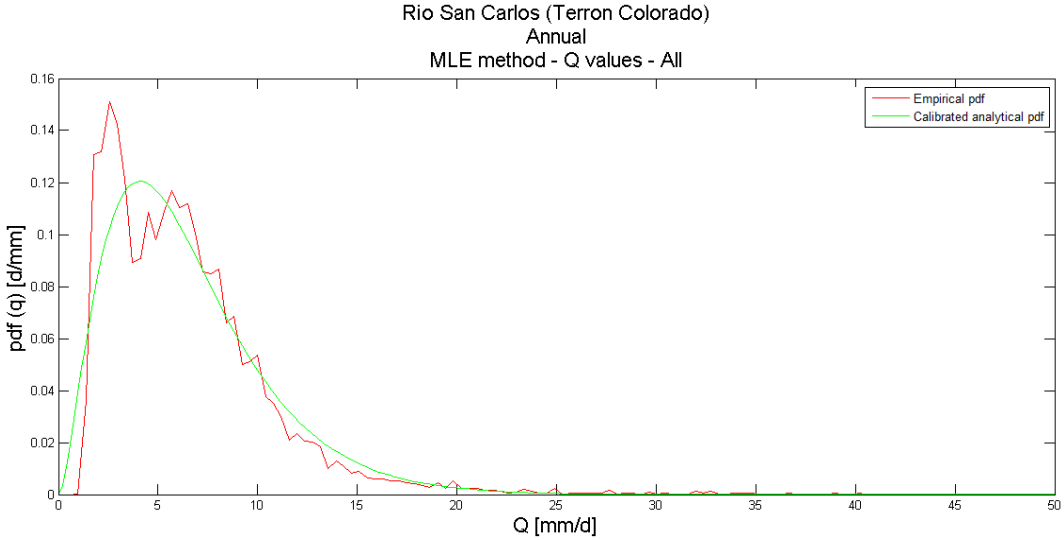

Figure III.3 –Rio San Carlos, calibrated pdf according to MLE method.

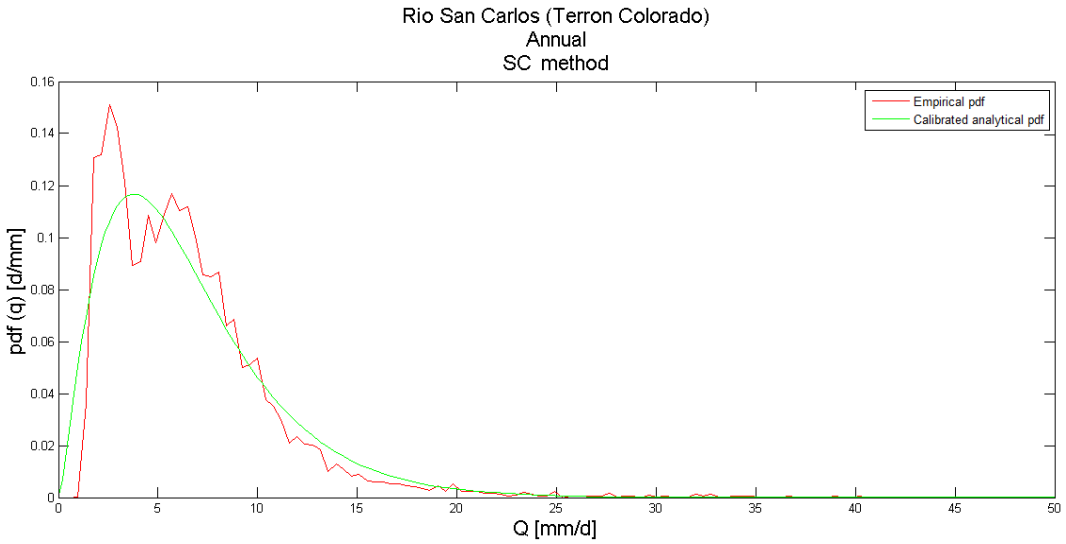

Figure III.4 –Rio San Carlos, calibrated pdf according to SC method.

The SC method, whose corresponding analytical pdf is shown in figure III.4 plot and is able to have a visual fitting pretty similar to the pdf obtained with the MLE method. The best Q% removal gives, in this case, the same result of the classic MLE and the code returns, as best data interval, the entire dataset. The method of moments, on the other hand, even if it's able to perfectly replicate mean, variance and coefficient of variation, is not able to provide a fitting remarkably different than other methods, being the pdf deduced with this method pretty similar to the other one estimated by the other calibration method (figure III.5).

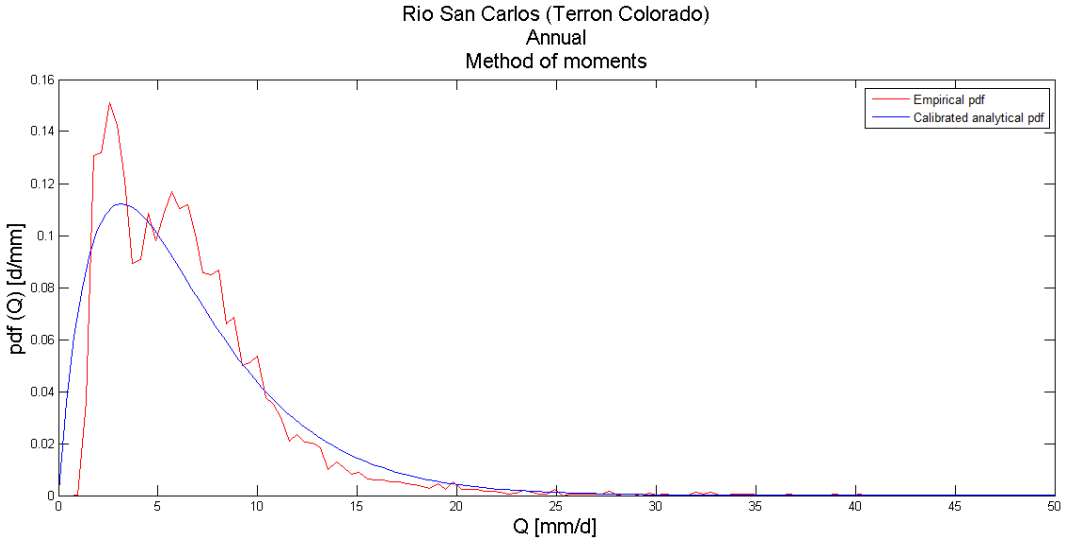

Figure III.5 –Rio San Carlos, calibrated pdf according to method of moments.

The performance can be observed in the following table in which every calibration method is linked to the correspondent sum of squared difference value. The best-fitting model is obtained with the SC calibration:

MLE		SC		Best Q% removal				Method of moments	
$\Delta_1 = \Delta_2$	SSD	$\Delta_1 = \Delta_2$	SSD	%Q used	Δ_1	Δ_2	SSD	$\Delta_1 = \Delta_2$	SSD
0.9807	0.0149	**1.1067**	**0.0138**	100%	0.9807	0.9807	0.0149	1.3530	0.0171

Table III.3 – Rio San Carlos. Annual pdf after calibration results

It's interesting to spot how the initial model without calibration, had a performance (obtained with the linear regression method 3a) equal to 0.01466, lower than any other calibrated method except than SC one. Therefore even without calibration and a seasonality characterization, the model is still able to obtain a reasonable fit with the observed annual pdf.

3.2.2 – Rio Tenorio

The following plots collected in figure III.6 will show the results of the application of the linear model (using regression methods 1a, 1b, 3a) and the non-linear one.

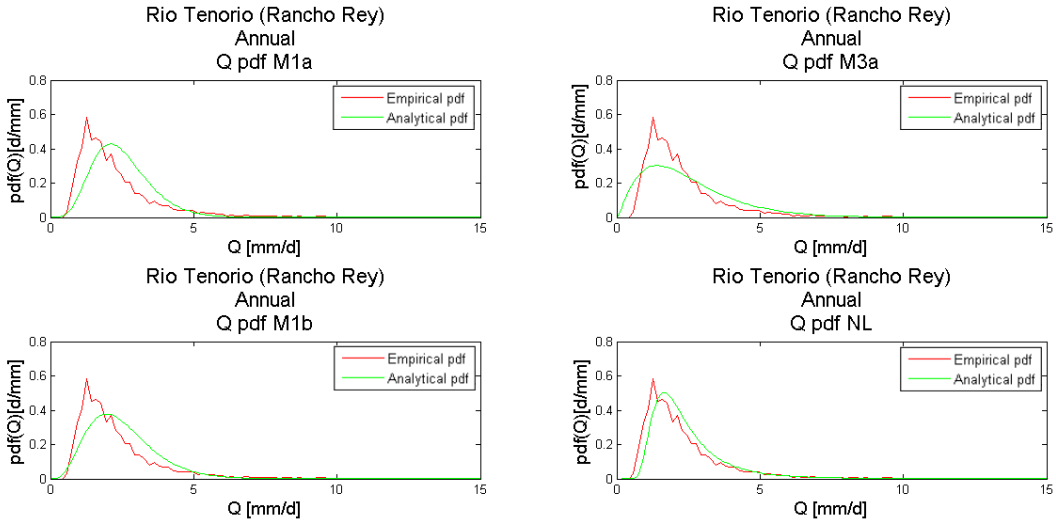

Figure III.6 –Rio Tenorio, Annual pdf with different regression methods.

The non-linear model shows a similar behavior to the observed pdf, but it is slightly shifted on the right, thus this recession method overestimates the discharge associated to certain probabilities and, in terms of SSD, the corresponding pdf is less performing than the pdf obtained with M3a linear recession.

The flow duration curve can be observed in the next plot and Rio Tenorio shows a permanent discharge all year long.

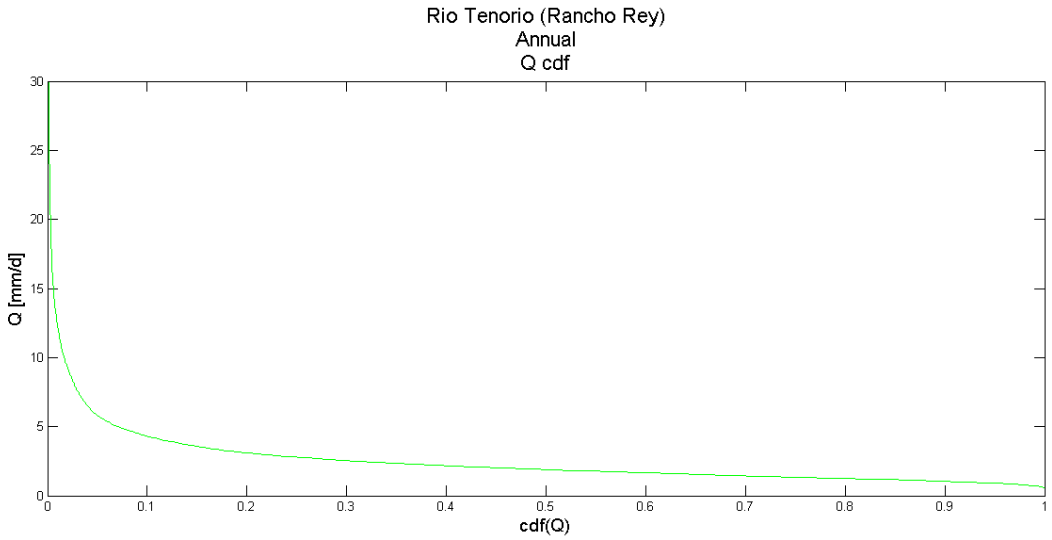

Figure III.7 –Rio Tenorio, flow duration curve.

$<Q>$ [mm/d]	2.5015	M1a SSD performance	0.56832
Var [mm^2/d^2]	5,695	M1b SSD performance	0.36661
CV_Q [-]	0,954	M3a SSD performance	**0.26579**
Best recession method	M3a	NL SSD performance	0.29543
α [mm]	7.8492	Q min [mm/d]	0.55
λ [1/d]	0.31869	Q max [mm/d]	42.12
k (M3a)	0,13861	Q dataset length	11322

Table III.4 – Rio Tenorio. Annual pdf pre-calibration results

After the calibration the model pdf increases performance only after the best Q% removal method. As the following plots (III.8-11) will show the visual fitting for the MLE and SC method is pretty similar and the method of moments is not able to represent both the position and the intensity of the peak of the pdf. It's also interesting to spot how the SC method gives $\Delta_1=\Delta_2\approx1$, and it has the same performance of the model without calibration. On the other hand, the best Q% removal method is able to reproduce better the shape of the peak allowing a visible increase of performance.

The table III.5 reassumes the calibrated-models properties (values of correction parameters, Δ_1 and Δ_2). The different performances for the different methods suggest that the fitting increases if compared to the previous uncalibrated case (0.26579). The only method which decreases the performances is the method of moments with a sum of squared difference equal to three times the not-calibrated one.

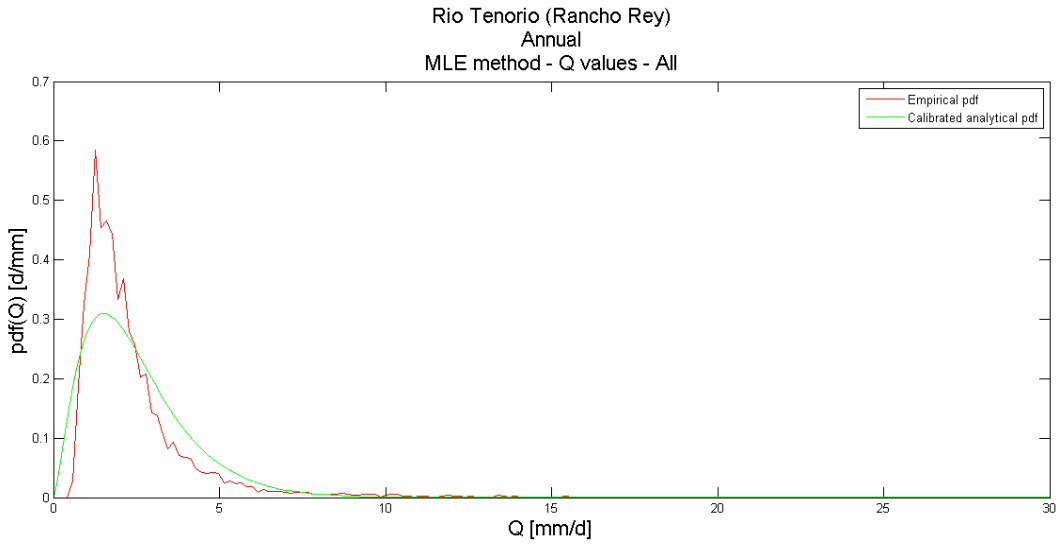

Figure III.8 –Rio Tenorio, calibrated pdf according to MLE method.

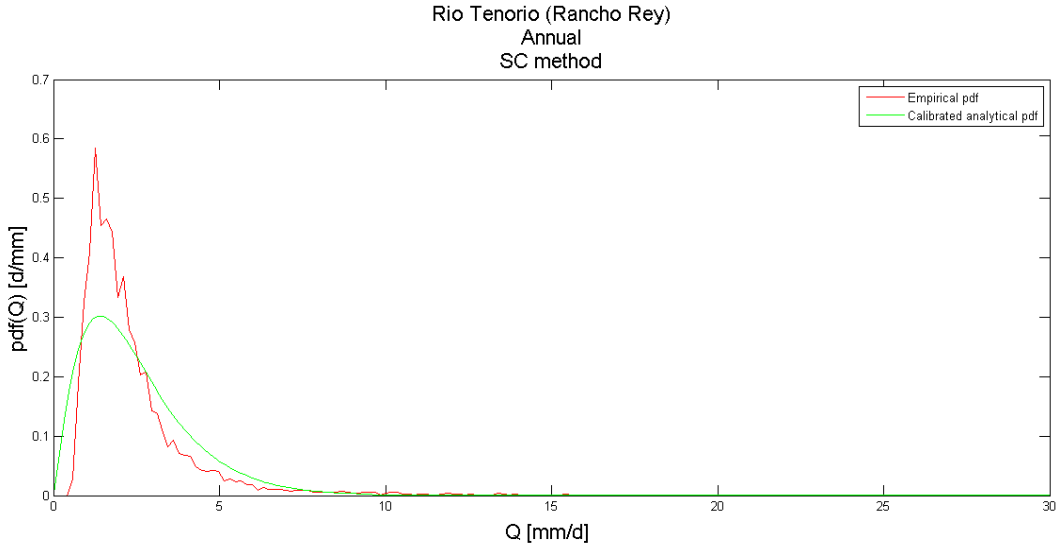

Figure III.9 –Rio Tenorio, calibrated pdf according to SC method.

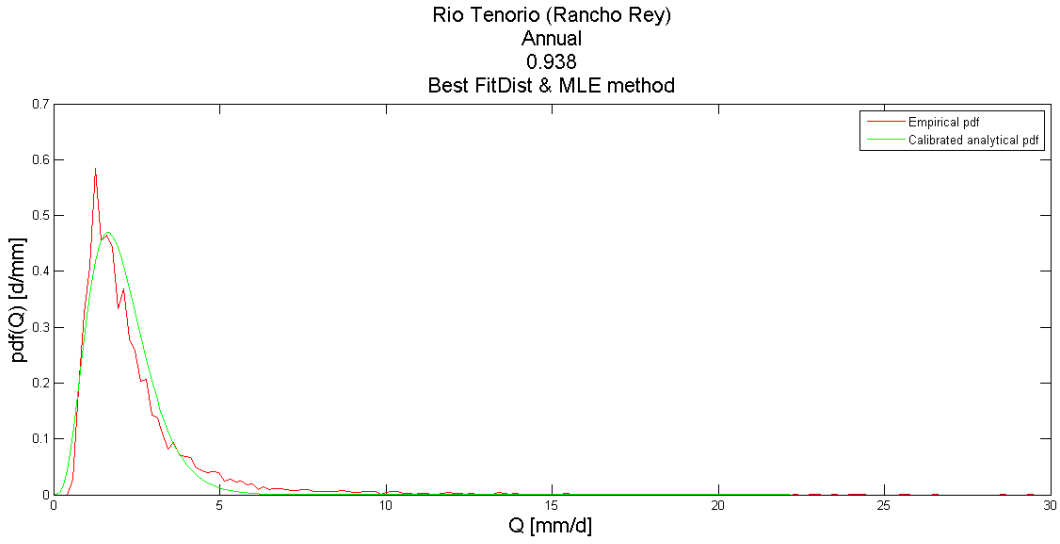

Figure III.10 –Rio Tenorio, calibrated pdf according to best Q% removal method.

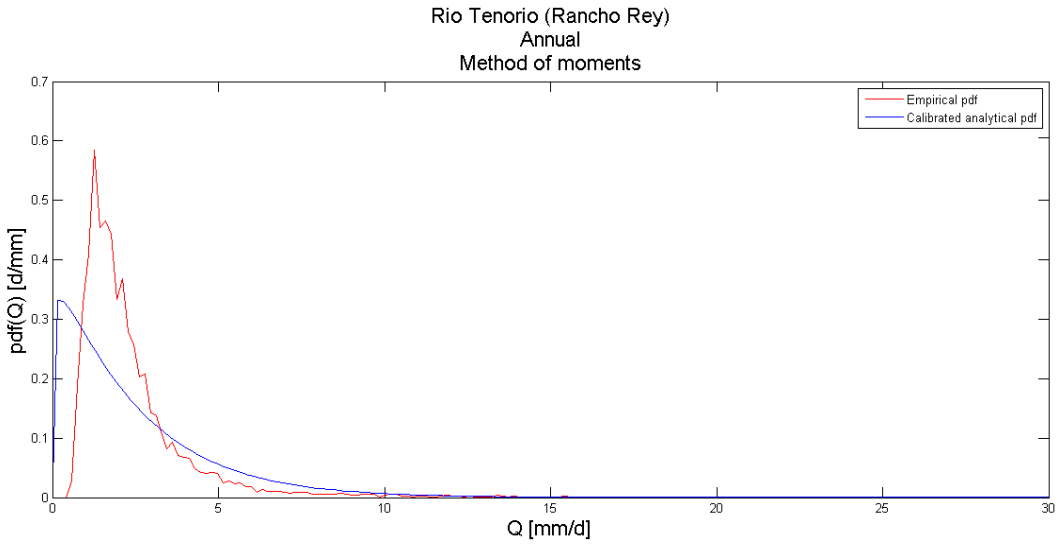

Figure III.11 –Rio Tenorio, calibrated pdf according to method of moments.

MLE		SC		Best Q% removal				Method of moments	
$\Delta_1 = \Delta_2$	SSD	$\Delta_1 = \Delta_2$	SSD	%Q used	Δ_1	Δ_2	SSD	$\Delta_1 = \Delta_2$	SSD
0.9045	0.2483	1.0001	0.2658	**93.8%**	**0.4732**	**0.3888**	**0.1250**	2.0924	0.687

Table III.5 – Rio Tenorio. Annual pdf after calibration results

3.2.3 – Rio Poas

The uncalibrated model is shown in Figure III.12 in with four cases (three for the linear regression and one for the non-linear).

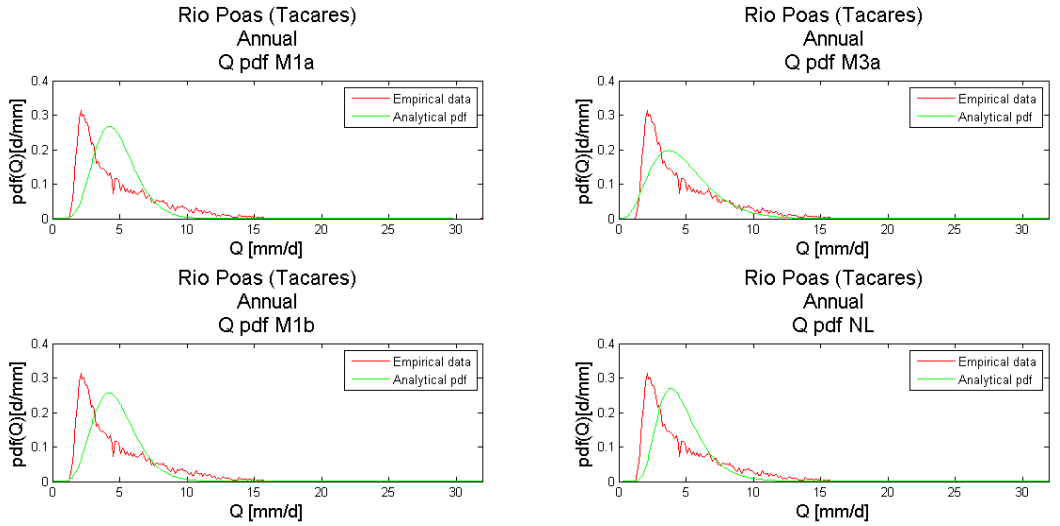

Figure III.12 –Rio Poas, Annual pdf with different regression methods.

As the flow duration curve indicates, Rio Poas is a permanent stream and its relatively high minimum flow is due to the climates of the region and the morphological properties of the Central Valley, which allow a continuous contribution to the stream from groundwater.

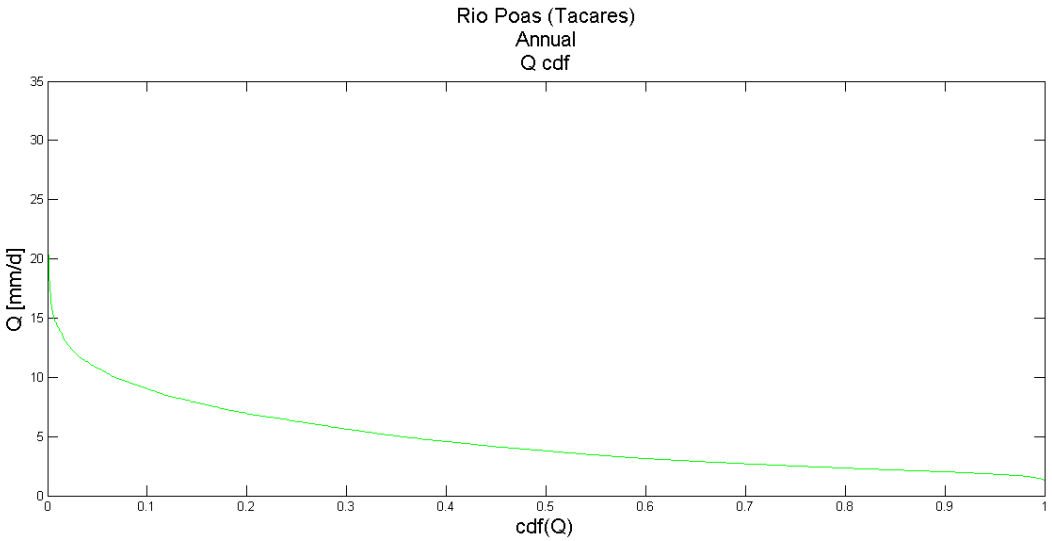

Figure III.13 –Rio Poas, flow duration curve.

$<Q>$ [mm/d]	4.76105	M1a SSD performance	0.76361
Var [mm^2/d^2]	8.8638	M1b SSD performance	0.68180
CV_Q [-]	0.6253	M3a SSD performance	**0.29211**
Best recession method	M3a	NL SSD performance	0.66488
α [mm]	13.1752	Q min [mm/d]	1.29
λ [1/d]	0.36136	Q max [mm/d]	31.94
k (M3a)	0,07961	Q dataset length	11322

Table III.6 – Rio Poas. Annual pdf pre-calibration results

As the table shows it's possible to observe how the best method to study the discharge recessions is given by the linear M3a model which is able to give the lowest SSD among all the possible methods.

The results of the application of different calibration methods are displayed in the following plots (III.14-17). The calibration allows an improvement in terms of sum of squared difference and, even if the MLE, moments and SC methods are able to show equally good performances, the best method is obtained using a certain Q% removal. The results can be analytically observed in the table present at the end of this section (III.7) and the different performances will be underlined by the SSD values listed. The different performances in terms of SSD of different calibrations is only qualitative, but not really remarkable, the SC method is able to give a better fitting than every other method except best Q% removal one. Every calibration method gives, more or less, very similar results in terms of visual fitting and sum of squared difference for many basins.

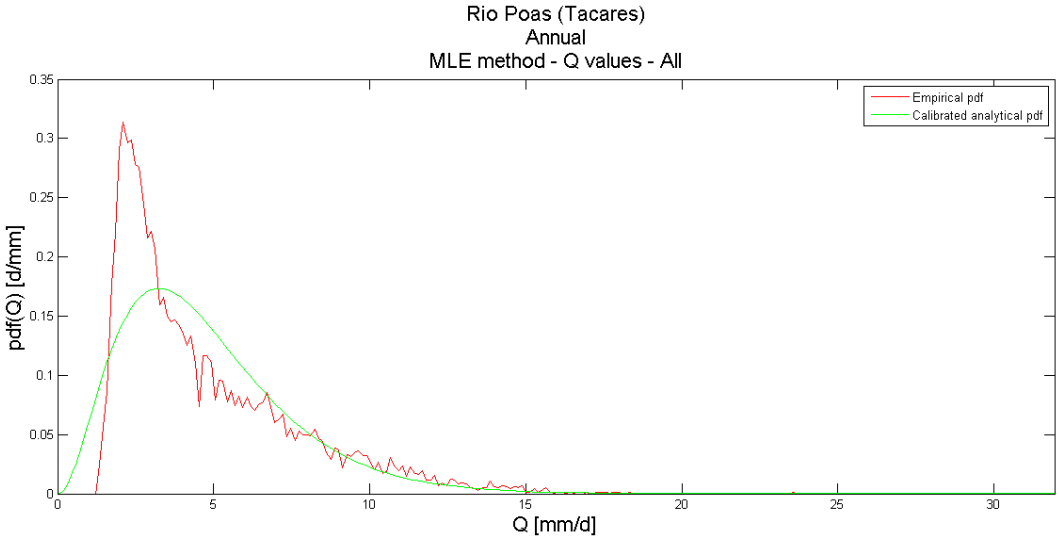

Figure III.14 –Rio Poas, calibrated pdf according to MLE method.

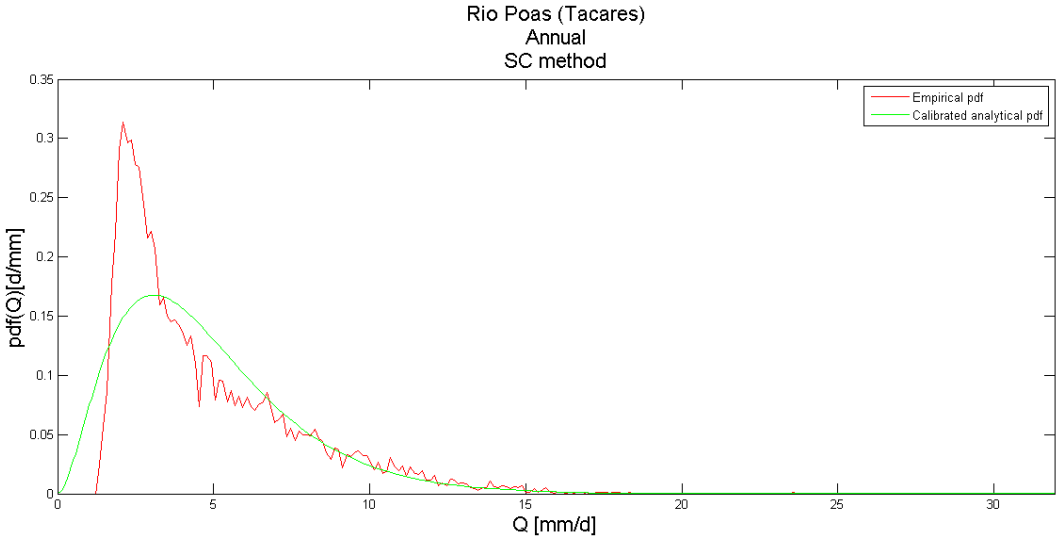

Figure III.15 –Rio Poas, calibrated pdf according to SC method.

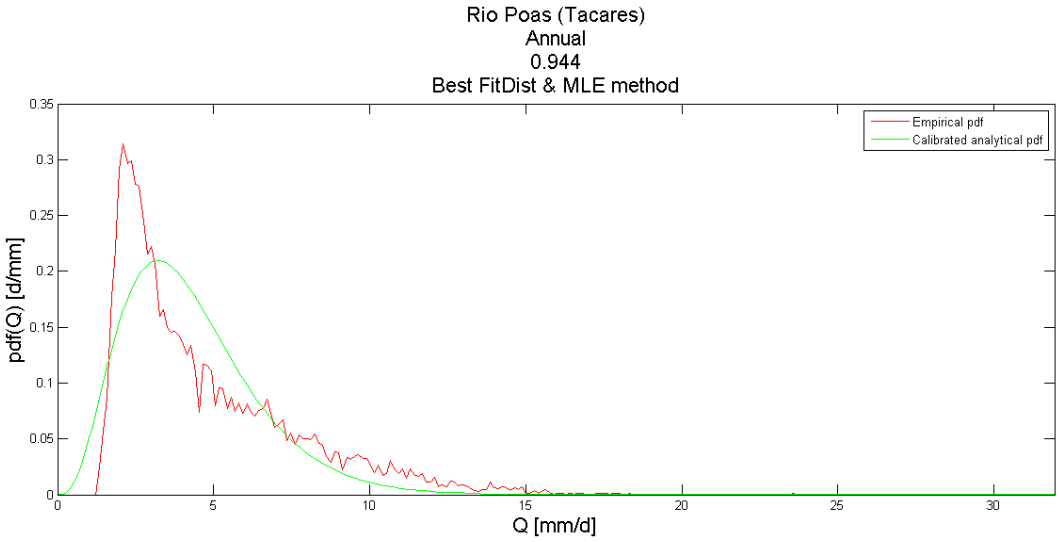

Figure III.16 –Rio Poas, calibrated pdf according to best Q% removal method.

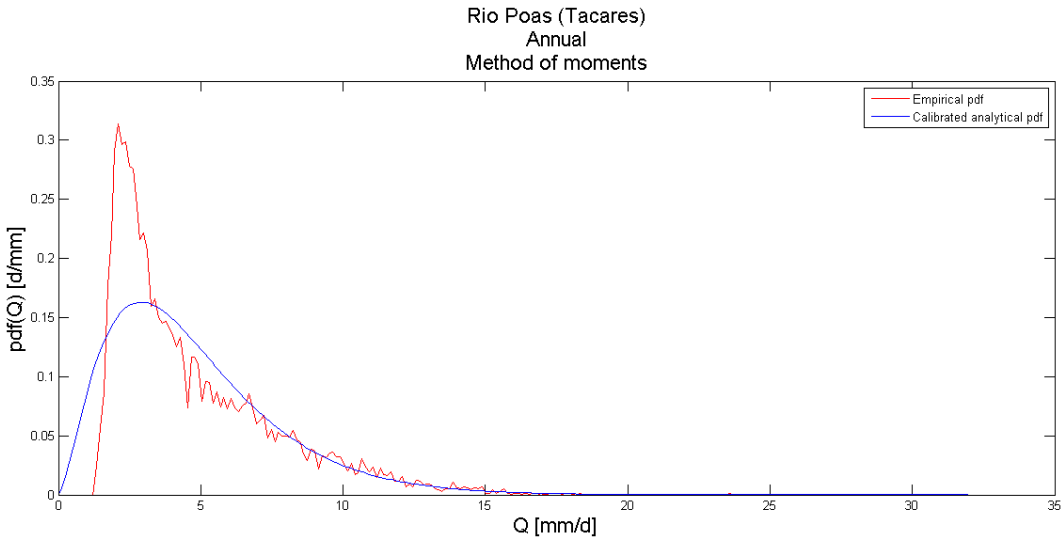

Figure III.17 –Rio Poas, calibrated pdf according to method of moments.

MLE		**SC**		**Best Q% removal**				**Method of moments**	
$\Delta_1 = \Delta_2$	SSD	$\Delta_1 = \Delta_2$	SSD	%Q used	Δ_1	Δ_2	SSD	$\Delta_1 = \Delta_2$	SSD
1.4419	0.20302	1.5999	0.1976	**94.4%**	**1.1319**	**1.01927**	**0.1906**	1.7748	0.2008

Table III.7 – Rio Poas. Annual pdf after calibration results

3.2.4 – Rio Naranjo

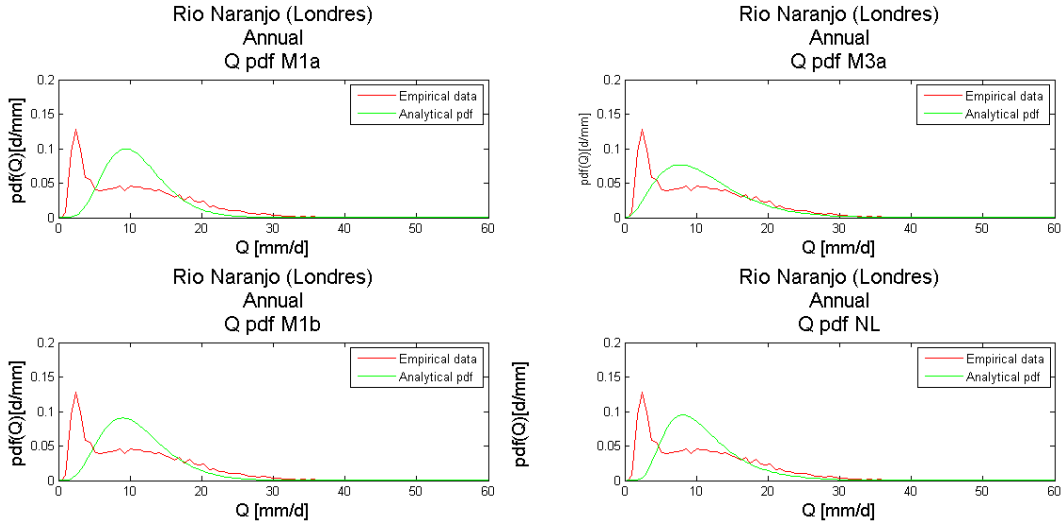

Figure III.18 –Rio Naranjo, Annual pdf with different regression methods.

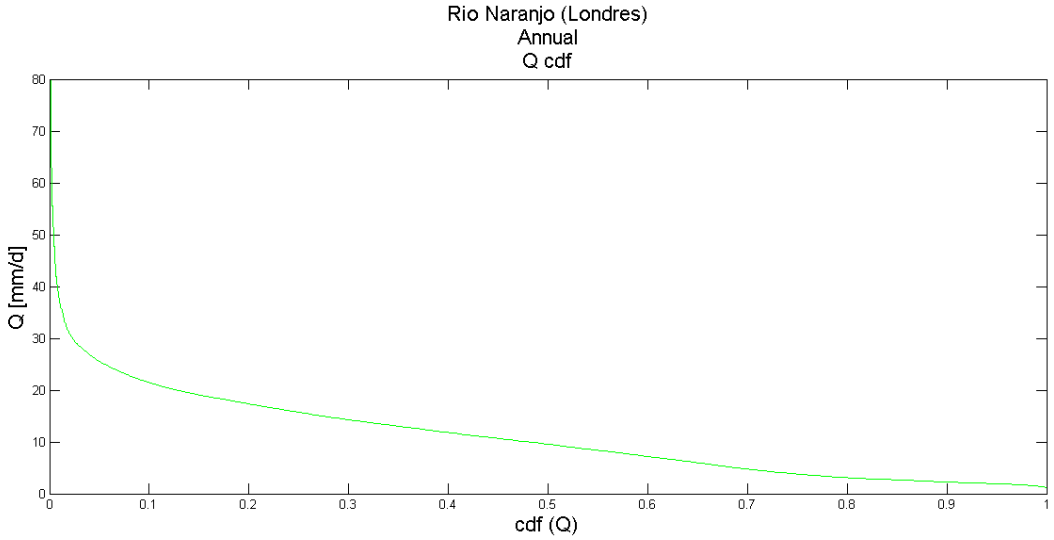

Figure III.19 –Rio Naranjo, flow duration curve.

$<Q>$ [mm/d]	11.021	M1a SSD performance	0.6122
Var [mm^2/d^2]	82.0393	M1b SSD performance	0.0513
CV_Q [-]	0.8218	M3a SSD performance	**0.0337**
Best recession method	M3a	NL SSD performance	0.0543
α [mm]	32.0246	Q min [mm/d]	1.18
λ [1/d]	0.3441	Q max [mm/d]	172.41
k (M3a)	0.1015	Q dataset length	11322

Table III.8 – Rio Naranjo. Annual pdf pre-calibration results

The calibrated model will be displayed in the next four plots (figure III.20-22). It's possible to remark a similar behavior of the pdf obtained with MLE, and moments methods, the SC one, on the contrary, is able to represent better the position of the peak of the bell and the curve evolution allows a sum of squared difference slightly inferior than one obtained with the other methods.

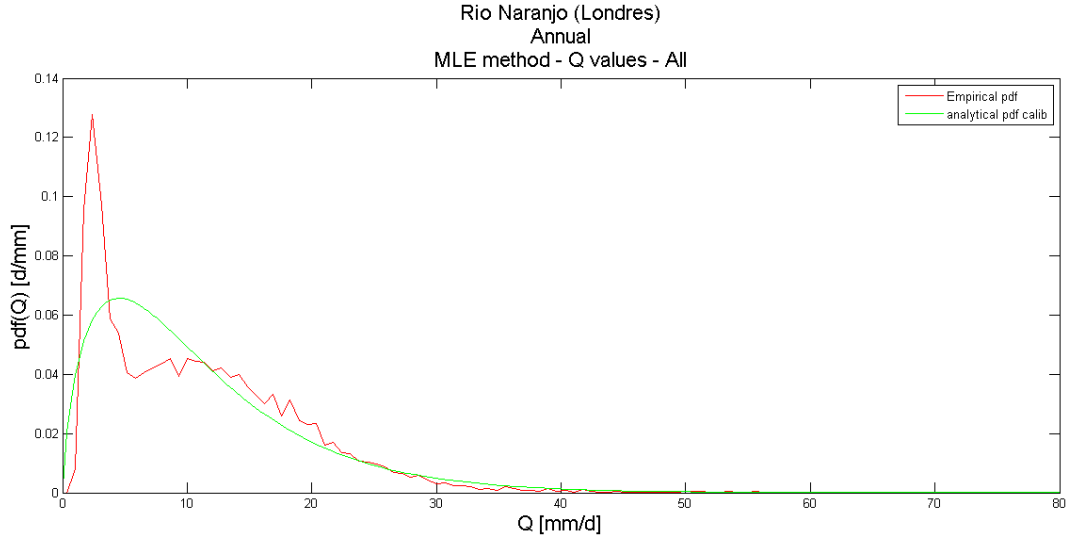

Figure III.20 –Rio Naranjo, calibrated pdf according to MLE method.

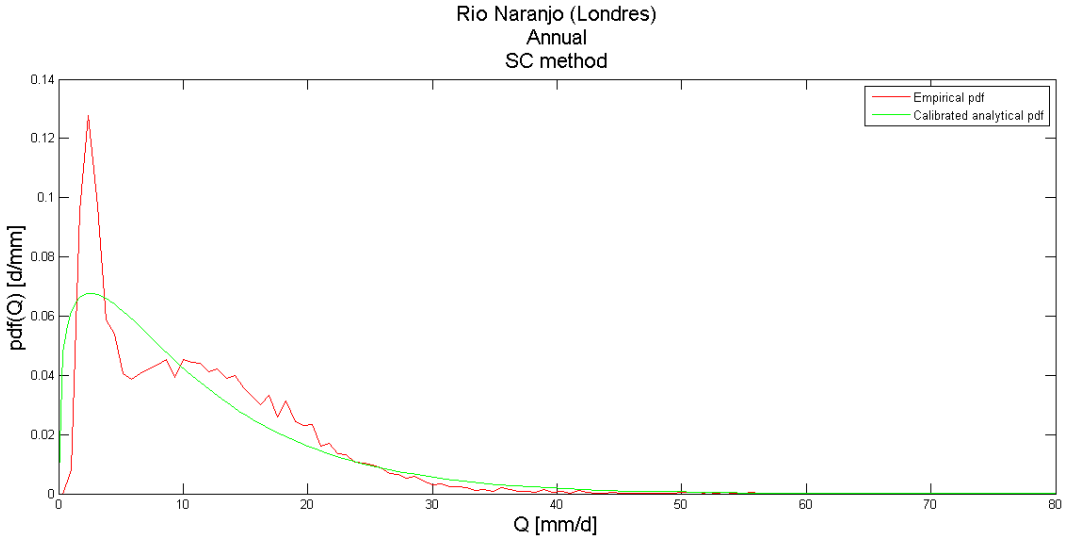

Figure III.21 –Rio Naranjo, calibrated pdf according to SC method.

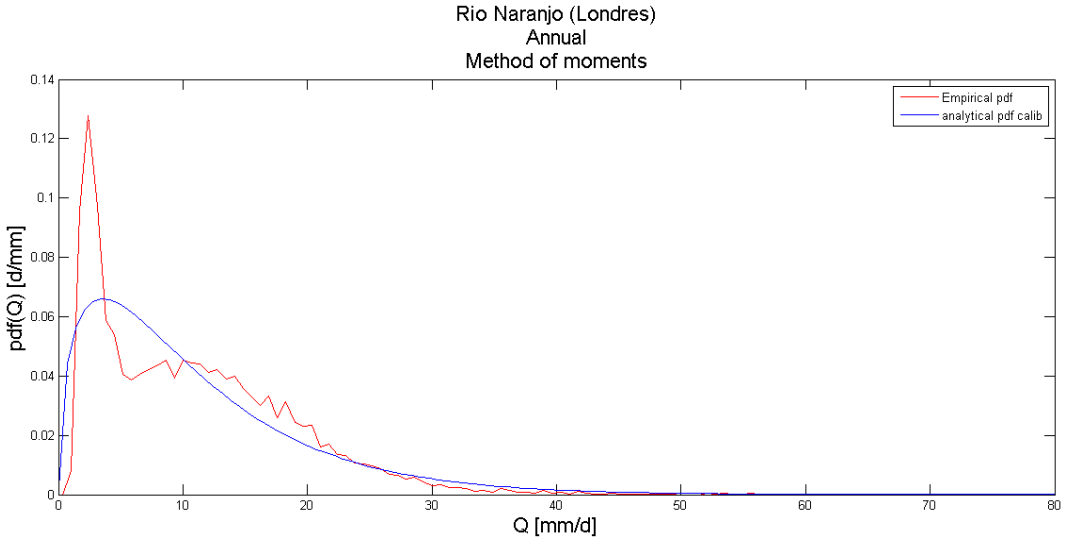

Figure III.22 –Rio Naranjo, calibrated pdf according to method of moments.

A summary of the properties of the calibration methods used for the annual fitting of Rio Naranjo is displayed in the following table III.9.

MLE		**SC**		**Best Q% removal**				**Method of moments**	
$\Delta_1 = \Delta_2$	SSD	$\Delta_1 = \Delta_2$	SSD	%Q used	Δ_1	Δ_2	SSD	$\Delta_1 = \Delta_2$	SSD
1.9859	0.0128	**2.59990**	**0.0105**	100%	1.9859	1.9859	0.0128	2.2883	0.0111

Table III.9 – Rio Naranjo. Annual pdf after calibration results

Best Q% removal gives, as result, a percentage of streamflow data used equal to 100%. Therefore the results are identical to the MLE method. The SC method shows a slight increase in term of performances, passing from 0.0337 to 0.0105 as sum of squared difference between calibrated pdf and empirical one deduced directly by the dataset.

3.2.5 – Rio Grande de Terraba

This river is located in the *Meridian Valley* area, in the South Pacific and it borders to Panama. It is located in an inter-mountainous valley between two sections of the *Cordillera*. Two major watersheds of opposite character (Rio General and Rio Coto Brus) confluence in this river which breaks through the small *Fila Brunqueña* to flow into the Pacific Ocean.

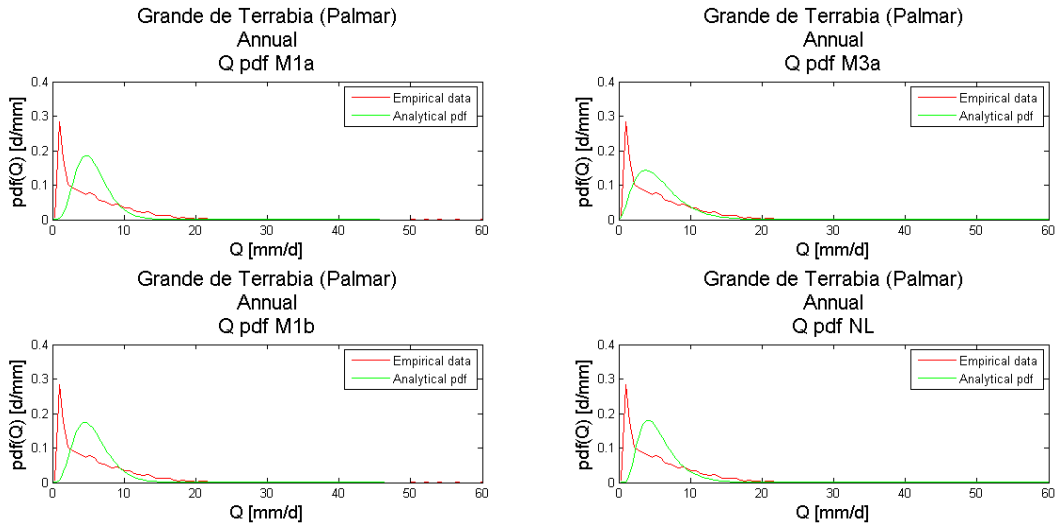

Figure III.23 –Rio Grande de Terraba, Annual pdf with different regression methods.

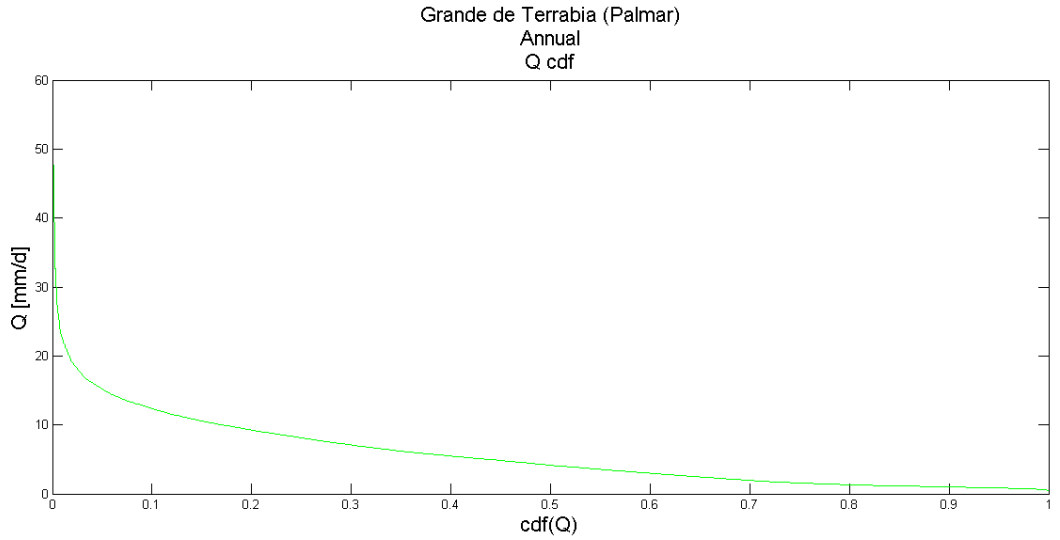

Figure III.24 –Rio Grande de Terraba, flow duration curve.

The theoretical uncalibrated model was applied using three different linear methods to study the recessions and the non-linear method (results plotted in Figure III.23). Even if the entire range is pretty wide (from 0.4 to 154 mm/d) the plots show the pdf using a shorter scale (up to 60 mm/d), in order to appreciate better the shape of the pdf. The empirical pdf shows a high peak and a sudden decrease of the slope, a clue that suggest a further necessary seasonality characterization and study.

The performances of the methods used to study the recession, the parameters value and indications about streamflow data and moments of the distribution are listed in the following table III.10:

$<Q>$ [mm/d]	5.6553	M1a SSD performance	0.17617
Var [mm^2/d^2]	30.7964	M1b SSD performance	0.16018
CV_Q [-]	0.9813	M3a SSD performance	**0.10605**
Best recession method	M3a	NL SSD performance	0.16081
α [mm]	15.0519	Q min [mm/d]	0.4
λ [1/d]	0.37571	Q max [mm/d]	154.27
k (M3a)	0.12670	Q dataset length	11322

Table III.10 – Rio Grande de Terraba. Annual pdf pre-calibration results

The calibration was performed and the best-fitting analytical pdf was modified in order to deduce the best gamma distribution and its relative parameters. In the following plots (figure III.25-27) the calibrated pdfs will be displayed. The best Q% removal calibration method, using as best percentage of discharge dataset the entire interval of values, gives the same result obtained by the MLE method and it is not shown. The method of moments is able to give a good fitting (figure III.27) and its relative SSD is close to that of the SC method. even if no method is able to reproduce accurately the peak of the pdf.

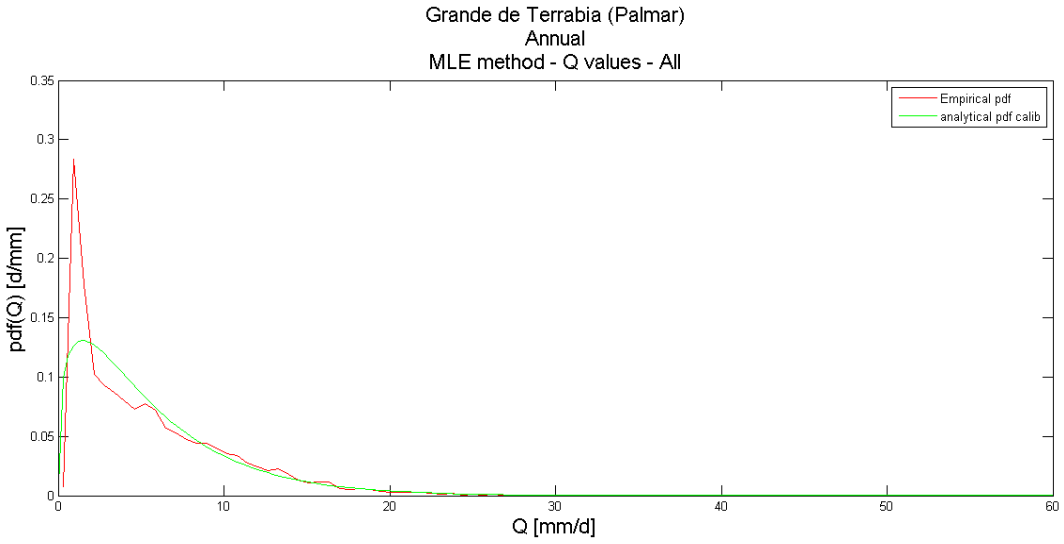

Figure III.25 –Rio Grande de Terraba, calibrated pdf according to MLE method.

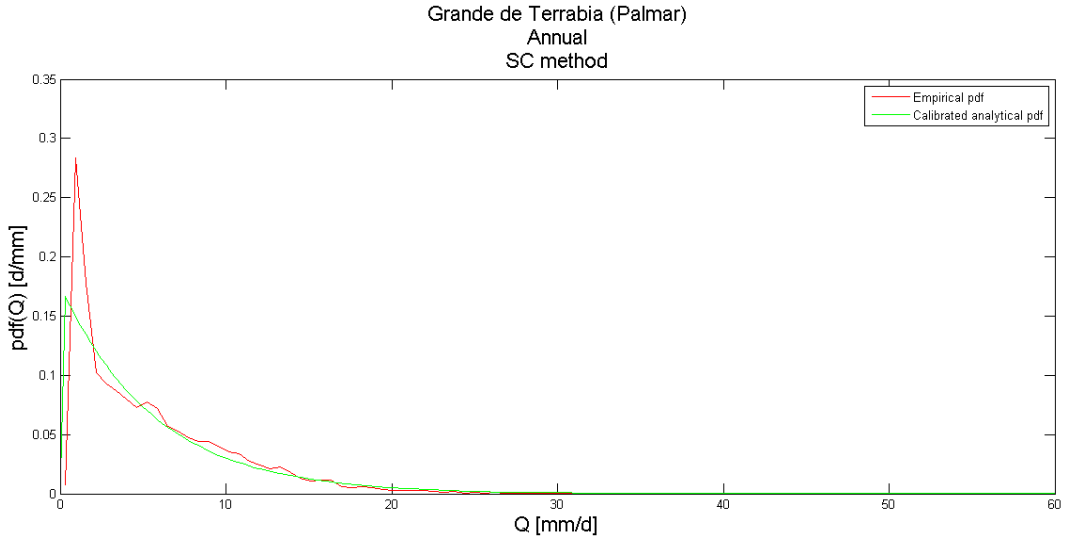

Figure III.26 –Rio Grande de Terraba, calibrated pdf according to SC method.

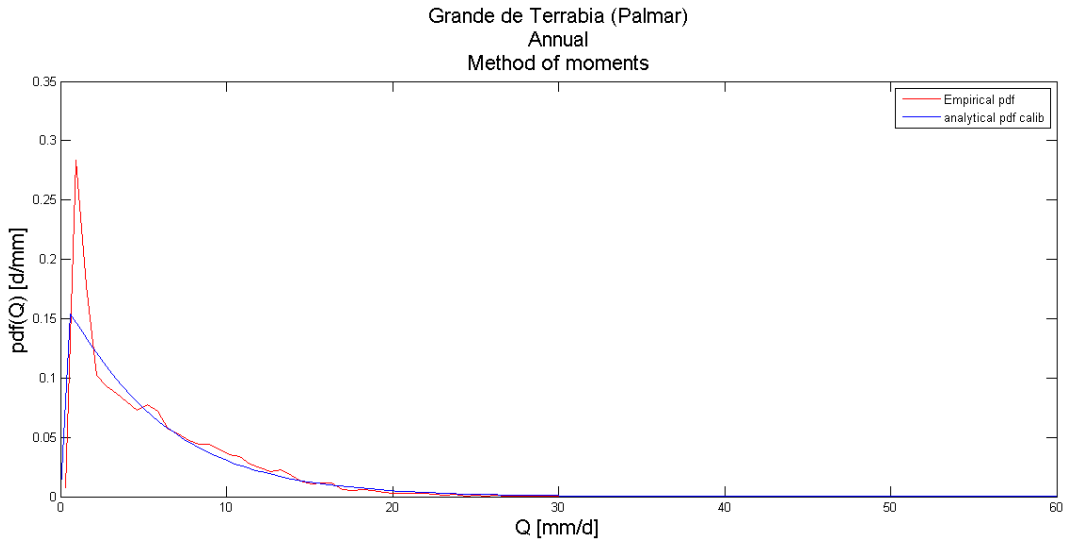

Figure III.27 –Rio Grande de Terraba, calibrated pdf according to method of moments.

A summary of the properties of the calibration methods used for the annual fitting of Rio Grande de Terraba can be observed in the following table in which SSD obtained with different methods are displayed.

MLE		**SC**		**Best Q% removal**				**Method of moments**	
$\Delta_1 = \Delta_2$	SSD	$\Delta_1 = \Delta_2$	SSD	%Q used	Δ_1	Δ_2	SSD	$\Delta_1 = \Delta_2$	SSD
2.19129	0.0340	**2.9599**	**0.0188**	100	2.19129	2.19129	0.0340	2.8553	0.0202

Table III.11 – Rio Grande de Terraba. Annual pdf after calibration results

3.2.6 – Rio Pejibaye

Being on the Caribbean side, Rio Pejibaye has a precipitation pattern (and a related streamflow annual trend) showing a continuous form with a weak distinction between dry and wet season. The annual pdf of the analytical model was derived using the same linear and non-linear methods used before and the plots in the following figure (III.28) will display the graphical results obtained.

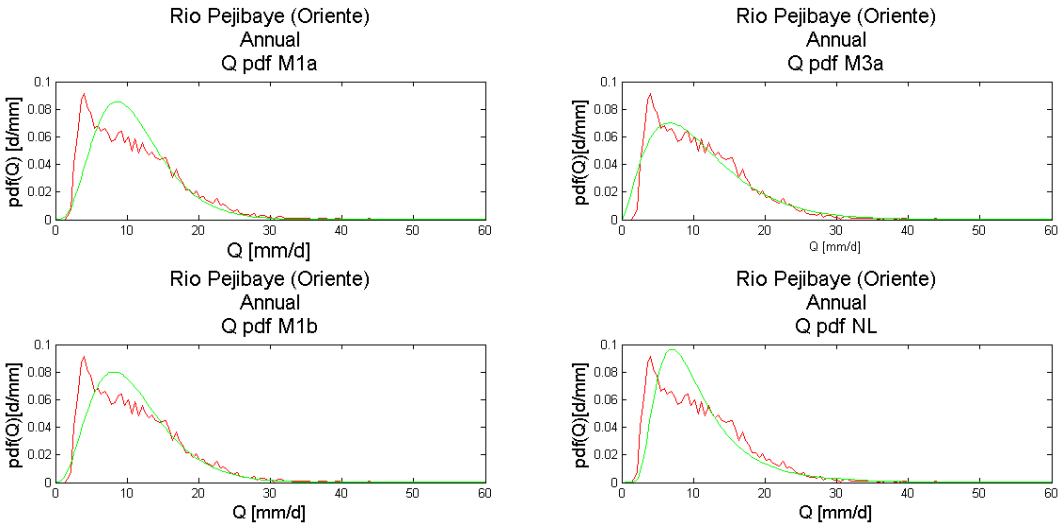

Figure III.28 –Rio Pejibaye, Annual pdf with different regression methods.

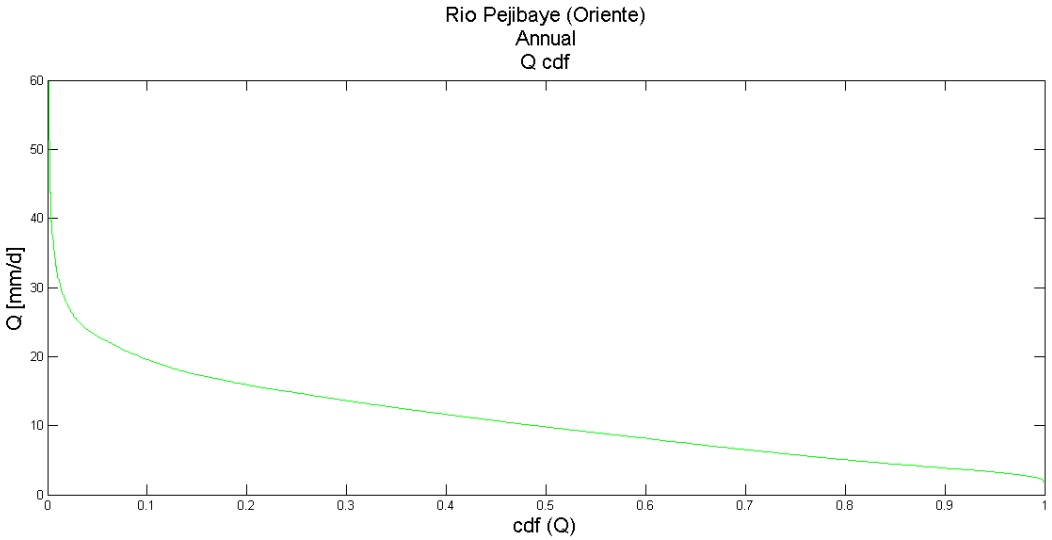

Figure III.29 –Rio Pejibaye, flow duration curve.

The performance of the different models are presented in table III.6. The most performing model pdf is, again, the one obtained using the *k* estimated from the linear recession method M3 (SSD 0.00524). Observing the shape of the empirical pdf deduced

directly from data it's possible to note a variation of the steepness in the descending part of the bell, a clue of the double-bell shape pdf.

$<Q>$ [mm/d]	11.0434	M1a SSD performance	0.01900
Var [mm^2/d^2]	47.8194	M1b SSD performance	0.01283
CV_Q [-]	0.6262	M3a SSD performance	**0.00524**
Best recession method	M3a	NL SSD performance	0.02021
α [mm]	29.9311	Q min [mm/d]	1.72
λ [1/d]	0.36896	Q max [mm/d]	118.47
k (M3a)	0.14663	Q dataset length	11322

Table III.12 – Rio Pejibaye. Annual pdf pre-calibration results

The model was then calibrated and the results are plotted and displayed in the next figures (III.30-32).

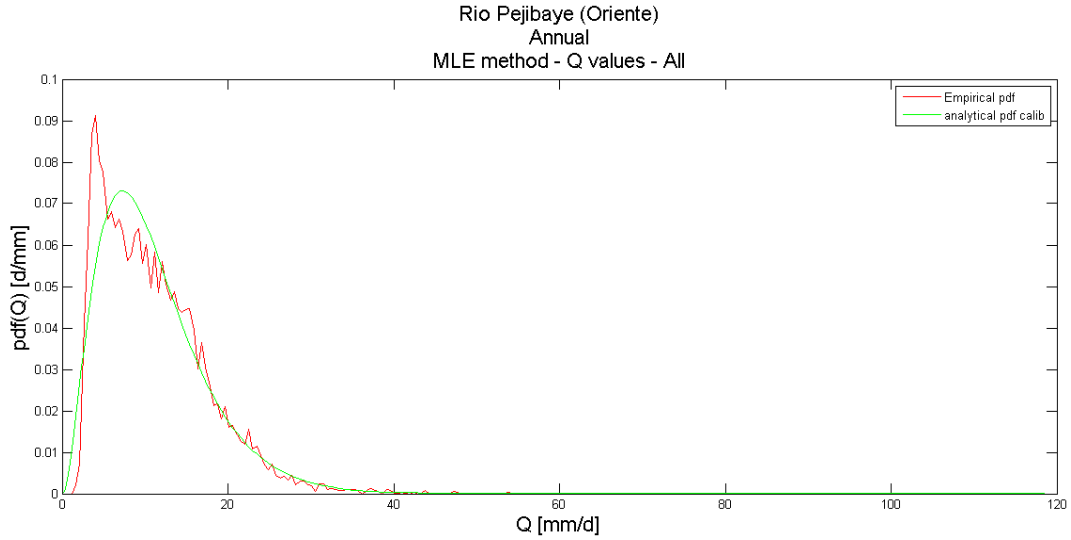

Figure III.30–Rio Pejibaye, calibrated pdf according to MLE method.

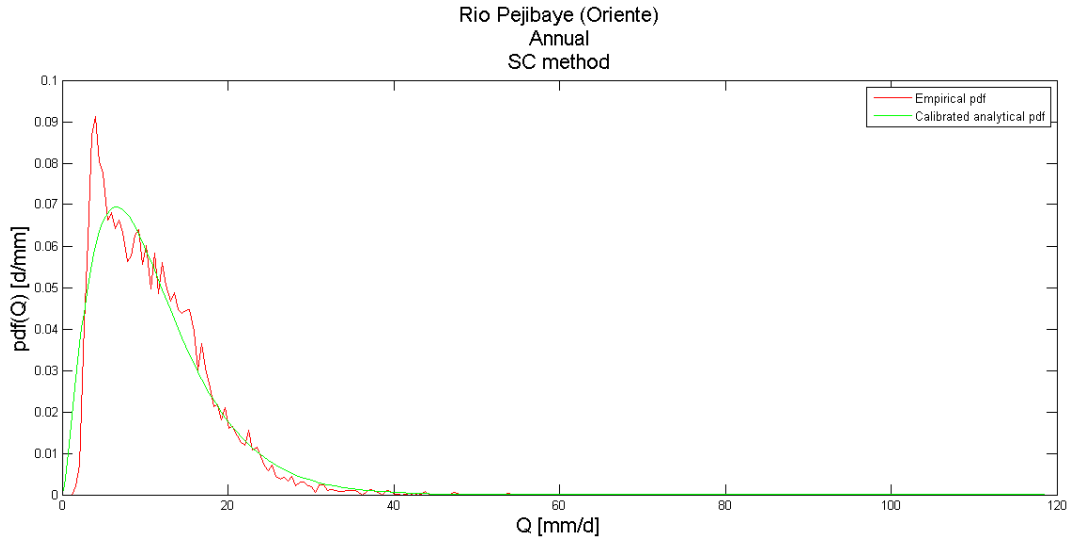

Figure III.31–Rio Pejibaye, calibrated pdf according to SC method.

As often happen when the calibration is applied on an annual-estimated pdf, the Best Q% removal method gives the entire list of the streamflow dataset to get the best evaluation. On the other hand the capacity of this method to improve the performances respect the initial uncalibrated model will be more clear when the seasonal study will be carried out and the final table in section 3.1.7 will display this property as well.

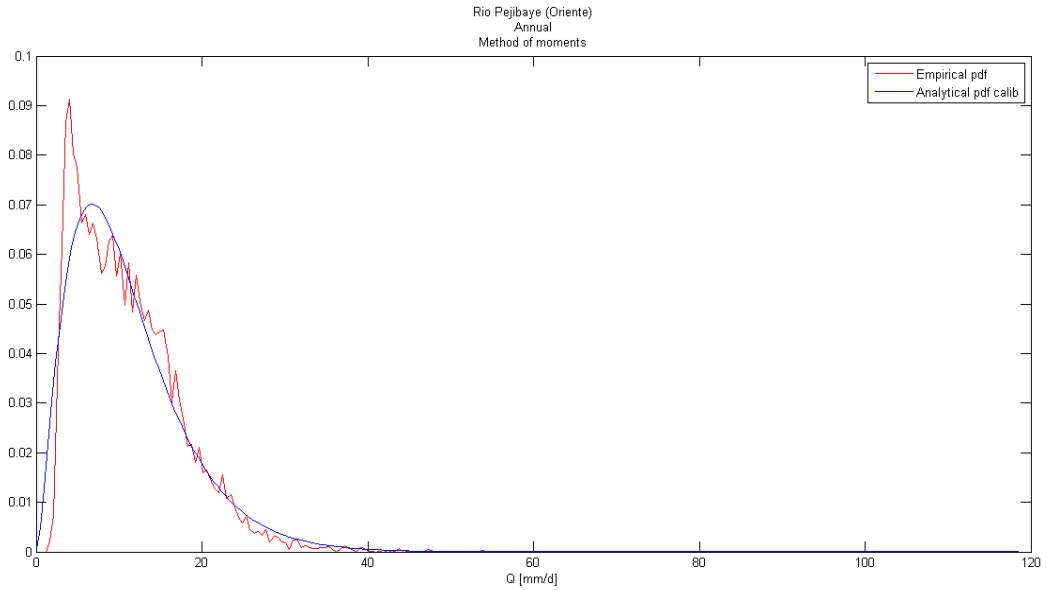

Figure III.32–Rio Pejibaye, calibrated pdf according to method of moments

The performances and a quick summary of the calibration methods and different performances obtained are collected in the table III.13. The SC, MLE and moments methods are pretty similar, giving a final value of SSD pretty equal to the initial one. It is possible to say, in this case, that the calibration didn't improve remarkably the performance of the model, being the initial theoretical pdf already

MLE		**SC**		**Best Q% removal**				**Method of moments**	
$\Delta_1 = \Delta_2$	SSD	$\Delta_1 = \Delta_2$	SSD	%Q used	Δ_1	Δ_2	SSD	$\Delta_1 = \Delta_2$	SSD
0.8587	0.0064	**1.0281**	**0.0052**	100%	0.8587	0.8587	0.0064	0.98659	0.0053

Table III.13 – Rio Pejibaye. Annual pdf after calibration results

3.2.7 – Summary table

In the table III.14 all the properties deduced by the analytical study of the annual streamflow pdf in the 6 basins will be shown. The table will illustrate the SSD (considered as a performance index) of the theoretical model according to different regression methods, and the moments of the observed distribution. The correction parameters (Δ_1 and Δ_2) as well as the relative SSD for different calibration techniques will allow the reader to appreciate the cases where the calibration increases the performance of the model.

River	Dataset information			Before calibration			After Calibration										Best calibration	Performance increasing (%)	$(k/\lambda)^{1/2}$ calibrated model	
							MLE		*SC*		*Best Q% removal*				*Method of moments*				*SC*	*Q%*
	Mean [mm/d]	*Variance [mm^2/d^2]*	CV_Q	Best recession method	SSD	$(k/\lambda)^{1/2}$ theoretical model	Δ	SSD	Δ	SSD	%Q Used	Δ_1	Δ_2	SSD	Δ_1	SSD				
Rio Frio (Guatuso)	10.16	89.727	0.93	M3a	0.0096	0.6986	1.09	0.0088	1.17	**0.0087**	99.4	0.99	0.95	0.0087	3.39	0.0148	SC	9.89	0.7585	0.6974
Rio San Carlos (Terron Colorado)	6.52	21.875	0.71	M3a	0.0146	0.6161	0.98	0.0149	1.10	**0.0138**	100	0.98	0.98	0.0149	1.77	0.0171	SC	5.35	0.6481	0.6101
Rio Sarapiqui (Cariblanco)	10.23	66.773	0.79	M3a	0.0076	0.5854	1.46	0.0078	1.00	0.0076	97.6	0.76	0.69	**0.0045**	4.08	0.0245	BestQ	40.39	0.5854	0.5111
Rio Tempisque (Guardia)	2.25	17.190	1.83	M3a	0.3678	0.6463	1.96	0.1962	2.07	0.1954	94.2	0.91	0.61	**0.09801**	2.28	inf	BestQ	73.35	0.9301	0.6172
Rio Tenorio (Rancho Rey)	2.50	5.695	0.95	M3a	0.2657	0.6596	0.9	0.2483	1.00	0.2658	93.8	0.47	0.38	**0.1250**	3.31	0.687	BestQ	52.96	0.6595	0.4536
Rio Barranca (Guapinol)	4.31	29.436	1.25	M3a	0.0928	0.6817	1.68	0.0462	2.15	**0.0355**	100	1.68	1.68	0.0462	2.85	inf	SC	61.73	0.9999	0.8845
Rio Poas (Tacares)	4.76	8.863	0.62	M3a	0.2921	0.4693	1.44	0.2030	1.59	0.1976	94.4	1.13	1.02	**0.1906**	2.89	0.2008	BestQ	34.73	0.5937	0.4994
Rio G.Candelaria (El Rey)	4.08	29.173	1.32	M3a	0.1995	0.6543	2.24	0.0669	2.33	**0.0634**	100	2.24	2.24	0.0669	1.22	inf	SC	68.18	0.9999	0.9796
Rio Naranjo (Londres)	11.02	82.039	0.82	M3a	0.0337	0.5432	1.98	0.0128	2.59	**0.0105**	100	1.98	1.98	0.0128	0.98	0.0111	SC	68.83	0.8760	0.7656
Rio Savegre (Providencia)	4.70	19.346	0.93	M3a	0.3125	0.5129	2.29	0.1282	2.39	0.1277	92.4	1.63	1.30	**0.1117**	1.33	0.1568	BestQ	64.25	0.7933	0.6567
G. de Terraba (Palmar)	5.65	30.796	0.98	M3a	0.1060	0.5807	2.19	0.0340	2.95	**0.0188**	100	2.19	2.19	0.0340	3.15	0.0202	SC	82.19	0.9990	0.8596
Rio Coto Brus (Caracucho)	5.52	25.974	0.92	M3a	0.1242	0.5418	2.14	0.0415	2.80	**0.0362**	100	2.14	2.14	0.0415	3.24	0.0365	SC	70.83	0.9066	0.7938
Rio Reventazon (Palomo)	8.34	33.781	0.69	M3a	0.0130	0.6294	0.98	0.0132	1.11	**0.0121**	100	0.98	0.98	0.0132	1.42	0.0128	SC	6.48	0.6644	0.6250
Rio Pejibaye (Oriente)	11.04	47.819	0.62	M3a	0.0052	0.6304	0.85	0.0064	1.02	**0.0052**	100	0.85	0.85	0.0064	3.39	0.0053	SC	0.56	0.6392	0.5841
Rio Pacuare (Dos Montanas)	7.04	27.449	0.74	M3a	0.0070	0.6438	0.9	0.0075	1.00	**0.0070**	100	0.9	0.9	0.0075	1.77	0.0134	SC	0.00	0.6439	0.6122
Rio Banano (Asunciòn)	13.51	199.99	1.04	M1b	0.0043	0.5887	1.28	0.0039	1.21	0.0039	94.8	0.71	0.58	**0.0019**	4.08	inf	BestQ	56.02	0.6493	0.4981
Rio Estrella (Pandora)	6.24	85.966	1.48	M3a	0.0152	0.8249	0.95	0.0155	1.07	0.0151	96.4	0.57	0.46	**0.0114**	2.28	inf	BestQ	25.18	0.8546	0.6273
Rio Telire (Bratsi)	6.38	19.163	0.68	M3a	0.0098	0.5749	0.91	0.0099	1.00	**0.0098**	99.8	0.84	0.83	0.0098	3.31	0.0192	SC	0.00	0.5749	0.5286

Table III.14 – Initial dataset information, best recession and its corresponding SSD value before calibration, correction parameters and SSD values obtained after calibration.

3.2.8 – Streamflow regime characterization

Here some considerations about the theoretical model and the calibration methods applied to the annual characterization of the analyzed catchments are listed.

- The best recession method for the estimation of the hydrograph recession rate, *k*, is given using the linear M3a method;
- The theoretical model pdfs, even if able to give a good visual fitting with the empirical pdf, are not always able to give a corresponding coefficient of variation (deduced by the square root of the ratio k/λ, see section 1.2) with the same, or similar, value of the empirical streamflow dataset. The classification of the streamflow regime is therefore not univocally defined;
- The best pdf obtained after the calibration is given most of the time using the SC method;
- The performance increment from the theoretical model to the calibrated one, deduced on the base of the sum of squared difference, is a questionable factor. For Rio Sarapiqui, for instance, the theoretical model is already able to give a good fitting with a SSD equal to 0.0076 and, after the calibration with the best Q% removal, the SSD drops down to 0.0045. The calibration, in a strictly analytical way, gives an increase of the performances equal to 40%. However this number has not a real meaning, being the initial SSD value of the theoretical model already small;
- The *inf* value expressed in some results of the method of moments is a consequence of the shape of the analytical deduced pdf. The SSD evaluation is expressed by the equation I.19 and the first interval of the analytical pdf comprehends the value $Q=0$ mm/d. If the shape of the gamma function presents a positive asymptote in correspondence of $Q=0$ value it means that the first subtraction of the summation will give an infinite number and, therefore, the final value of the SSD will be an infinite number as well. This result is a nice clue to recognize which streamflow presents an *erratic* behavior being the monotonically-decreasing shape of a gamma function the typical pdf shape for streamflow with *erratic* regime [Botter et al; 2013]
- After the calibration there's a better correspondence between the empirical coefficient of variation and the square root of the ratio k/λ obtained by the model, but the equation that define the perfect theoretical correspondence between the model and the dataset is not satisfied. The equation that rules the perfect streamflow regime classification reads:

$$CV_Q = \sqrt{\frac{k}{\lambda}} \qquad \text{(I. 17)}$$

Therefore, to obtain a perfect regime characterization this equation should be always verified and the CV_Q obtained from experimental dataset would be exactly equal on the right-side term, where k and λ are obtained through an analysis on daily discharge data and daily rainfall intensity data, as expressed in section 1.3. Having a perfect theoretical-empirical link, the couples (CV_Q, $(k/\lambda)^{1/2}$) obtained for every application of the model on the studied catchment, should lay on the bisector line of a CV_Q Vs $(k/\lambda)^{1/2}$ plot.

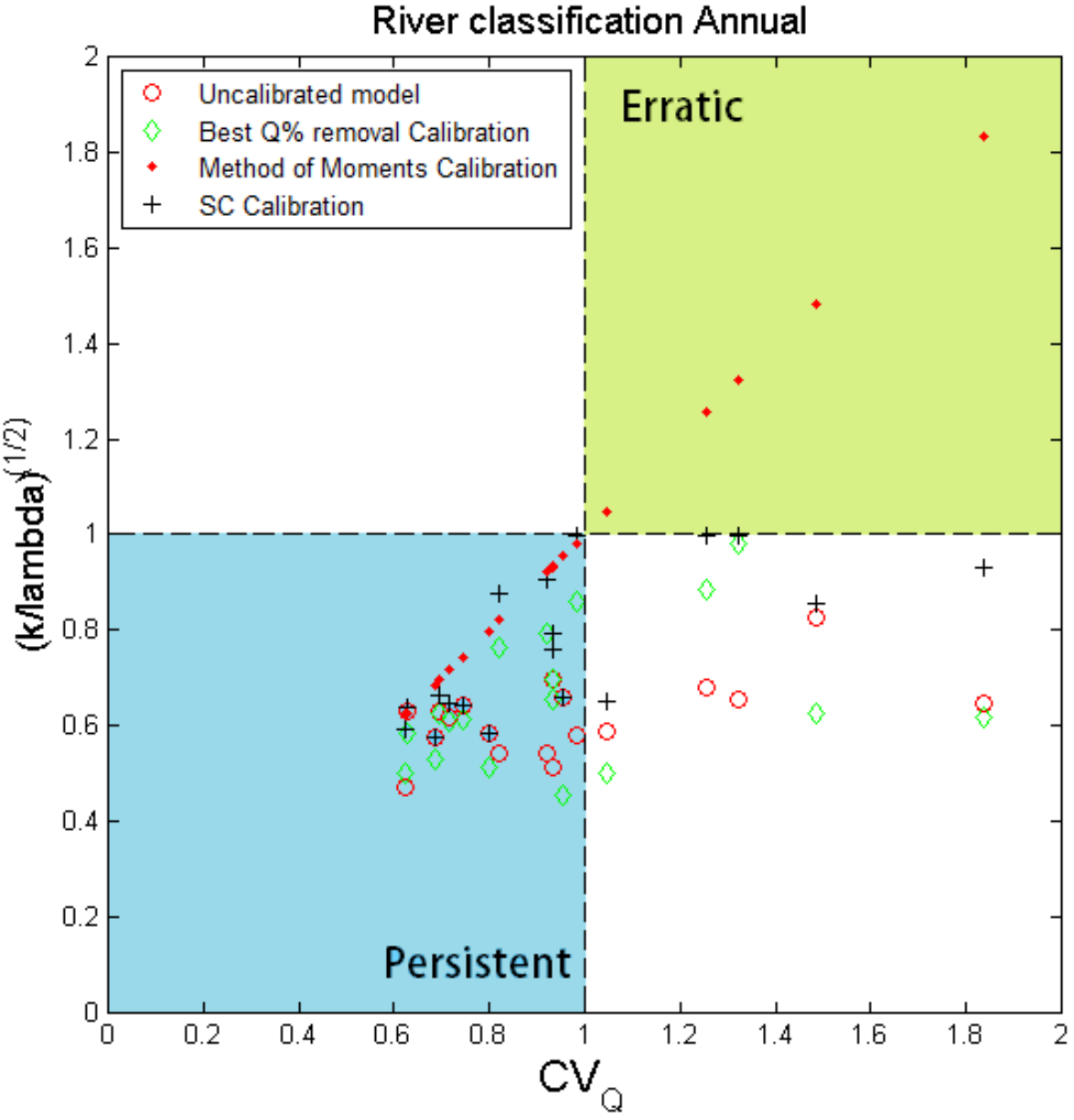

Figure III.33 – Annual streamflow characterization through CV_Q *Vs* $(k/\lambda)^{1/2}$ plots for non-calibrated model and for different calibration options.

Let's remember that:

- *Persistent regime*. Obtained when then mean frequency of effective rainfall is higher than the flow decay rate ($\lambda/k > 1$). Discharge pulses triggered by a certain rainfall event are relatively frequent. The mean interarrival time is smaller than the mean duration of the flow pulse. In stochastic terms the discharge data are less distributed around the mean (relatively low variance if compared to the mean), $CV_Q < 1$, coherently to what is expressed by equation I.17.
- *Erratic Regime.* Obtained when the mean frequency of effective rainfall is smaller than the flow decay rate ($\lambda/k < 1$). The precipitation events have a main interarrival long enough to allow the streamflow to dry between one event and the successive. In stochastic terms the range of observed values of q is wide around the mean, the variance is relatively high compared to the mean and the $CV_Q > 1$, coherently to what is defined to equation I.17.

Therefore, the more a certain catchment is able to show a good correspondence between CV_Q and $(k/\lambda)^{1/2}$ the more the resulting point will be near the bisector line of a CV_Q Vs $(k/\lambda)^{1/2}$ plot. In the figure III.33 the square root of the ratio between the mean frequency of flow-producing rainfall events and the inverse of mean response time have been plotted with the observed CV_Q in order to evaluate the accuracy of the analytical prediction on the streamflow regime according to the uncalibrated and calibrated model for the 18 catchments.

The best Q% fitting method even if it is able to give good calibrated pdf and to return nice performances in terms of SSD it is the worst one in terms of streamflow regime characterization. The way this method is defined, discarding a certain percentage of streamflow data, allows the analytical curve to fit better the bell-shape of the observed pdf, but doesn't allow the model to take in account all the streamflow events, overestimating therefore the shape parameter of the pdf. The method of moments, on the other hand, even if it never shows the best SSD among the other methods, it perfectly fits the empirical CV_Q of the observed streamflow data by definition. The results are displayed in the figure III.33 and all the points (representing a basin) are lined on the bisector: the method of moments totally satisfies equation I.17 .

3.3 – Characterization of the streamflow during dry season

In this chapter the same catchments analyzed in section 3.2 will be studied in order to show how the subdivision into two seasons (dry and wet) can improve the initial fitting of the analytical pdf. At the end, a streamflow regime characterization will be discussed in order to appreciate both in a visual and in analytical way the differences and the performances of the methods and which river displays an *erratic* or a *persistent* regime.

As was shown in the precedent section, many plots concerning the observed and calibrated pdf according to SC, MLE and best Q% removal methods show a similar trend. In order to not fill this work with many useless plots in the following sections only few, but more explicative, plots will be displayed:

- Uncalibrated model using four different regression fitting methods, as used before;
- The best-fitting calibrated model, specifying, time after time, the analytical difference with other methods using a table;
- The methods of moments calibrated model. This method is able to return a perfect streamflow regime characterization, it's therefore interesting to observe which kind of analytical pdf gives as result

The wet season characterization will be studied in the section 3.4.

3.3.1 – Rio San Carlos

The theoretical model has been evaluated according to the M1a, M1b, M3a and Non-linear regression method. The analytical pdf are plotted in the following figure III.34:

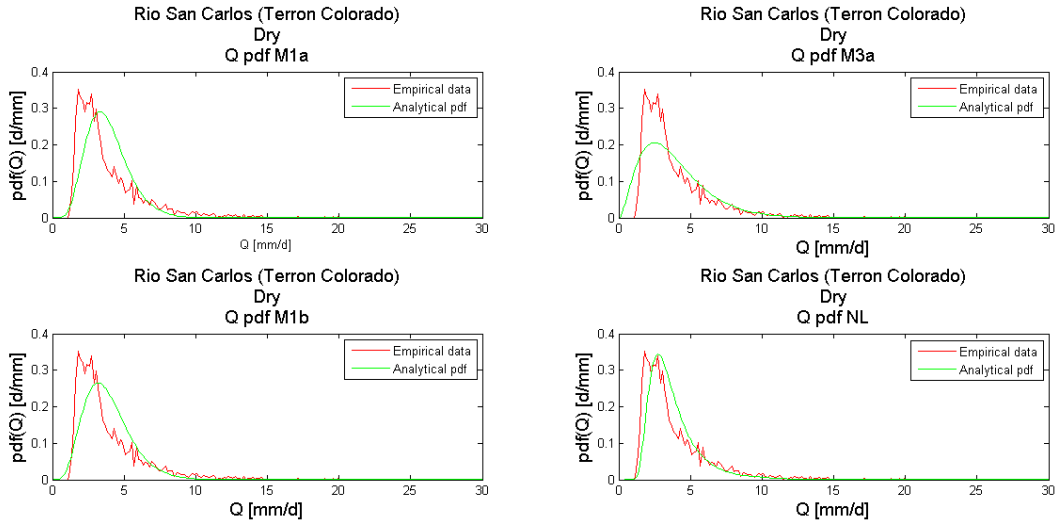

Figure III.34 –Rio San Carlos, Dry Season pdf with different regression methods.

The best-fitting calibrated model can be obtained with the best Q% removal method which is able to return a good-fitting pdf discarding 7.8% of the dataset. The properties of the dataset used and the theoretical model results are listed in table III.15.

It's interesting to spot how the linear M3a method is still the best according to the performance evaluation defined by the SSD. The non-linear one, even if it's able to represent better the bell-shape of the pdf, is not able to perfectly fit the dataset being the curve shifted on the right. This small difference gives, as consequence, a SSD slightly major of the one deduced by M3a method.

$<q>$ [mm/d]	3.867	M1a SSD performance	0.3867
Var [mm^2/d^2]	6.502	M1b SSD performance	0.2840
CV_Q [-]	0.659	M3a SSD performance	**0.2060**
Best recession method	M3a	NL SSD performance	0.2411
α [mm]	12.004	q min [mm/d]	1.16
λ [1/d]	0.322	q max [mm/d]	39.07
k (M3a)	0.1148	q dataset length	4657

Table III.15 – Rio San Carlos. Pdf pre-calibration results for dry season

The seasonality characterization gives, as consequence, different interval in terms of data analyzed, as it's possible to understand comparing the first table in section 3.1.1 and the one showed in this paragraph. The range of possible streamflow value will be different, and shorter, as well.

The best calibration methods resulted to be the Best Q% removal with a percentage of streamflow dataset used equal to 92.2%. The increase of performance can be evaluated graphically in the following figure III.35

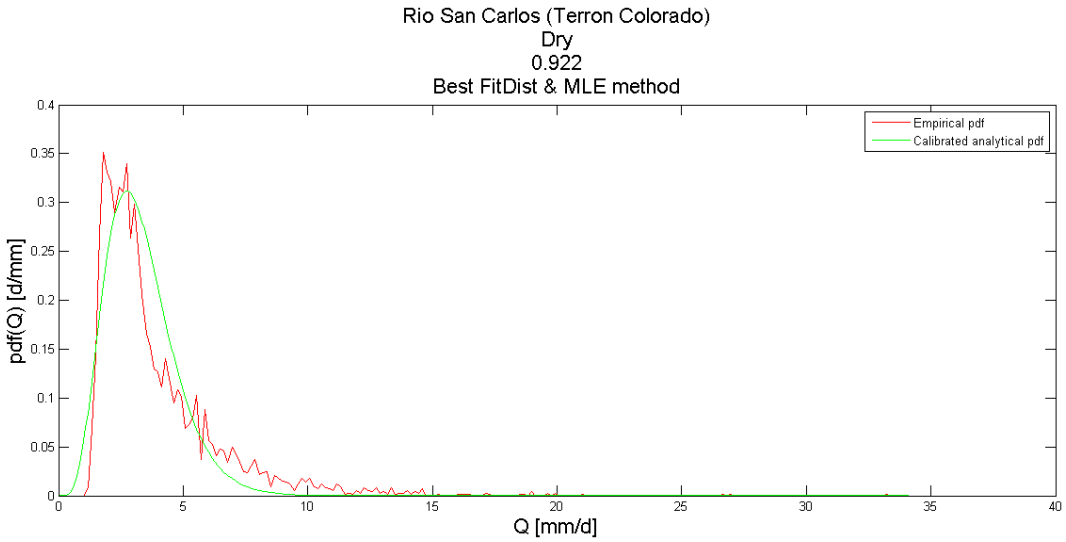

Figure III.35 –Rio San Carlos, Dry Season best-fitting calibrated pdf using best Q% removal method

The methods of moments will display the worse pdf, a result that can be both by plots in figure III.36 and underlined by the high SSD (see the table III.16)..

MLE		**SC**		**Best Q% removal**				**Method of moments**	
$\Delta_1 = \Delta_2$	SSD	$\Delta_1 = \Delta_2$	SSD	%Q used	Δ_1	Δ_2	SSD	$\Delta_1 = \Delta_2$	SSD
0.8073	0.1897	1.0001	0.2060	**92.2%**	**0.4886**	**0.4186**	**0.1383**	1.2191	0.2494

Table III.16 – Rio San Carlos. Dry season pdf after calibration results

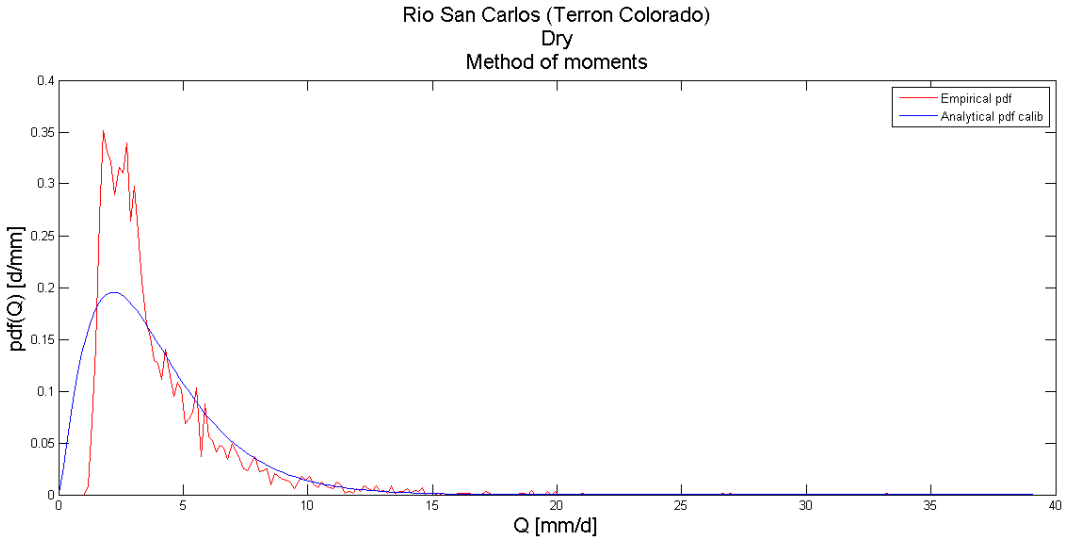

Figure III.36 –Rio San Carlos, dry Season, calibrated pdf according to method of moments

3.3.2 – Rio Tenorio

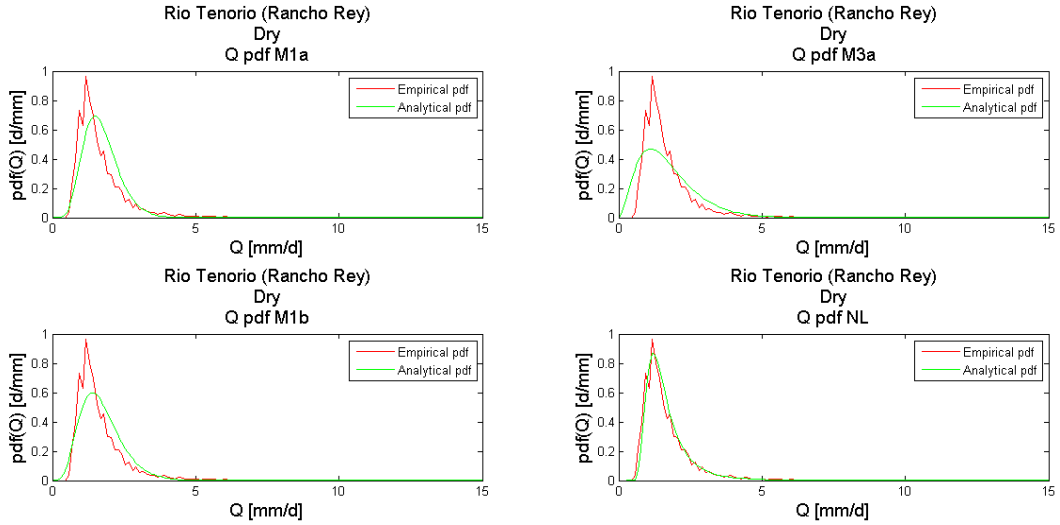

Figure III.37 –Rio Tenorio, Dry Season pdf with different regression methods.

It's quickly deducible how, this time, the non-linear model is able to give a good performance and its graphical behavior is able to describe the empirical data pdf.

$<q>$ [mm/d]	1.7067	M1a SSD performance	0.8355
Var [mm^2/d^2]	1.3533	M1b SSD performance	0.5705
CV_Q [-]	0.6816	M3a SSD performance	0.7438
Best recession method	NL	NL SSD performance	**0.2929**
α [mm]	5.8098	q min [mm/d]	0.55
λ [1/d]	0.2937	q max [mm/d]	31.05
k (M1b)	0.0530	q dataset length	5618

Table III.17 – Rio Tenorio. Pdf pre-calibration results for dry season

This observation can be underlined in an analytical way considering the SSD values displayed in the following table. In order to increase the performances of the model the calibration codes were applied only on the linear model, starting from the hydroclimatical parameters showed in the table. The hydrograph recession rate is, this time, considered starting from a linear recession analysis that uses the M1b method, the most performing one.

The calibration was able to return a better estimation of the pdf using the best Q% removal method. It's interesting to note how, even if the performance of the linear model increased (passing from a SSD of 0.5705 given by the M1b recession technique, to 0.32), the final performance is still lower than the original one obtained by the non-linear method.

The graphical results relative to the best Q% removal and methods of moments pdf are respectively displayed in the figure III.38 and III.39.

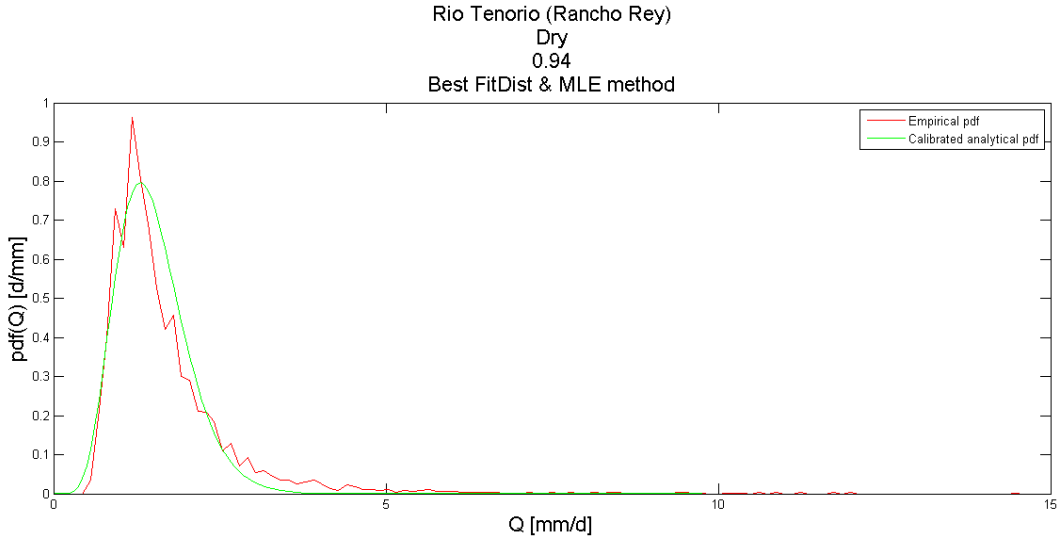

Figure III.38 –Rio Tenorio, Dry Season best-fitting calibrated pdf using best Q% removal method

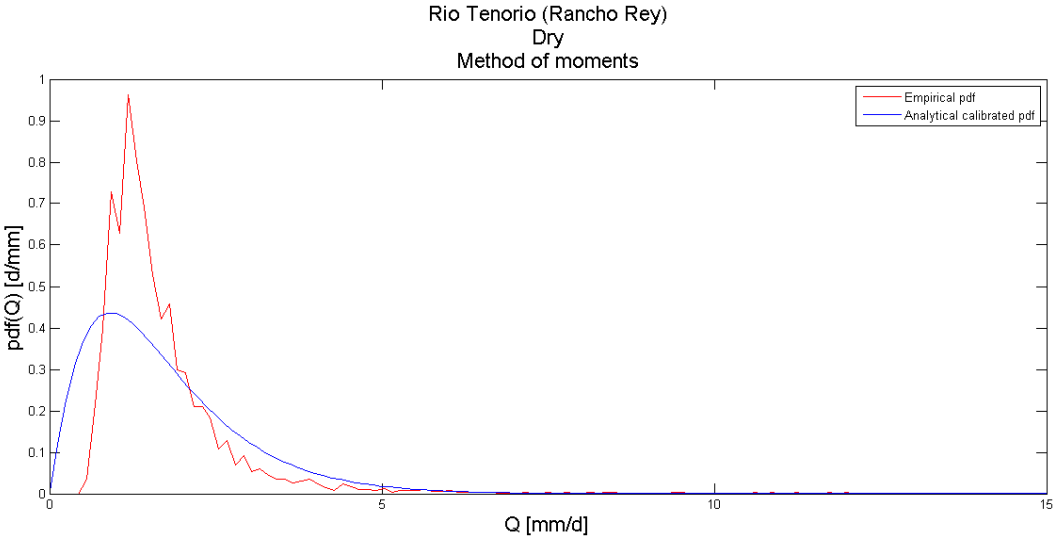

Figure III.39 – Rio Tenorio, dry Season, calibrated pdf according to method of moments

The calibration methods and their results are expressed by the table III.18:

MLE		**SC**		**Best Q% removal**				**Method of moments**	
$\Delta_1 = \Delta_2$	SSD	$\Delta_1 = \Delta_2$	SSD	%Q used	Δ_1	Δ_2	SSD	$\Delta_1 = \Delta_2$	SSD
1.2359	0.5441	1.1259	0.5353	**94%**	**0.6511**	**0.5707**	**0.3200**	2.41041	1.0538

Table III.18 – Rio Tenorio. Dry season pdf after calibration results

3.3.3 – Rio Poas

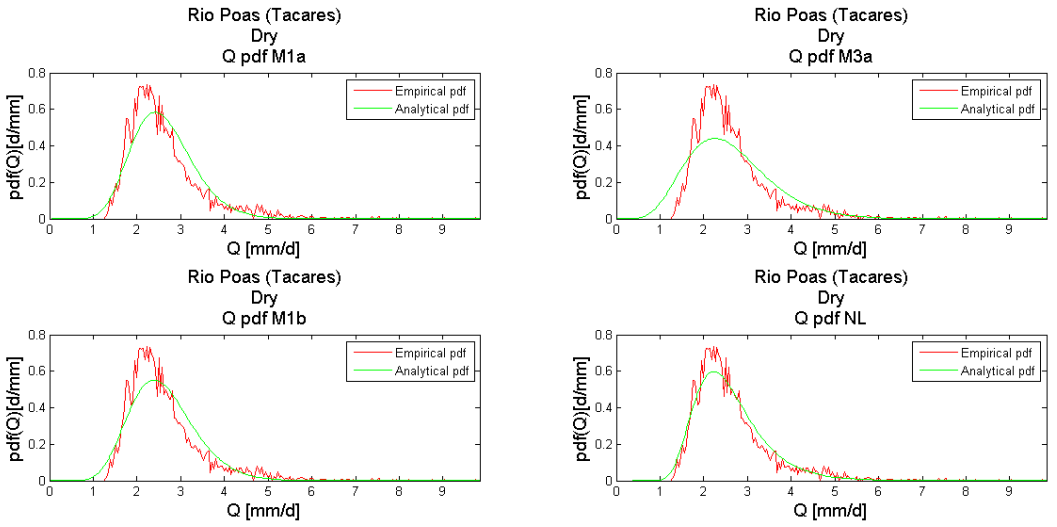

Figure III.40 –Rio Poas, Dry Season pdf with different regression methods.

The theoretical model has been evaluated according to the M1a, M1b, M3a and Non-linear regression method. The analytical pdf are plotted in the following figure III.40. The non-linear regression method is able to return the best pdf in term of visual-fitting with the observed-data pdf. This result is underlined by the table III.19. Moreover, among the linear-techniques to study the regressions, the M1a method displays a better result than the M3a and M1b one giving, as result, the pdf with smallest SSD.

$<q>$ [mm/d]	2.6056	M1a SSD performance	0.8479
Var [mm^2/d^2]	0.7322	M1b SSD performance	0.8583
CV_Q [-]	0.3284	M3a SSD performance	1.5253
Best recession method	NL	NL SSD performance	**0.3899**
α [mm]	7.2133	q min [mm/d]	1.29
λ [1/d]	0.3612	q max [mm/d]	9.84
k (M1a)	0.0264	q dataset length	4688

Table III.19 – Rio Poas. Pdf pre-calibration results for dry season

The calibration started from the results obtained from the M1a method and the best result has been obtained with the best Q% removal as the following table III.20 underlines.

MLE		**SC**		**Best Q% removal**				**Method of moments**	
$\Delta_1 = \Delta_2$	SSD	$\Delta_1 = \Delta_2$	SSD	%Q used	Δ_1	Δ_2	SSD	$\Delta_1 = \Delta_2$	SSD
1.1917	0.8828	1.0447	0.8434	**94.2%**	**0.7557**	**0.7127**	**0.4608**	1.4721	1.0975

Table III.20 – Rio Poas. Dry season pdf after calibration results

The following pictures will display the pdf obtained with the best calibration and the worse one:

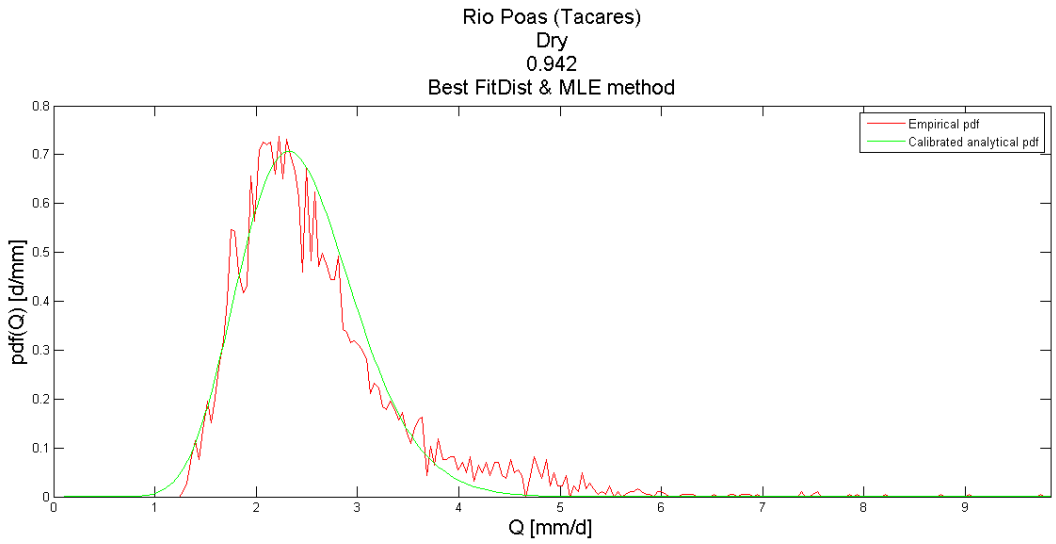

Figure III.41 –Rio Poas, Dry Season best-fitting calibrated pdf using best Q% removal method

The calibration was able to return a better estimation of the pdf using the best Q% removal method, obtaining a SSD value of 0.4608, way lower than the initial one (equal to 0.8479) discarding 5.8% of the dataset (corresponding to the most intense streamflow). Again this calibration applied on the linear model was not able to give a totally satisfactory result, being the non-linear uncalibrated model still better than the calibrated linear model. The method of moments, on the contrary, represent the worse calibration and its performances are lower than the initial model one.

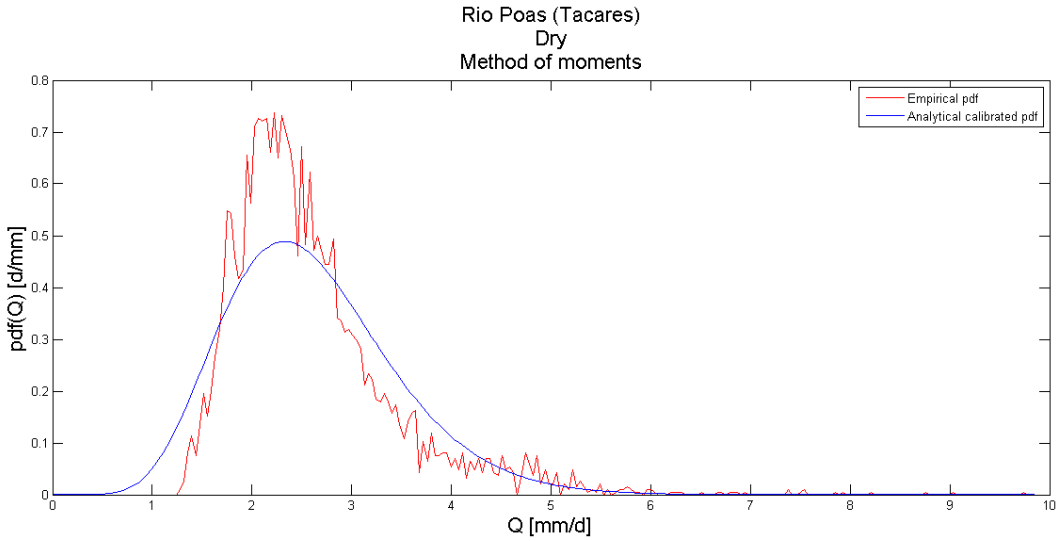

Figure III.42 – Rio Poas, dry Season, calibrated pdf according to method of moments

3.3.4 – Rio Naranjo

The theoretical model has been evaluated according to the M1a, M1b, M3a and Non-linear regression method. The analytical pdf are plotted in the following figure III.43:

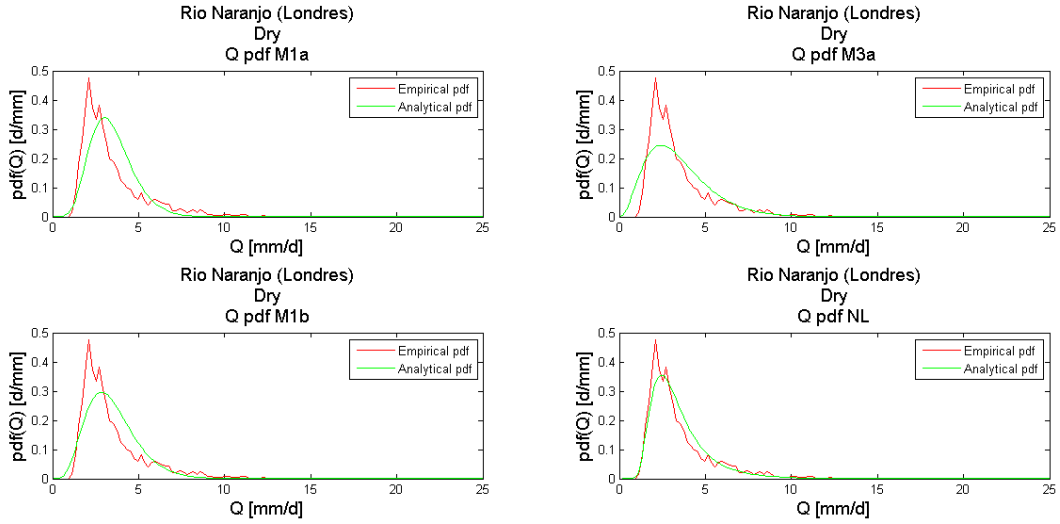

Figure III.43 –Rio Naranjo, Dry Season pdf with different regression methods

The non-linear regression method is able to return the best pdf in term of visual-fitting with the observed-data pdf. Moreover, among the linear-techniques to study the regressions, the M3a method displays a better result than the M1a and M1b one. These result can be underlined in the table III.21.

$<q>$ [mm/d]	3.4567	M1a SSD performance	0.3143
Var [mm^2/d^2]	4.595	M1b SSD performance	0.2133
CV_Q [-]	0.6201	M3a SSD performance	0.1932
Best recession method	NL	NL SSD performance	**0.0950**
α [mm]	13.4024	q min [mm/d]	1.18
λ [1/d]	0.2579	q max [mm/d]	50.5
k (M3a)	0.7585	q dataset length	3727

Table III.21 – Rio Naranjo. Pdf pre-calibration results for dry season

The calibration was performed in order to increase the performances of the linear best-fitting model which is, in this case, the one deduced by the pdf parameters obtained with the regression M3a method. The calibration results can be expressed in table III.22 and in the following plots (III.44-45) and they underline the performance increment obtained by the method described in section 1.5.

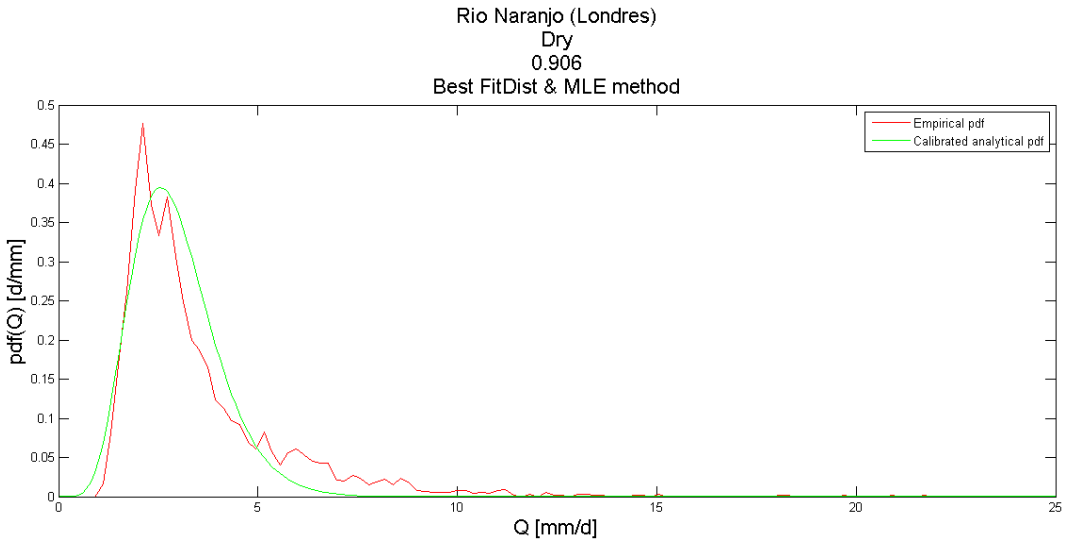

Figure III.44 –Rio Naranjo, Dry Season best-fitting calibrated pdf using best Q% removal method

The calibration was able to return a better estimation of the pdf using the best Q% removal method, obtaining a SSD value of 0.1154 starting from the 0.1953, a slight increment of the performance that was possible using the MLE method on a dataset in which the 9.4% of the most intense streamflow values were discarded. Again this calibration applied on the linear model was not able to give a totally satisfactory result, being the non-linear uncalibrated model still better (with a SSD of 0.095) than the

calibrated linear model. The method of moments, on the other hand, is able to reproduce in the general behavior the dataset-deduced pdf, but its performances are better solely of the analytical pfd deduced by a M1a recession method estimation. The best Q% removal and method of moments results can be appreciated in the figures III.44 and III.45.

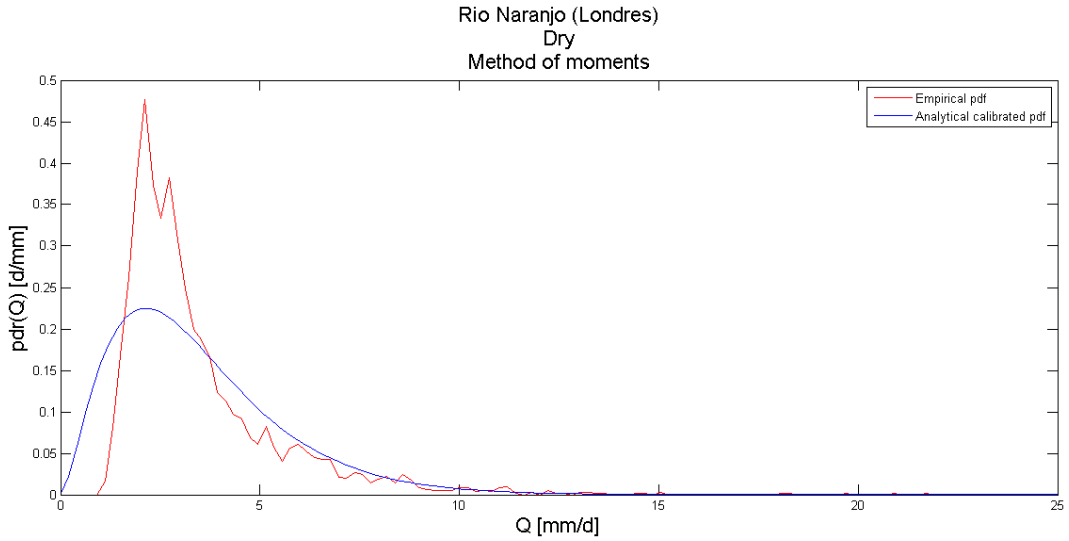

Figure III.45 – Rio Naranjo, dry Season, calibrated pdf according to method of moments

MLE		**SC**		**Best Q% removal**				**Method of moments**	
$\Delta_1 = \Delta_2$	SSD	$\Delta_1 = \Delta_2$	SSD	%Q used	Δ_1	Δ_2	SSD	$\Delta_1 = \Delta_2$	SSD
0.8237	0.1818	1.0001	0.1933	**90.6**	**0.4492**	**0.3831**	**0.1154**	1.3075	0.2444

Table III.5 – Rio Naranjo. Dry season pdf after calibration results

3.3.5 – Rio Grande de Terraba

The theoretical model has been evaluated according to the M1a, M1b, M3a and Non-linear regression method. The analytical pdf are plotted in the figure III.46.

Every method used, both non-linear and linear, is not able to give a satisfactory pdf able to well represent the empirical pdf deduced by the dataset. The best pdf was obtained considering the hydrograph recession rate obtained from the linear method M3a.

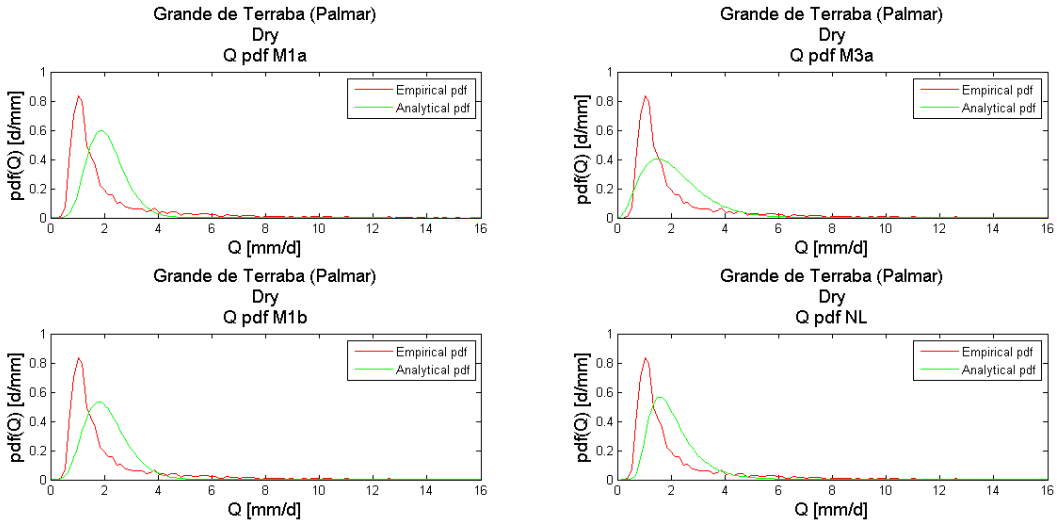

Figure III.46 –Rio Grande de Terraba, Dry Season pdf with different regression methods.

$<q>$ [mm/d]	2.1063	M1a SSD performance	2.4146
Var [mm^2/d^2]	4.4304	M1b SSD performance	1.9122
CV_Q [-]	0.9993	M3a SSD performance	**1.0018**
Best recession method	M3a	NL SSD performance	1.6778
α [mm]	5.6705	q min [mm/d]	0.4002
λ [1/d]	0.3714	q max [mm/d]	39.605
k (M3a)	0.1067	q dataset length	4688

Table III.23 – Rio Grande de Terraba. Pdf pre-calibration results for dry season

The better result obtained still has a relatively high SSD value, if compared to other similar cases. The performance methods were done starting from the pdf data showed in the last table. The results can be quickly represented in the table III.24.

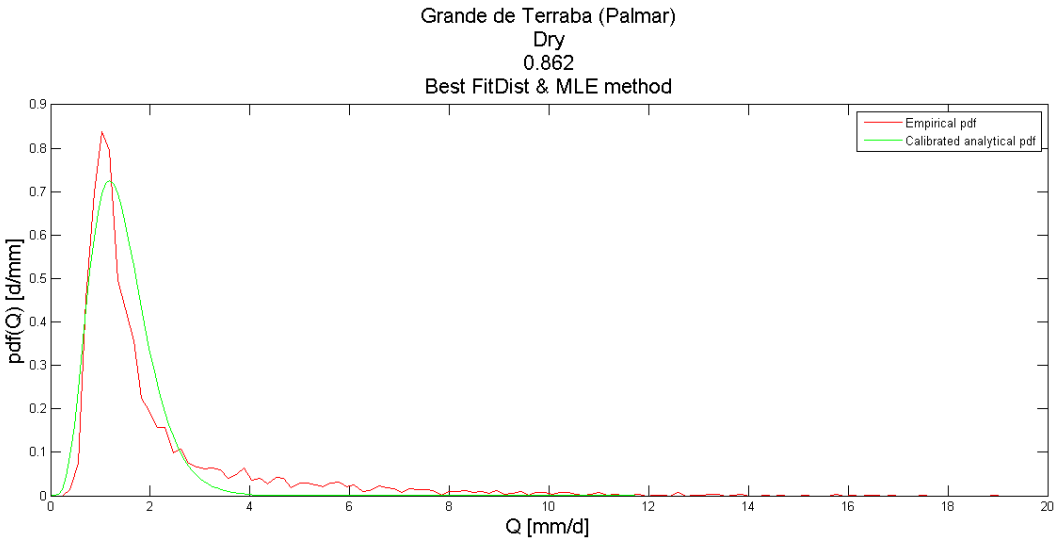

Figure III.47 – Rio Grande de Terraba, Dry Season best-fitting calibrated pdf using best Q% removal method

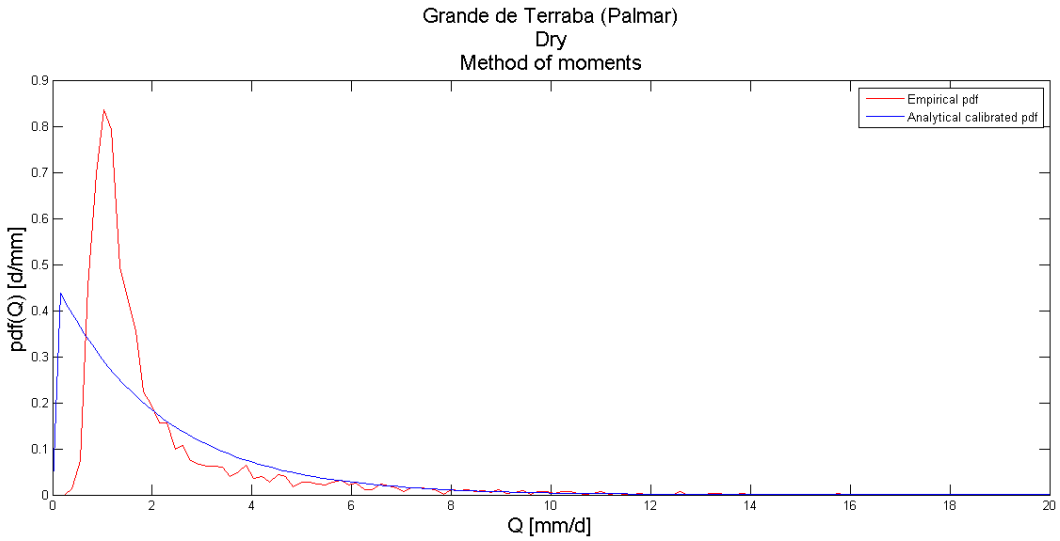

Figure III.48 – Rio Grande de Terraba, dry Season, calibrated pdf according to method of moments

The performance increase obtained with best Q% method is able to lower the SSD from 1.0018 to 0.3924, but the relative percentage of high flow discarded is pretty high, 13.8%. The visual fitting on the peak of the empirical pdf deduced by observed data can be graphically appreciated in the III.47 figure. The pdf obtained from the methods of moments, even if by definition, is able to give the same mean, variance and, therefore, coefficient of variation of the empirical dataset. The scarce data-fitting can be seen in the figure III.48.

MLE		**SC**		**Best Q% removal**				**Method of moments**	
$\Delta_1 = \Delta_2$	SSD	$\Delta_1 = \Delta_2$	SSD	%Q used	Δ_1	Δ_2	SSD	$\Delta_1 = \Delta_2$	SSD
1.7317	0.8326	1.5713	0.8246	**86.2%**	**0.5999**	**0.4072**	**0.3924**	3.4740	1.2789

Table III.24 – Rio Grande de Terraba. Dry season pdf after calibration results

3.3.6 – Rio Pejibaye

The theoretical model has been evaluated according to the M1a, M1b, M3a and Non-linear regression method and, starting from the parameter evaluated, the pdfs were built and, for every method, the performance, in terms of SSD, were estimated.

The analytical pdf are plotted in the following figure III.49 and the performances of the methods used are listed in table III.25.

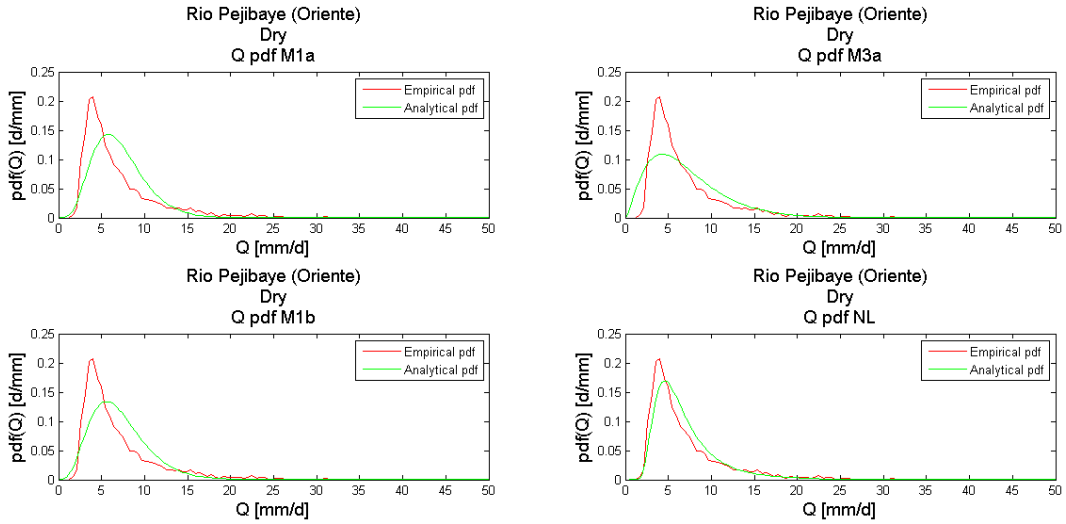

Figure III.49 –Rio Pejibaye, Dry Season pdf with different regression methods.

$<q>$ [mm/d]	7.0946	M1a SSD performance	0.0663
Var [mm^2/d^2]	31.7777	M1b SSD performance	0.0537
CV_Q [-]	0.7946	M3a SSD performance	0.0407
Best recession method	NL	NL SSD performance	**0.0283**
α [mm]	20.2752	q min [mm/d]	1.72
λ [1/d]	0.3499	q max [mm/d]	118.47
k (M3a)	0.1388	q dataset length	4688

Table III.25 – Rio Pejibaye. Pdf pre-calibration results for dry season

The non-linear regression method is able to return the best pdf in term of visual-fitting with the observed-data pdf a result confirmed by the lowest SSD obtained. Moreover, among the linear-techniques to study the regressions, the M3a method displays a better result than the M1a and M1b one. The calibration was performed in order to increase the performances of the linear best-fitting model which is the one deduced by the pdf parameters obtained with the regression M3a method. The calibration results can be expressed in the following table.

MLE		**SC**		**Best Q% removal**				**Method of moments**	
$\Delta_1 = \Delta_2$	SSD	$\Delta_1 = \Delta_2$	SSD	%Q used	Δ_1	Δ_2	SSD	$\Delta_1 = \Delta_2$	SSD
0.8629	0.0389	1.0001	0.0407	**91.4%**	**0.4672**	**0.3837**	**0.0257**	1.5907	0.0648

Table III.26 – Rio Pejibaye. Dry season pdf after calibration results

After the calibration the linear model modified according to the best Q% removal approach is able to give a SSD value inferior of the best initial non-calibrated model.

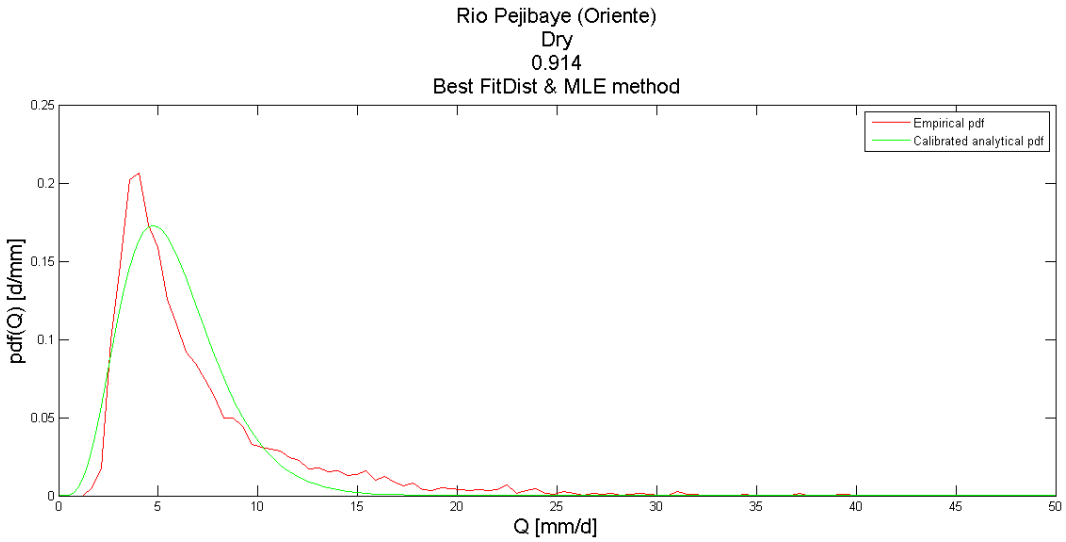

Figure III.50 – Rio Pejibaye, Dry Season best-fitting calibrated pdf using best Q% removal method

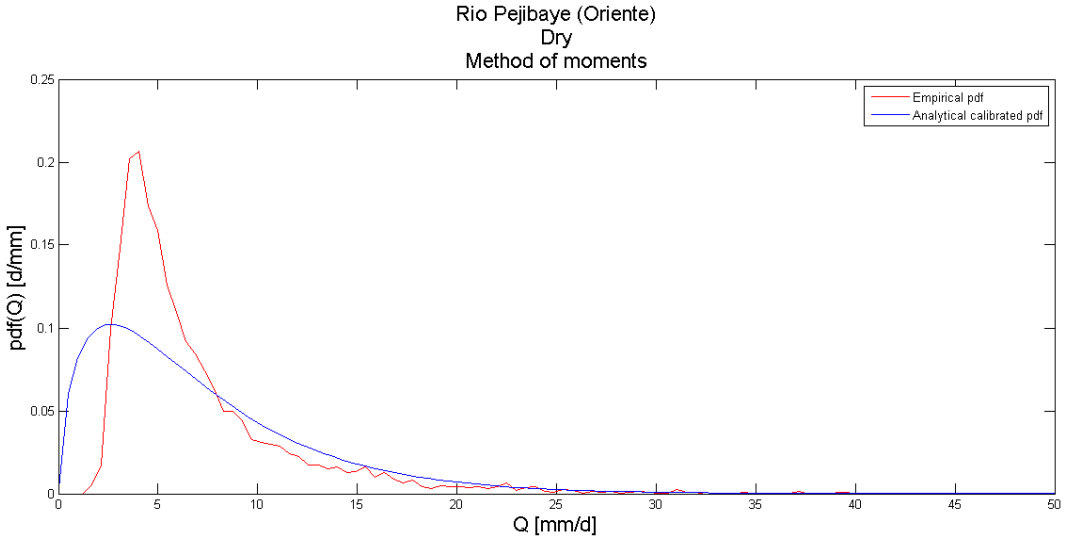

Figure III.51 – Rio Pejibaye, Dry Season best-fitting calibrated pdf using method of moments

3.3.7 – Summary table

In the following table all the properties deduced by the analytical study of the basins using the datasets and considering only the dry-season data will be shown. The table III.28 illustrates the SSD (considered as a performance index) of the theoretical model according to different regression methods, and the moments of the observed distribution. The values of the correction parameters (Δ_1 and Δ_2) as well as the relative SSD for different calibration techniques allow inferring whether the calibration induces an increase in model performances or not.

River	Dataset information			Before calibration			After Calibration										Best calibration	Performance increasing (%)	$(k/\lambda)^{1/2}$ calibrated model	
							MLE		*SC*		*Best Q% removal*				*Method of moments*				*SC*	*Q%*
	Mean [mm/d]	*Variance [mm^2/d^2]*	CV_Q	Best recession method	SSD	$(k/\lambda)^{1/2}$ theoretical model	Δ	SSD	Δ	SSD	%Q Used	Δ_1	Δ_2	SSD	Δ_1	SSD				
Rio Frio (Guatuso)	5.53	27.558	0.94	M3a	0.1143	0.9489	1.10	0.1148	1.03	0.1142	90	0.52	0.39	**0.0778**	2.18	0.0185	Best Q	31.95	0.6530	0.4642
Rio San Carlos (Terron Colorado)	3.86	6.502	0.65	M3a	0.2060	0.6594	0.80	0.1897	1.00	0.2060	92.2	0.48	0.41	**0.1383**	1.21	0.2494	BestQ	32.86	0.5971	0.4174
Rio Sarapiqui (Cariblanco)	7.26	36.913	0.83	NL	0.0313	0.8357	0.95	0.0329	1.00	0.0337	95.4	0.54	0.47	**0.0201**	2.08	0.0838	BestQ (M3a)	40.23	0.5791	0.4268
Rio Tempisque (Guardia)	1.001	3.081	1.75	M2	0.5652	1.7536	2.21	0.2822	2.32	0.2801	99.8	1.52	1.41	**0.2475**	17.87	inf	BestQ	71.13	0.6327	0.5115
Rio Tenorio (Rancho Rey)	1.70	1.353	0.68	NL	*0.2929*	0.6816	1.23	0.5441	1.12	0.5355	94	0.65	0.57	**0.3200**	2.41	1.0538	BestQ (M2)	41.79	0.4658	0.3542
Rio Barranca (Guapinol)	1.98	4.316	1.04	M3a	1.6010	1.0447	1.27	1.6269	1.08	1.5916	84.6	0.37	0.24	**0.7001**	2.74	Inf	BestQ	56.26	0.6572	0.3838
Rio Poas (Tacares)	2.60	0.732	0.32	NL	*0.3899*	0.3284	1.19	0.8828	1.04	0.8434	94.2	0.75	0.71	**0.4608**	1.47	1.0975	BestQ (M1a)	45.65	0.2766	0.2353
Rio G.Candelaria (El Rey)	1.21	1.740	1.08	M3a	1.7031	1.0824	1.56	1.6480	1.28	1.5650	93.2	0.65	0.51	**0.7406**	4.26	Inf	BestQ	56.50	0.5935	0.4235
Rio Naranjo (Londres)	3.45	4.595	0.62	NL	*0.0950*	0.6201	0.82	0.1818	1.00	0.1933	90.6	0.44	0.38	**0.1154**	1.30	0.2444	BestQ (M3a)	40.28	0.5423	0.3634
Rio Savegre (Providencia)	1.92	1.24	0.57	M3a	0.6710	0.5778	1.21	0.6886	1.05	0.6673	91.8	0.66	0.58	**0.4198**	1.95	1.0578	BestQ	37.43	0.4244	0.3373
G. de Terraba (Palmar)	2.10	4.430	0.99	M3a	1.0018	0.9993	1.73	0.8326	1.57	0.8246	86.2	0.59	0.40	**0.3924**	3.47	1.2789	BestQ	60.82	0.6720	0.4152
Rio Coto Brus (Caracucho)	2.26	3.362	0.81	M3a	1.3062	0.8107	1.48	1.2998	1.22	1.2496	86.8	0.52	0.39	**0.5025**	2.72	2.0165	BestQ	61.53	0.5432	0.3570
Rio Reventazon (Palomo)	4.90	18.885	0.88	NL	0.0671	0.8862	0.96	0.0780	1.00	0.0790	92.4	0.49	0.40	**0.0437**	2.06	0.1729	BestQ (M3a)	44.66	0.6170	0.4335
Rio Pejibaye (Oriente)	7.09	31.777	0.79	NL	0.0283	0.7946	0.86	0.0389	1.00	0.0407	91.4	0.46	0.38	**0.0257**	1.59	0.0648	BestQ (M3a)	36.85	0.6300	0.4306
Rio Pacuare (Dos Montanas)	4.54	19.250	0.96	NL	0.0406	0.9645	0.85	0.0625	1.00	0.0678	93.6	0.45	0.37	**0.0381**	2.08	0.1611	BestQ (M3a)	43.71	0.6673	0.4507
Rio Banano (Asunciòn)	13.14	196.861	1.06	NL	0.0016	1.0678	0.87	0.0029	1.00	0.0033	96.2	0.52	0.44	**0.0012**	2.38	Inf	BestQ (M3a)	61.54	0.6914	0.4987
Rio Estrella (Pandora)	5.99	61.408	1.30	NL	0.0203	1.3078	0.88	0.0202	0.89	0.0202	95	0.51	0.40	**0.0128**	2.60	Inf	BestQ (M3a)	38.00	0.7674	0.5798
Rio Telire (Bratsi)	4.78	12.045	0.72	M3a	0.0752	0.7254	0.91	0.0756	1.00	0.0752	98.2	0.72	0.67	**0.0718**	1.51	0.1069	BestQ	4.49	0.5892	0.5018

Table III.28 – Dry season analysis. Initial dataset information, best recession and its corresponding SSD value before calibration, correction parameters and SSD values obtained after calibration.

3.3.8 – Streamflow regime characterization

Some considerations about the theoretical model, the calibration methods applied to the dry season characterization of the analyzed catchments and the table showed in the previous section can be mentioned.

- The best method for the estimation of the hydrograph recession rate, *k*, is obtained most of the time with the linear M3a method even if, the 50% of the cases the best performances are obtained using the non-linear method;
- As for the annual characterization of the streamflow, the theoretical model is not able to give a value of the square root of the ratio k/λ equal to the coefficient of variation obtained by the empirical dataset. This consequence leads to a not perfect correspondence between *erratic* and *persistent* streamflow regimes defined by equation I.17;
- For the dry season characterization the best method able to return a better-fitting pdf to the empirical data is given by the best Q% removal method. It's important to spot how, when non-linear theoretical model showed better performances than the other techniques, the model calibrated was the linear model with smallest SSD, it is indicated in round parenthesis in the "*Best calibration*" column;
- Even if the calibration is always able to improve the performances of the linear model (see the column "*Performance increasing*") it's not always true that the linear model is then able to express better performances than the non-linear method. In fact, let's focus the sight on those catchments which have a good initial theoretical fitting with the non-linear model (Rio Sarapiqui, Rio Tenorio, Rio Poas, Rio Naranjo, Rio Reventazon, Rio Pejibaye, Rio Pacuare, Rio Banano, Rio Estrella, column "*Before Calibration – Best recession method*". Their correspondent SSD is, sometimes, smaller than the SSD deduced by the best linear-calibrated model. These case were underlined in the column using a cursive font;
- The *inf* value expressed in some results of the method of moments, as underlined before in section 3.2.8 gives a quick indication about the streamflow regime and underline its *erratic* behavior.

According to the considerations done in section 3.2.8 about the definition of a certain streamflow regime, it's possible to analyze how the different calibration methods are able to give different performances in terms of CV_Q and $(k/\lambda)^{0.5}$.

The SC method leads to negligible differences with respect to the results obtained before the calibration. The best Q% removal, on the other hand, shows a decrease of performance and a higher spreading around the bisector. This spreading stands for a lower link between observed value CV_Q and theoretical estimated $(k/\lambda)^{0.5}$, this characteristic is

due to the main idea behind this method: remove some streamflow value implies a better fitting in the bell-part of the curve, but, on the other hands, underestimate the k over λ ratio. The graphical characterization between *erratic* and *persistent* flow regime can be quickly done looking at the "*Dataset information* – CV_Q" column in the 3.3.7 section and remembering the rules in 1.2 section. A qualitative and graphical Costa Rican dry-season streamflow regime characterization can be done looking at the following plots.

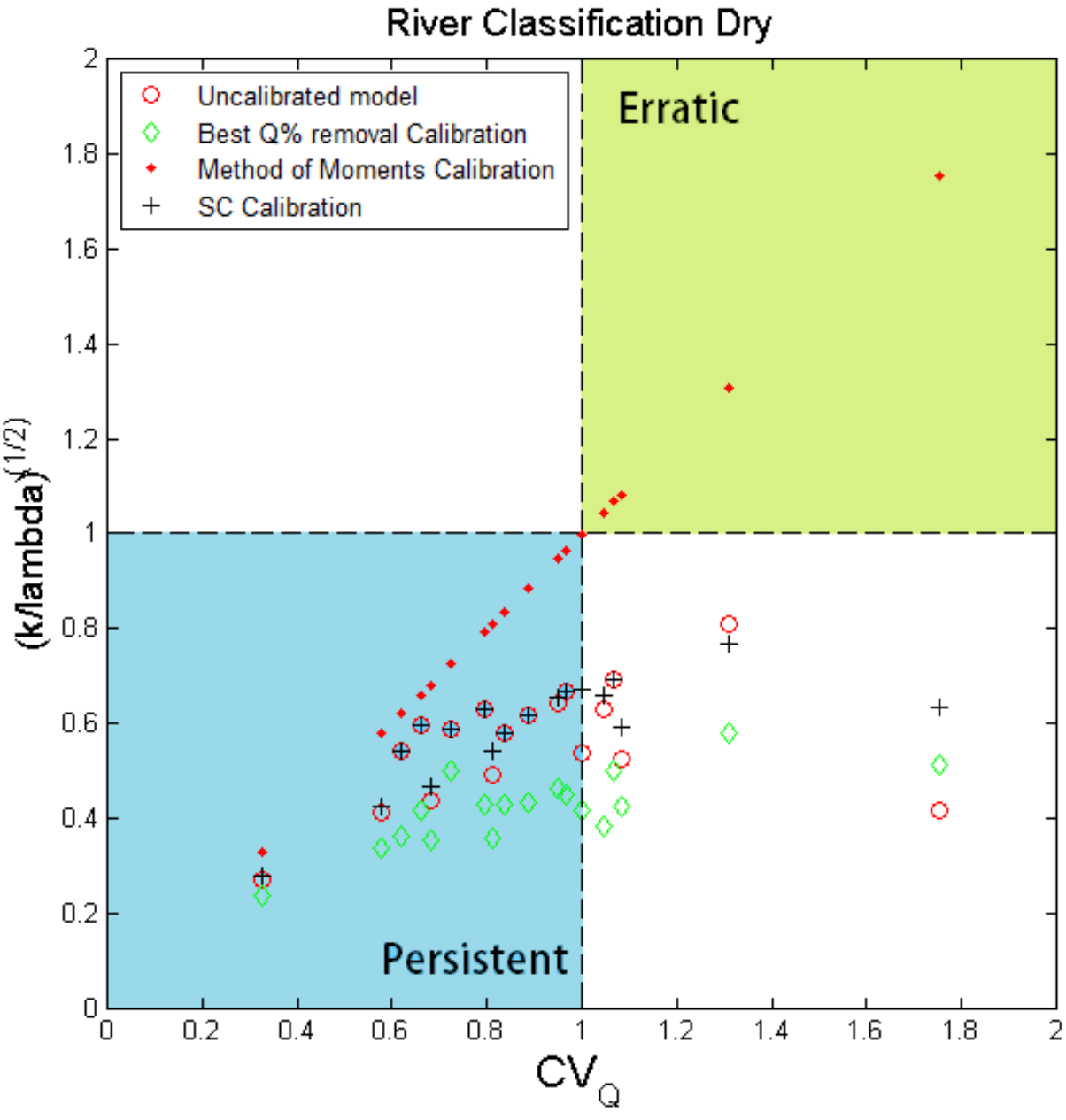

Figure III.52 – Dry season streamflow characterization through CV_Q *Vs* $(k/\lambda)^{1/2}$ plots for non-calibrated model and for different calibration options.

3.4 – Characterization of the streamflow during wet season

In this chapter the same catchments analyzed in section 3.2 and 3.3 will be studied in order to show how the subdivision into two seasons (dry and wet) can improve the initial fitting of the analytical pdf. The uncalibrated models will be displayed showing three different linear methods and the non-linear one used to study the recessions and to deduce the relative pdf. Every catchment will be described with tables in order to give information on the streamflow regime, calibrated and uncalibrated models. At the end, the streamflow regime characterization will be discussed in order to distinguish between *erratic* or *persistent* regimes.

3.4.1 – Rio San Carlos

The best theoretical pdf can be obtained using the M1a regression method, the non-linear technique, on the contrary, is no able to return a pdf due to the extremely low K parameter deduced from recession analysis.

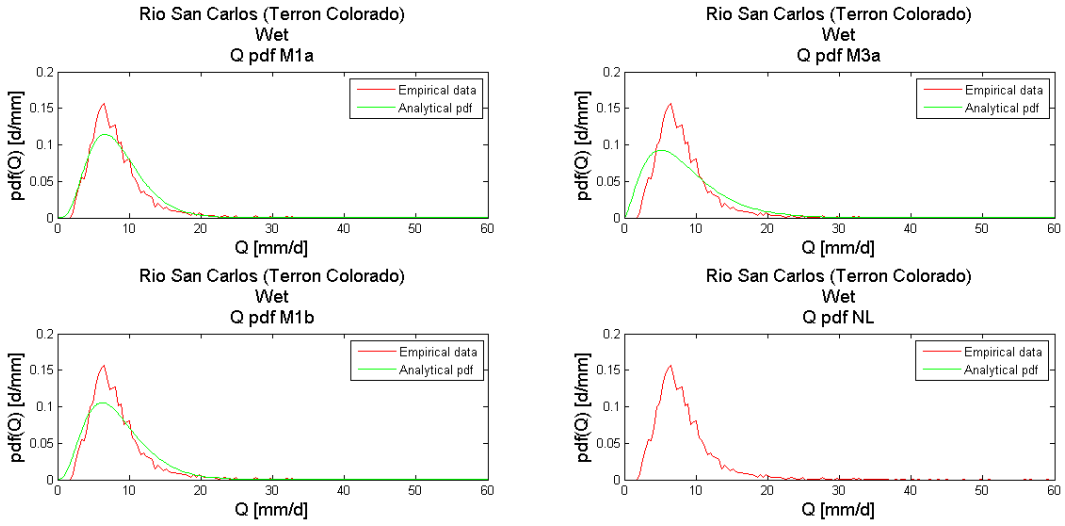

Figure III.53 –Rio San Carlos, Wet Season pdf with different regression methods.

$<q>$ [mm/d]	8.3834	M1a SSD performance	**0.0113**
Var [mm^2/d^2]	24.2287	M1b SSD performance	0.0157
CV_Q [-]	0.5871	M3a SSD performance	0.0351
Best recession method	M1a	NL SSD performance	NaN
α [mm]	22.7656	q min [mm/d]	2.13
λ [1/d]	0.3682	q max [mm/d]	98.1
k (M1a)	0.07711	q dataset length	6665

Table III.29 – Rio San Carlos. Pdf pre-calibration results for wet season

In the next figures (III.54-55) the best calibrated method, best Q% removal, will be displayed. The following table (III.30) will show the values of SSD obtained from pdfs deduced by different calibration methods. The pdf in figure III.54 is able to show accurately both the peak of the pdf and the descending slope of the curve. The method of moments, on the contrary, thanks to a perfect link between mean and variance between observed pdf and theoretical one, is able to give a perfect correspondence in term of observed CV_Q and the squared root of the ratio between hydrograph recession rate and mean effective-rainfall frequency, but it's not able to represent in a reliable way the shape of the observed pdf.

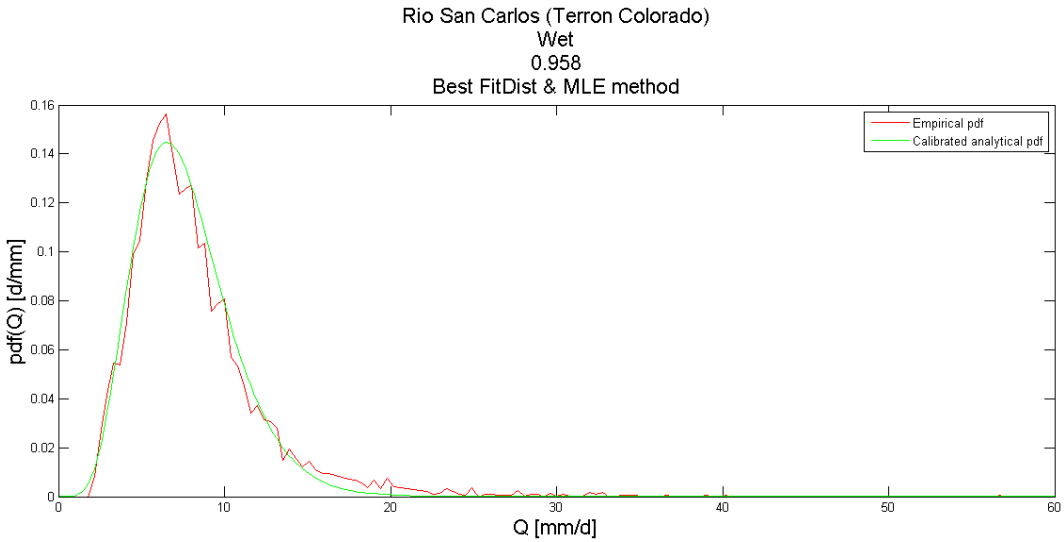

Figure III.54 – Rio San Carlos, Wet Season best-fitting calibrated pdf using best Q% removal method

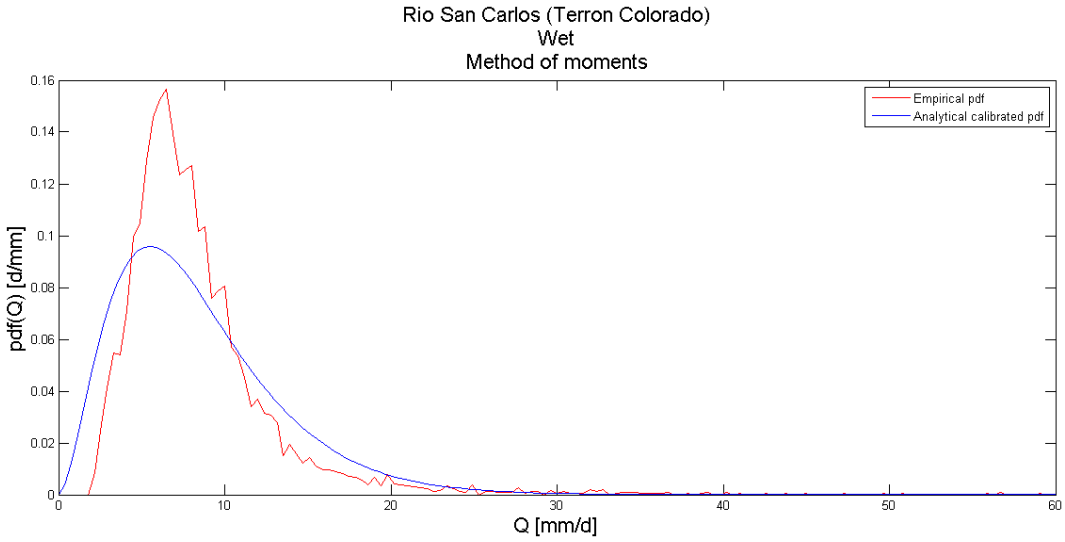

Figure III.55 – Rio San Carlos, Wet Season, calibrated pdf according to method of moments

The graphical fitting or discordance between theoretical pdf and empirical one will be linked with the corresponding SSD evaluated for every calibration method. The results can be reassumed in the table III.30:

MLE		SC		Best Q% removal				Method of moments	
$\Delta_1 = \Delta_2$	SSD	$\Delta_1 = \Delta_2$	SSD	%Q used	Δ_1	Δ_2	SSD	$\Delta_1 = \Delta_2$	SSD
1.0608	0.01211	1.0001	0.01135	**95.8**	**0.7042**	**0.6435**	**0.0040**	2.0392	0.0281

Table III.30 – Rio San Carlos. Wet season pdf after calibration results

3.4.2 – Rio Tenorio

In this case the best-fitting pdf was obtained using the non-linear recessions method, the curve is able to well represent the behavior of the observed pdf and the relative error associated is relatively low with a SSD value of 0.0998. The best linear method is given by the M1b method and it was calibrated using MLE, SC, best Q% removal and method of moments applications. The best result was obtained through the best Q% removal technique using 92% of the entire dataset interval.

These considerations lead to the following plots in figure III.56.

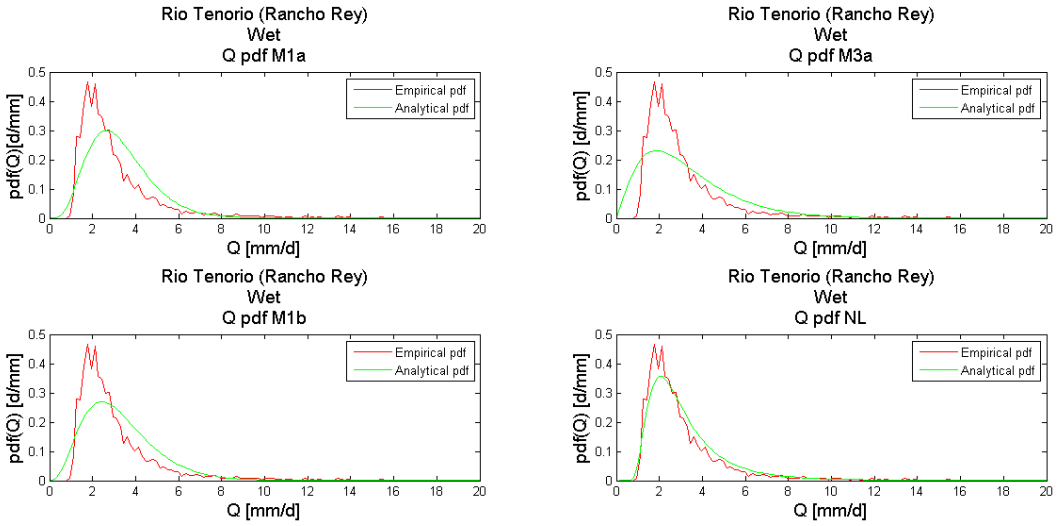

Figure III.56 –Rio Tenorio, Wet Season pdf with different regression methods.

$<q>$ [mm/d]	3.2844	M1a SSD performance	0.3428
Var [mm^2/d^2]	8.736	M1b SSD performance	0.2752
CV_Q [-]	0.8999	M3a SSD performance	0.3222
Best recession method	NL	NL SSD performance	**0.0998**
α [mm]	9.5275	q min [mm/d]	0.91
λ [1/d]	0.3447	q max [mm/d]	42.12
k (M1b)	0.0679	q dataset length	5704

Table III.31 – Rio Tenorio. Pdf pre-calibration results for wet season

The different theoretic methods appreciated in the previous picture can find a numerical correspondence in terms of good/bad fitting considering the SSD values listed in the table III.31.

In the next pictures two calibrated model results will be displayed: best Q% removal method and method of moments. In this way it's possible to appreciate the qualitative difference between a method able to return the best graphical-fitting, but the worst streamflow regime characterization (best Q% removal) and a method able to return the worst graphical-fitting but the most coherent regime characterization (method of moments).

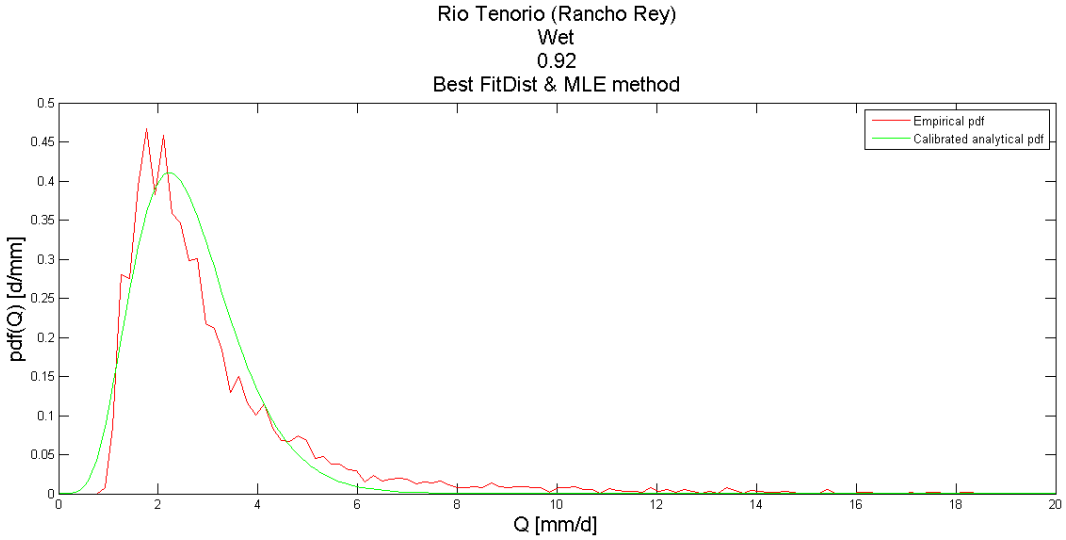

Figure III.57 – Rio Tenorio, Wet Season best-fitting calibrated pdf using best Q% removal method

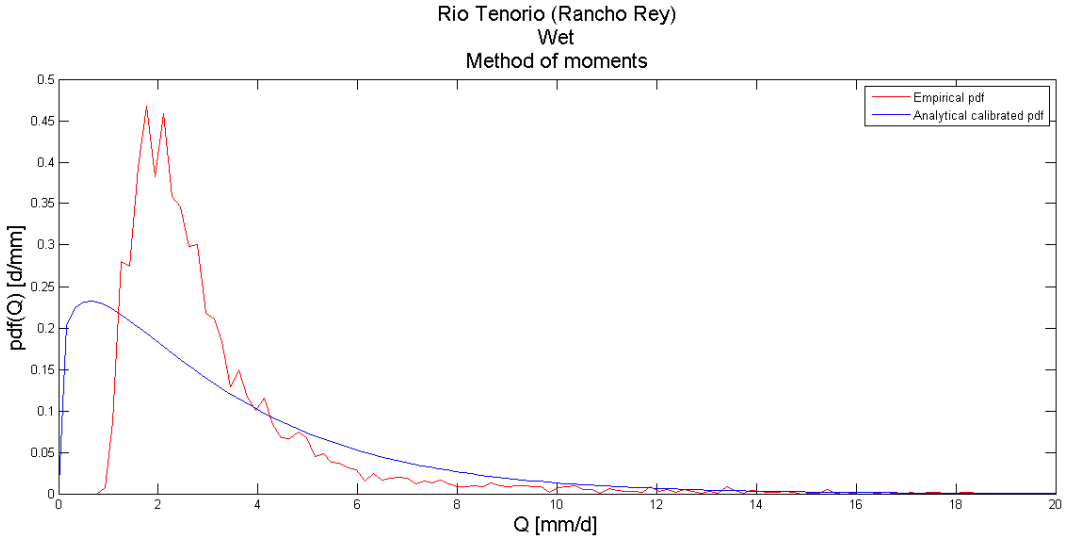

Figure III.58 – Rio Tenorio, Wet Season, calibrated pdf according to method of moments

The better graphical fitting of the calibrated model using the Best Q% removal approach can be underlined in the following table and comparing the figure III.57 with

the III.58. From the table it's possible to note how all SSD values are listed as well as the corresponding value of correction parameters, Δ_1 and Δ_2. The methods of moments is able to display a bad-fotting pdf, and this wrong lack of correspondence can be observed in its SSD value and observing the Δ values associated, being one order of magnitude higher than the one estimated with best Q% method.

MLE		**SC**		**Best Q% removal**				**Method of moments**	
$\Delta_1 = \Delta_2$	SSD	$\Delta_1 = \Delta_2$	SSD	%Q used	Δ_1	Δ_2	SSD	$\Delta_1 = \Delta_2$	SSD
0.8274	0.2806	1.0001	0.3222	**92.0**	**0.3615**	**0.2900**	**0.1252**	1.8727	0.6372

Table III.32 – Rio Tenorio. Wet season pdf after calibration results

3.4.3 – Rio Poas

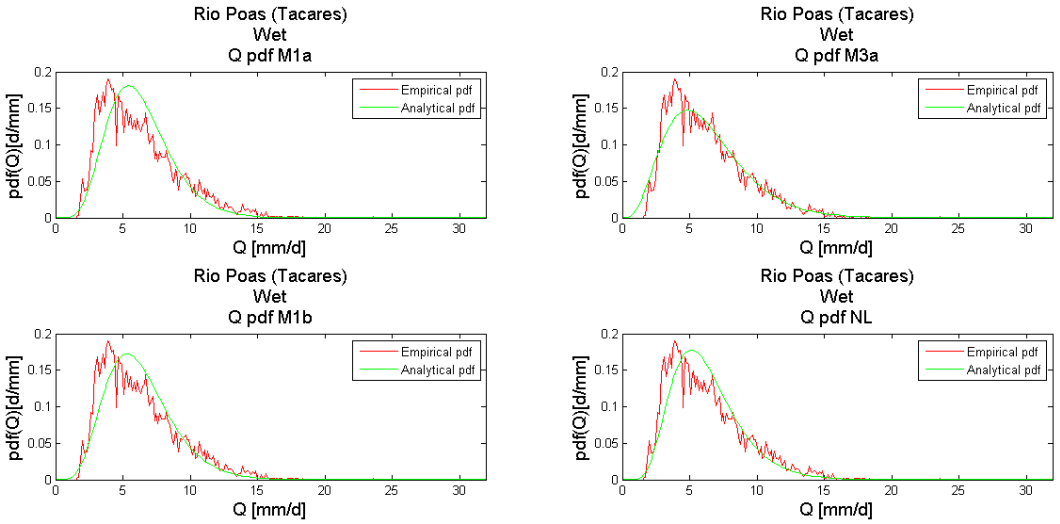

Figure III.59 –Rio Poas, Wet Season pdf with different regression methods.

The streamflow dataset is able to show a good fitting with all the pdf deduced with different theoretical approaches. The non-linear method displays no the best analytical and graphical fitting while the best result can be identified by pdf deduced by the linear M3a method. The linear pdf and its parameters were then calibrated in order to increase the performances. It's interesting to spot how, even without calibration, the theoretical models are able to give a good graphical fitting, a result that can be appreciated in the SSD results listed in the table III.33.

$<q>$ [mm/d]	6.2843	M1a SSD performance	0.1017
Var [mm^2/d^2]	9.0067	M1b SSD performance	0.0767
CV_Q [-]	0.4776	M3a SSD performance	**0.0403**
Best recession method	M3a	NL SSD performance	0.0718
α [mm]	17.3681	q min [mm/d]	1.59
λ [1/d]	0.3618	q max [mm/d]	31.94
k (M3a)	0.0831	q dataset length	6634

Table III.33 – Rio Poas. Pdf pre-calibration results for wet season

It's interesting to note, as it'll be displayed in the following plots and tables, how the calibration has no effect on the model, giving, as result, the same initial values deduced in a strictly analytical way. Moreover, the method of moments is able to return a good results in terms of graphical fitting pdf and SSD associated.

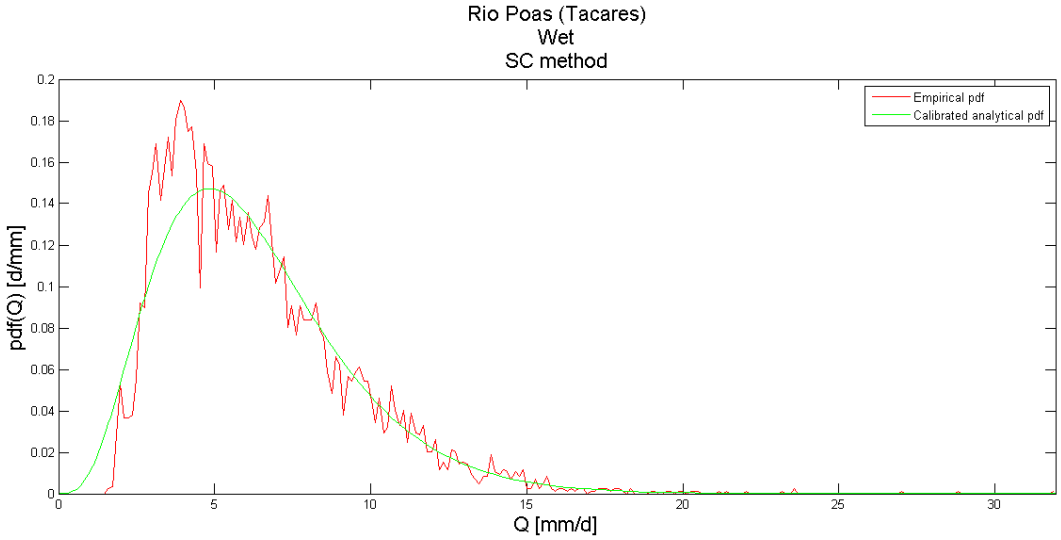

Figure III.60 – Rio Poas, Wet Season best-fitting calibrated pdf using best Q% removal method

The best Q% removal method is not able to return a satisfactory result and the associated dataset of streamflow used corresponds to the entire dataset recorded (100% of discharge-dataset used), its analytical result is, this, totally equal to the one obtained with MLE method. The calibration can still be considered pretty ineffective being the best-fitting pdf after calibration (the one obtained with SC technique) almost equal to the original theoretical model, the two SSD have indeed the same value (a difference can be appreciated only considering the from the 6th decimal number).

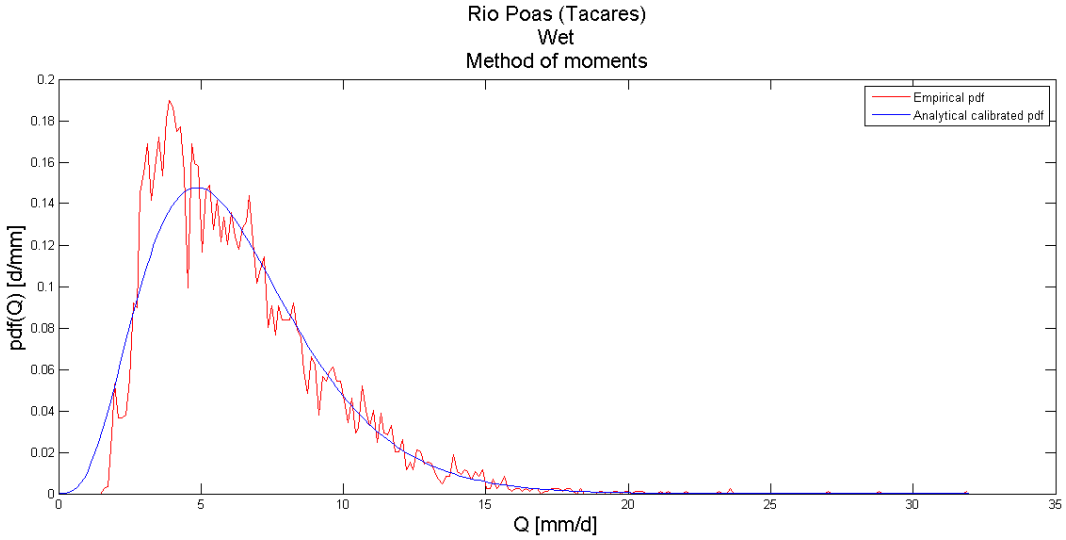

Figure III.61 – Rio Poas, Wet Season, calibrated pdf according to method of moments

MLE		**SC**		**Best Q% removal**				**Method of moments**	
$\Delta_1 = \Delta_2$	SSD	$\Delta_1 = \Delta_2$	SSD	%Q used	Δ_1	Δ_2	SSD	$\Delta_1 = \Delta_2$	SSD
0.8887	0.0434	**1.0001**	**0.0403**	100	0.8887	0.8887	0.0403	0.9921	0.0404

Table III.34 – Rio Poas. Wet season pdf after calibration results

3.4.4 – Rio Naranjo

In the following figure III.62 the results obtained with non-calibrated model of the wet-season study of Rio Naranjo is displayed.

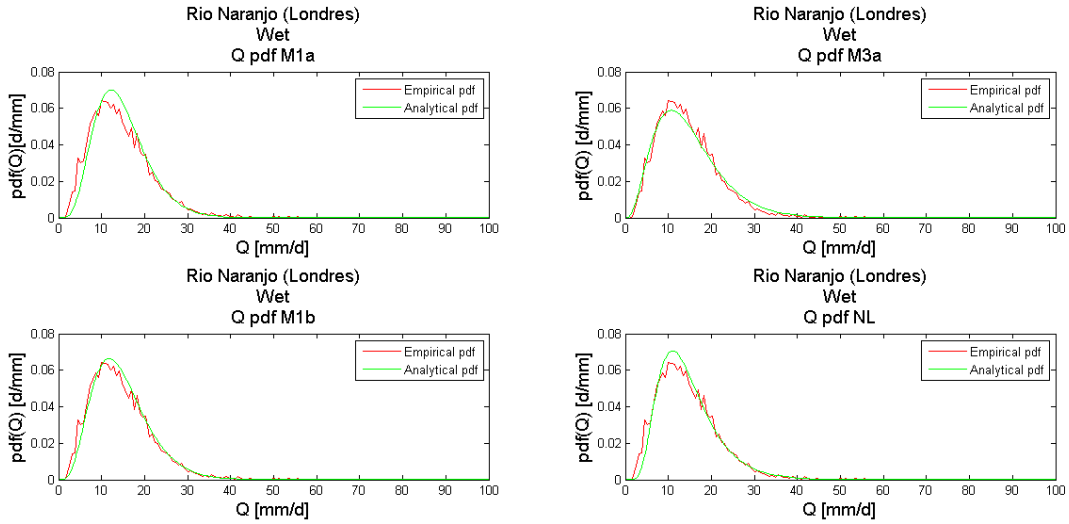

Figure III.62 – Rio Naranjo, Wet Season pdf with different regression methods.

It's possible to observe how the pdf deduced by the model is able to fit in a very good way the observed pdf. This qualitative and graphic result finds a numerical link as well: the SSD evaluated for every pdf shows value with an order of magnitude of 10^{-3} and, the best-fitting pdf, which is obtained with M3a method, returns a SSD even lower, 0.0006. All the results can be displayed in the table III.35.

$<q>$ [mm/d]	14.733	M1a SSD performance	0.0027
Var [mm^2/d^2]	78.1858	M1b SSD performance	0.0014
CV_Q [-]	0.6002	M3a SSD performance	**0.0006**
Best recession method	M3a	NL SSD performance	0.0017
α [mm]	37.9884	q min [mm/d]	1.96
λ [1/d]	0.33878	q max [mm/d]	172.41
k (M3a)	0.1059	q dataset length	7595

Table III.35 – Rio Naranjo. Pdf pre-calibration results for wet season

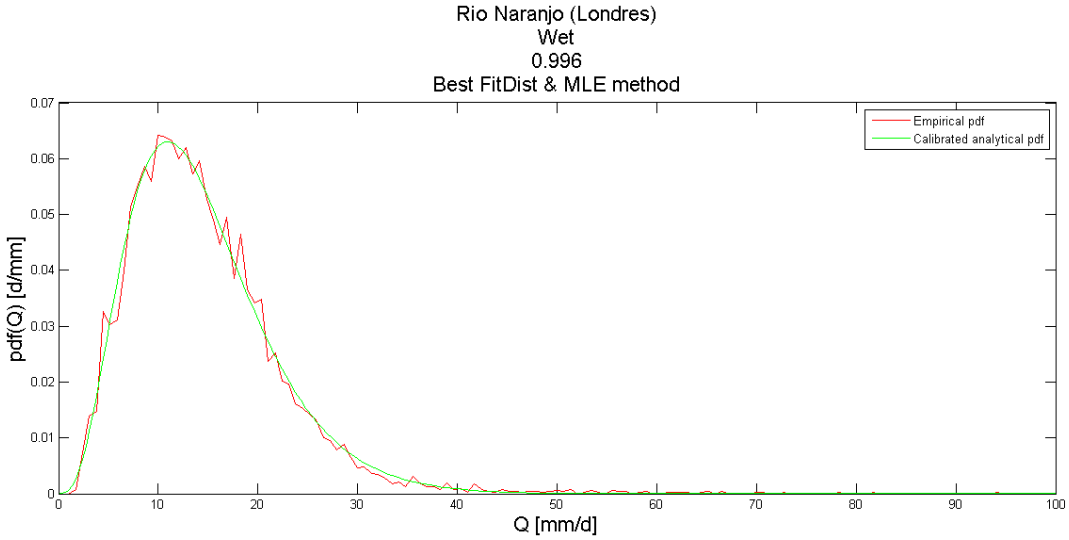

Figure III.63 – Rio Naranjo, Wet Season best-fitting calibrated pdf using best Q% removal method

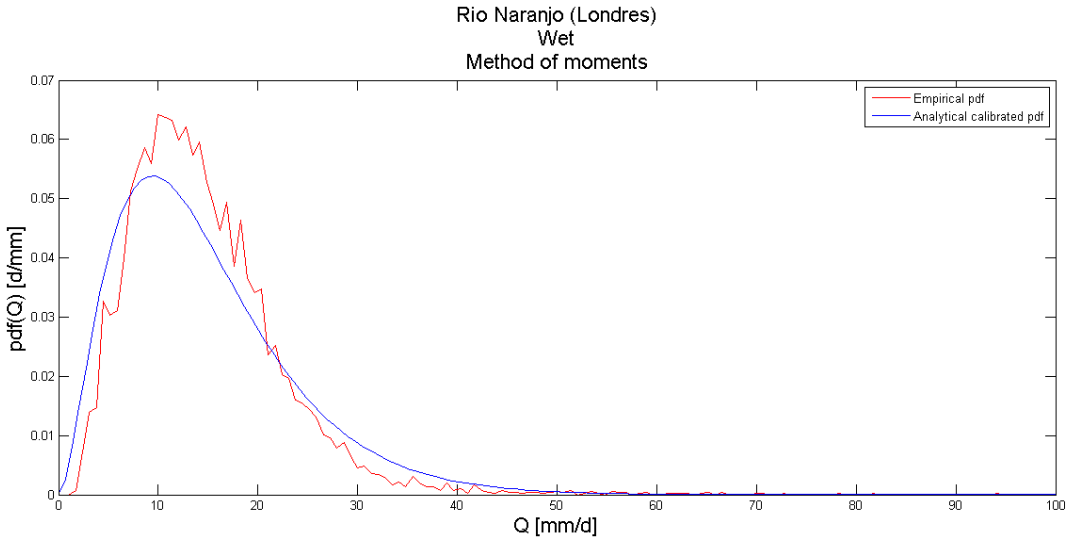

Figure III.64 – Rio Naranjo, Wet Season, calibrated pdf according to method of moments

The calibration method, which could be avoided considering the great performances of the theoretical model, was able to improve the SSD using the best Q% removal passing from 0.0006 to 0.00045 and considering a dataset of discharge equal to 99.6% of the total one, discarding 0.4% of the values corresponding to the most intense events. The SC calibration is not able to return an improvement of the performances being the final SSD equal to the initial one. The MLE shows a slight improvement and the method of moments decreases the performances, being the associated SSD higher than the initial value.

MLE		**SC**		**Best Q% removal**				**Method of moments**	
$\Delta_1 = \Delta_2$	SSD	$\Delta_1 = \Delta_2$	SSD	%Q used	Δ_1	Δ_2	SSD	$\Delta_1 = \Delta_2$	SSD
0.9664	0.0005	1.0001	0.0006	**99.6**	**0.8798**	**0.8620**	**0.00045**	1.3183	0.0022

Table III.36 – Rio Naranjo. Wet season pdf after calibration results

3.4.5 – Rio Grande de Terraba

In the following figure III.65 the results obtained with non-calibrated model of the wet-season study of Rio Grande de Terraba is displayed.

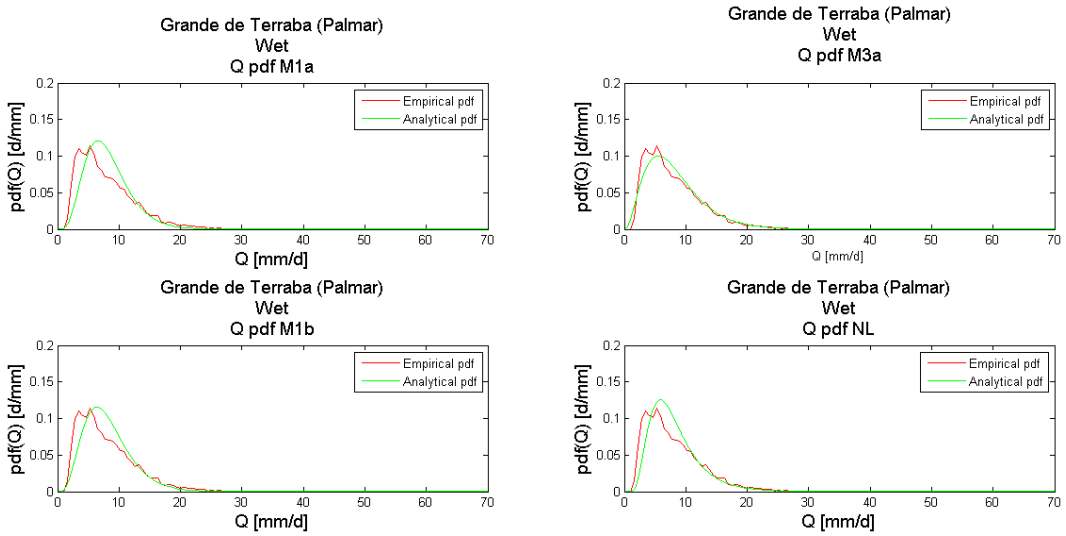

Figure III.65 – Rio Grande de Terraba, Wet Season pdf with different regression methods.

The graphical fitting with observed pdf reaches the maximum accuracy considering the theoretic curve deduced using the parameter estimated by the recession method M3a.

$<q>$ [mm/d]	8.1632	M1a SSD performance	0.0228
Var [mm^2/d^2]	34.2377	M1b SSD performance	0.0171
CV_Q [-]	0.7168	M3a SSD performance	**0.0052**
Best recession method	M3a	NL SSD performance	0.0180
α [mm]	20.9175	q min [mm/d]	1.32
λ [1/d]	0.3902	q max [mm/d]	154.27
k (M3a)	0.1272	q dataset length	6634

Table III.37 – Rio Grande de Terraba. Pdf pre-calibration results for wet season

The calibrated models are able to slightly improve the performances and, both MLE and best Q% removal methods will decrease the SSD associated. The best pdf can be obtained, on the other hand, with SC calibration which is able to lower the performance value from 0.0052 to 0.0035. The method of moments decreases the performances and returns a worst pdf in terms of SSD and its relative value passes from 0.0052 to 0.006.

The best Q% removal returns the same result obtained with the classic MLE calibration method, a result due to the optimal interval of dataset considered by the code, which is equal to the entire range of discharge values analyzed. The method of moments, on the other hand, even if it's not able to return the best fitting in terms of SSC is still able to give a good results, being the order of magnitude of the SSD equal to 10^{-3}.

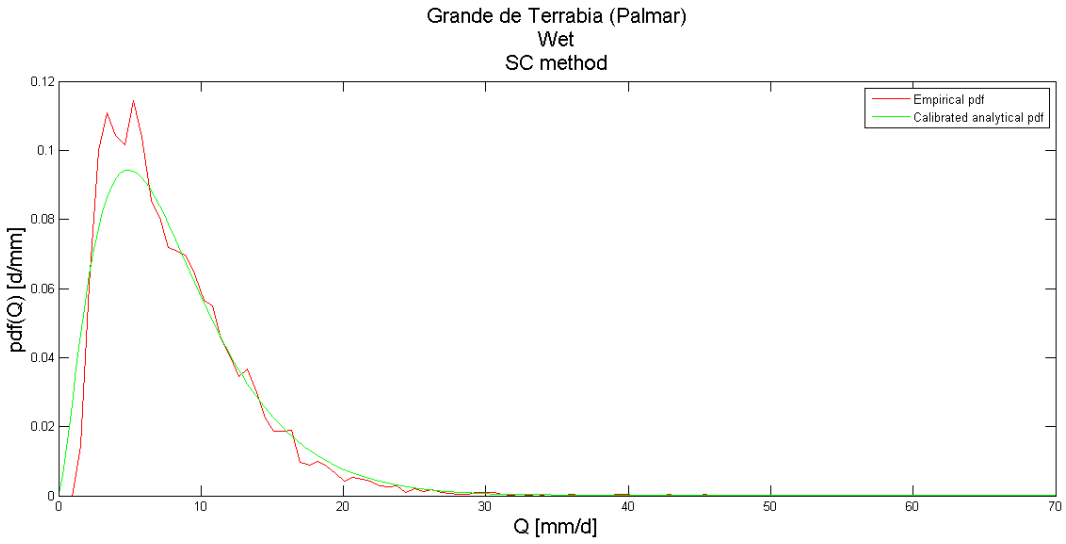

Figure III.66 – Rio Grande de Terraba, Wet Season best-fitting calibrated pdf using best Q% removal method

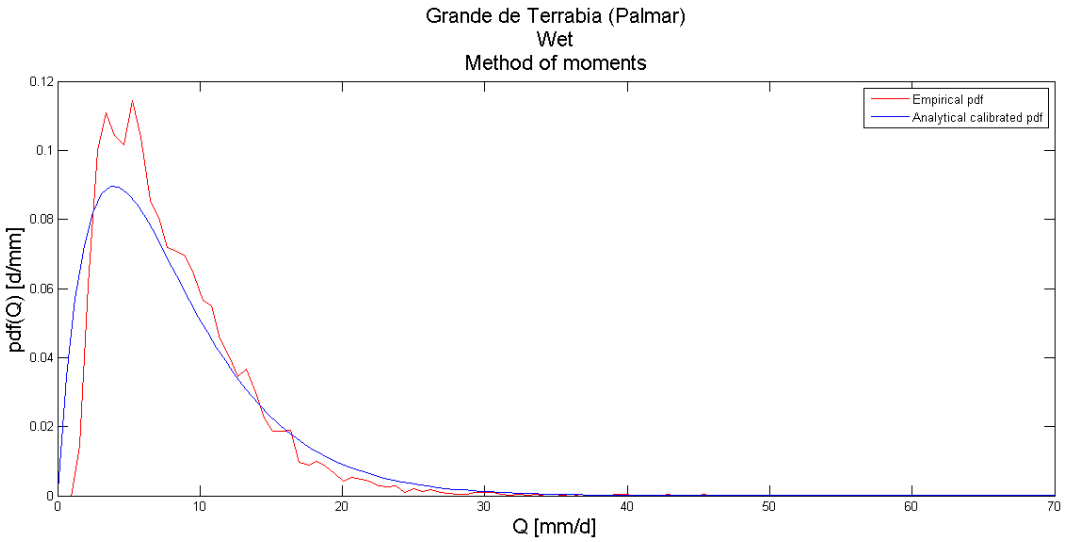

Figure III.67 – Rio Grande de Terraba, Wet Season, calibrated pdf according to method of moments

MLE		**SC**		**Best Q% removal**				**Method of moments**	
$\Delta_1 = \Delta_2$	SSD	$\Delta_1 = \Delta_2$	SSD	%Q used	Δ_1	Δ_2	SSD	$\Delta_1 = \Delta_2$	SSD
1.0656	0.0043	**1.2301**	**0.0035**	100	1.0656	1.0656	0.0043	1.5673	0.006

Table III.38 – Rio Grande de Terraba. Wet season pdf after calibration results

3.4.6 – Rio Pejibaye

In the following figure III.68 the results obtained with non-calibrated model of the wet-season study of Rio Pejibaye, on the Caribbean coast, is displayed.

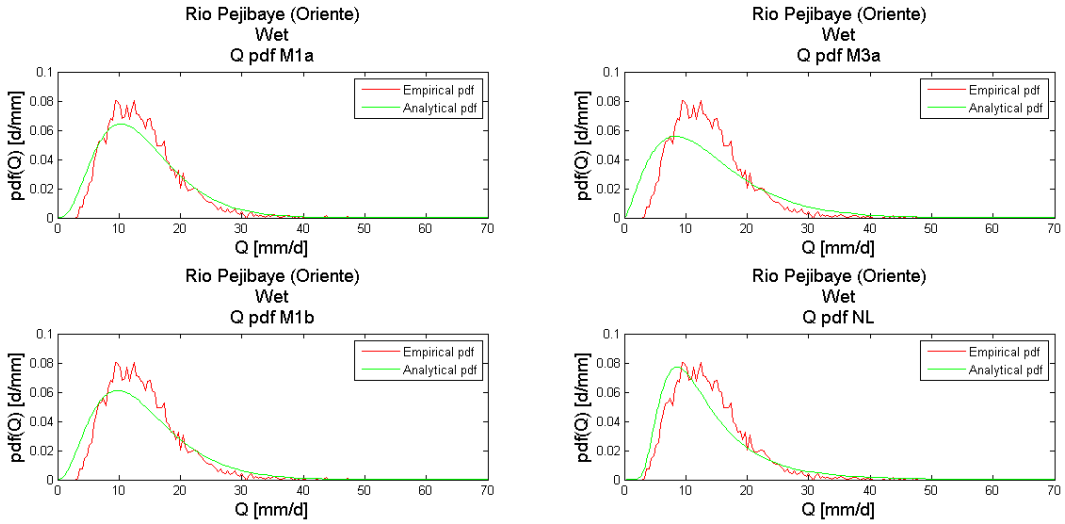

Figure III.68 – Rio Pejibaye, Wet Season pdf with different regression methods.

In this last basin analyzed during wet season the best theoretic pdf was obtained using the hydroclimatic parameters considered in the following table. The most performing hydrograph recession rate resulted to be the one deduced with a linear regression-fitting M1a technique.

$<q>$ [mm/d]	13.8339	M1a SSD performance	**0.0050**
Var [mm^2/d^2]	40.3499	M1b SSD performance	0.0086
CV_Q [-]	0.4592	M3a SSD performance	0.0194
Best recession method	M1a	NL SSD performance	0.0089
α [mm]	36.0549	q min [mm/d]	3.25
λ [1/d]	0.3836	q max [mm/d]	95.46
k (M1a)	0.0978	q dataset length	6634

Table III.39 – Rio Pejibaye. Pdf pre-calibration results for wet season

In this application the theoretical model is able to display a good graphical fitting, which find correspondence with the low SSD values estimated for different regression-evaluation methods.

The successively performed calibrations are able to increase slightly the performances and to give a consequent SSD decrease. The best calibrated pdf is obtained through the best Q% removal method, in which only 0.2% of the dataset was discarded, obtaining a final SSD of 0.0014.

The method of moments is able to improve the performances as well, passing from an initial SSD of 0.005 to a final one of 0.0022. The SC calibration returns the worst pdf, with a relative SSD of 0.0059, even higher than the initial one.

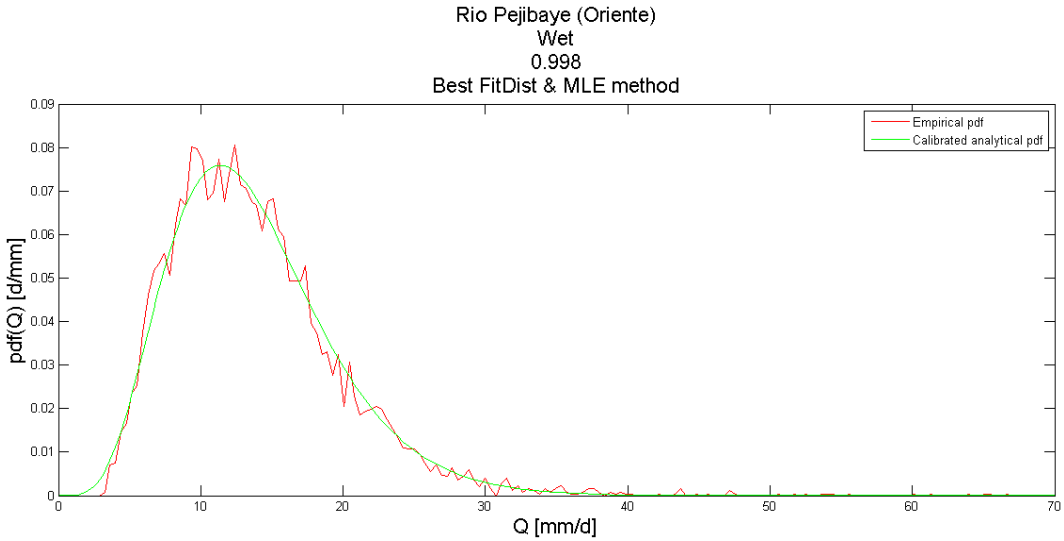

Figure III.69 – Rio Pejibaye, Wet Season best-fitting calibrated pdf using best Q% removal method

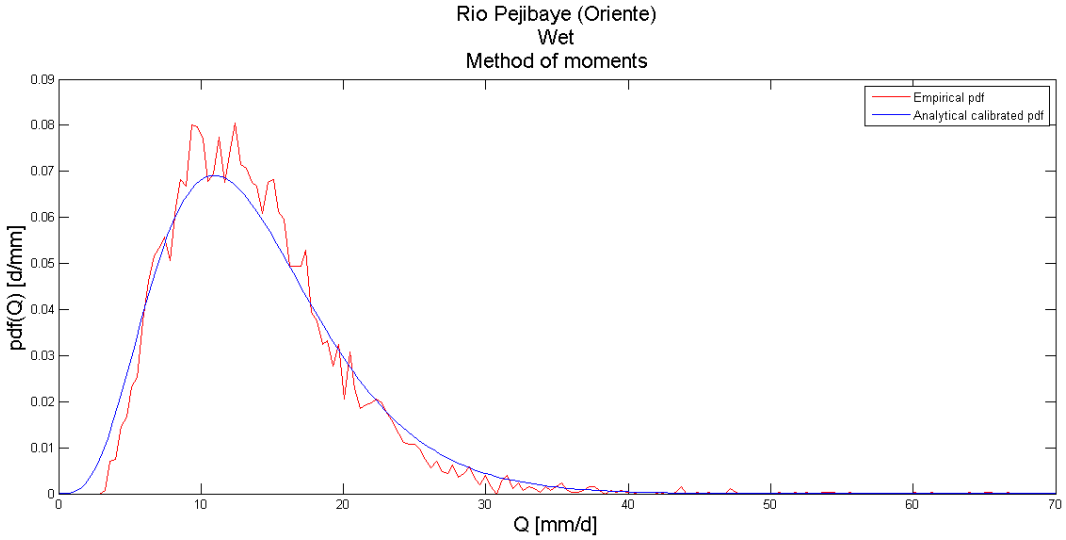

Figure III.70 – Rio Pejibaye, Wet Season, calibrated pdf according to method of moments

MLE		**SC**		**Best Q% removal**				**Method of moments**	
$\Delta_1 = \Delta_2$	SSD	$\Delta_1 = \Delta_2$	SSD	%Q used	Δ_1	Δ_2	SSD	$\Delta_1 = \Delta_2$	SSD
0.7031	0.0015	1.0001	0.0059	**99.8**	**0.6703**	**0.6650**	**0.0014**	0.8264	0.0022

Table III.10 – Rio Pejibaye. Wet season pdf after calibration results

3.4.7 – Summary table

In the following table all the properties deduced by the analytical study of the basins using the datasets and considering only the wet-season data will be showed. The table will display the SSD deduced from the theoretical model according to different regression methods, the moments of the observed distribution and the consequence of the calibration, according different methods. The final columns express the CV deduced by the pdf obtained after SC and best %Q removal calibrations.

River	Dataset information			Before calibration			After Calibration										Best calibration	Performance increasing (%)	$(k/\lambda)^{1/2}$ calibrated model	
	Mean [mm/d]	*Variance [mm^2/d^2]*	CV_Q	Best recession method	SSD	$(k/\lambda)^{1/2}$ theoretical model	*MLE*		*SC*		*Best Q% removal*				*Method of moments*				*SC*	*Q%*
							Δ	SSD	Δ	SSD	%Q Used	Δ_1	Δ_2	SSD	Δ	SSD				
Rio Frio (Guatuso)	13.40	107.672	0.77	NL	*0.0010*	0.5421	1.12	0.007	1.00	0.0073	**93.6**	**0.65**	**0.55**	**0.0029**	2.03	0,0188	Best Q (M1b)	60.26	0.5421	0.4384
Rio San Carlos (Terron Colorado)	8.38	24.228	0.58	M1a	0.0113	0.4576	1.06	0.0121	1.00	0.0113	**95.8**	**0.70**	**0.64**	**0.0040**	1.64	0,0281	BestQ	64.61	0.4576	0.3840
Rio Sarapiqui (Cariblanco)	13.15	79.008	0.67	NL	*0.0010*	0.4357	1.26	0.0249	1.00	0.0227	**91.6**	**0.52**	**0.44**	**0.0077**	2.40	0,0463	BestQ (M1a)	65.82	0.4357	0.3164
Rio Tempisque (Guardia)	3.13	25.127	1.60	M3a	0.3013	0.6640	1.65	0.2672	1.42	0.2602	**90.8**	**0.61**	**0.39**	**0.1204**	5.81	inf	BestQ	60.01	0.7920	0.5188
Rio Tenorio (Rancho Rey)	3.28	8.736	0.89	NL	*0.0064*	0.6575	0.82	0.280	1.00	0.3222	**92.0**	**0.36**	**0.29**	**0.1252**	1.87	0,6372	BestQ (M3a)	61.13	0.6576	0.3954
Rio Barranca (Guapinol)	6.59	43.486	0.99	M3a	0.0158	0.7001	1.00	0.0158	1.13	0.0151	**96.4**	**0.74**	**0.65**	**0.014**	2.03	0,0281	BestQ	8.317	0.7452	0.6046
Rio Poas (Tacares)	6.28	9.006	0.47	M3a	0.0403	0.4794	0.88	0.0434	**1.00**	**0.0403**	100	0.88	0.88	0.0434	0.99	0,0404	SC	0	0.4794	0.4519
Rio G.Candelaria (El Rey)	6.10	38.676	1.01	M3a	0.0307	0.6721	1.32	0.0212	1.42	0.0207	**95.4**	**0.98**	**0.82**	**0.0177**	2.29	inf	BestQ	42.30	0.8032	0.6661
Rio Naranjo (Londres)	14.73	78.185	0.60	M3a	0.0006	0.5227	0.96	0.0005	1.00	0.0006	**99.6**	**0.87**	**0.86**	**0.0004**	1.31	0,0022	BestQ	24.63	0.5227	0.4902
Rio Savegre (Providencia)	6.64	22.828	0.71	M3a	0.0552	0.4982	1.58	0.0224	1.59	0.0223	**96.2**	**1.29**	**1.17**	**0.0181**	2.08	0,0294	BestQ	67.09	0.6302	0.5663
G. de Terraba (Palmar)	8.16	34.237	0.71	M3a	0.0052	0.5710	1.06	0.0043	**1.23**	**0.0035**	100	1.06	1.06	0.0043	1.57	0,006	SC	32.07	0.6333	0.5895
Rio Coto Brus (Caracucho)	7.83	29.112	0.68	M3a	0.0115	0.5576	1.07	0.0104	**1.18**	**0.0098**	99.2	0.96	0.93	0.0102	1.52	0,0137	SC	14.74	0.6067	0.5469
Rio Reventazon (Palomo)	10.78	30.003	0.50	NL	0.0998	0.4890	0.78	0.0105	1.00	0.0165	**96.0**	**0.55**	**0.51**	**0.0051**	1.07	0,0196	BestQ (M1a)	68.94	0.4890	0.3651
Rio Pejibaye (Oriente)	13.83	40.349	0.45	M1a	0.0050	0.5050	0.70	0.0015	1.00	0.0050	**99.8**	**0.67**	**0.66**	**0.0014**	0.82	0,0022	BestQ	71.53	0.5051	0.4135
Rio Pacuare (Dos Montanas)	8.85	25.596	0.57	NL	0.0117	0.4676	0.94	0.0144	1.00	0.0154	**96.6**	**0.66**	**0.61**	**0.0072**	1.49	0,0344	BestQ (M1a)	53.11	0.4676	0.3815
Rio Banano (Asunciòn)	13.89	202.812	1.02	NL	0.0129	0.6518	1.10	0.0072	1.00	0.0071	**92.8**	**0.56**	**0.43**	**0.0031**	2.47	inf	BestQ (M1b)	55.20	0.6527	0.4885
Rio Estrella (Pandora)	6.48	109.734	1.61	M3a	0.0172	0.8461	1.00	0.0172	1.12	0.0168	**96.0**	**0.57**	**0.44**	**0.0121**	3.64	inf	BestQ	29.73	0.8954	0.6425
Rio Telire (Bratsi)	7.52	21.107	0.61	NL	*0.0056*	0.4389	1.10	0.0113	1.00	0.0107	**97.0**	**0.76**	**0.71**	**0.0062**	1.93	0,033	BestQ (M1a)	41.72	0.4390	0.3839

Table III.41 – Wet season analysis. Initial dataset information, best recession and its corresponding SSD value before calibration, correction parameters and SSD values obtained after calibration.

3.4.8 – Streamflow regime characterization

As well as for the annual streamflow characterization and dry season study it's possible to deduce some qualitative and quantitative considerations about the theoretical model, the calibration methods applied, the pre and after-calibration performances and the characterization of streamflow regimes related to the analyzed catchments.

- The best linear method for the estimation of the hydrograph recession rate, *k*, is obtained most of the time with the linear M3a recession, which resulted the most performing method for 50% of total cases. The other 9 catchments obtained a better fitting using the non-linear method (7 cases) and M1a (2 cases);
- As for the annual and wet-season characterization of the streamflow, the initial theoretical model is not able to give a value of the square root of the ratio k/λ equal to the coefficient of variation obtained by the empirical dataset. This consequence leads to a not perfect correspondence between *erratic* and *persistent* streamflow regimes and the uncalibrated model shows in the plot CV_Q Vs $(k/\lambda)^{0.5}$ couples of values which are not able to find a 1=1 association. Usually the $(k/\lambda)^{0.5}$ deduced from the model underestimates the coefficient of variation calculated using solely the daily discharge dataset;
- For the wet season characterization the best method able to return a better-fitting pdf to the empirical data is given by the best Q% removal method. It's important to spot how, when non-linear theoretical model showed better performances than the other linear techniques, the calibration was applied on the most performing linear model (the one with smallest SSD). When the best theoretical fitting is obtained from non-linear model, the calibrated linear model was indicated in round parenthesis in the "*Best calibration*" column;
- Even if the calibration is always able to improve the performances of the linear model (see the column "*Performance increasing*") it's not always true that the linear model is then able to express better performances than the non-linear method. In fact, let's focus the sight on those catchments which have a good initial theoretical fitting with the non-linear model (Rio Frio, Rio Sarapiqui, Rio Tenorio, Rio Reventazon, Rio Pejibaye, Rio Pacuare, Rio Banano, Rio Telire) in the column "*Before Calibration – Best recession method*". Their correspondent SSD is, sometimes, smaller than the SSD deduced by the best linear-calibrated model. These case were underlined in the column using a cursive font;
- The *inf* value expressed in some results of the method of moments, as underlined before in section 3.2.8 and 3.3.8 gives a quick indication about the streamflow regime and underline its *erratic* behavior, expressed also by a value higher than 1 in the "*Dataset information* – CV_Q" column.

According to the considerations done in section 3.2.8 about the perfect definition of a certain streamflow regime, it's possible to analyze how the different calibration methods are able to give different performances in terms of CV_Q and $(k/\lambda)^{0.5}$ correspondence.

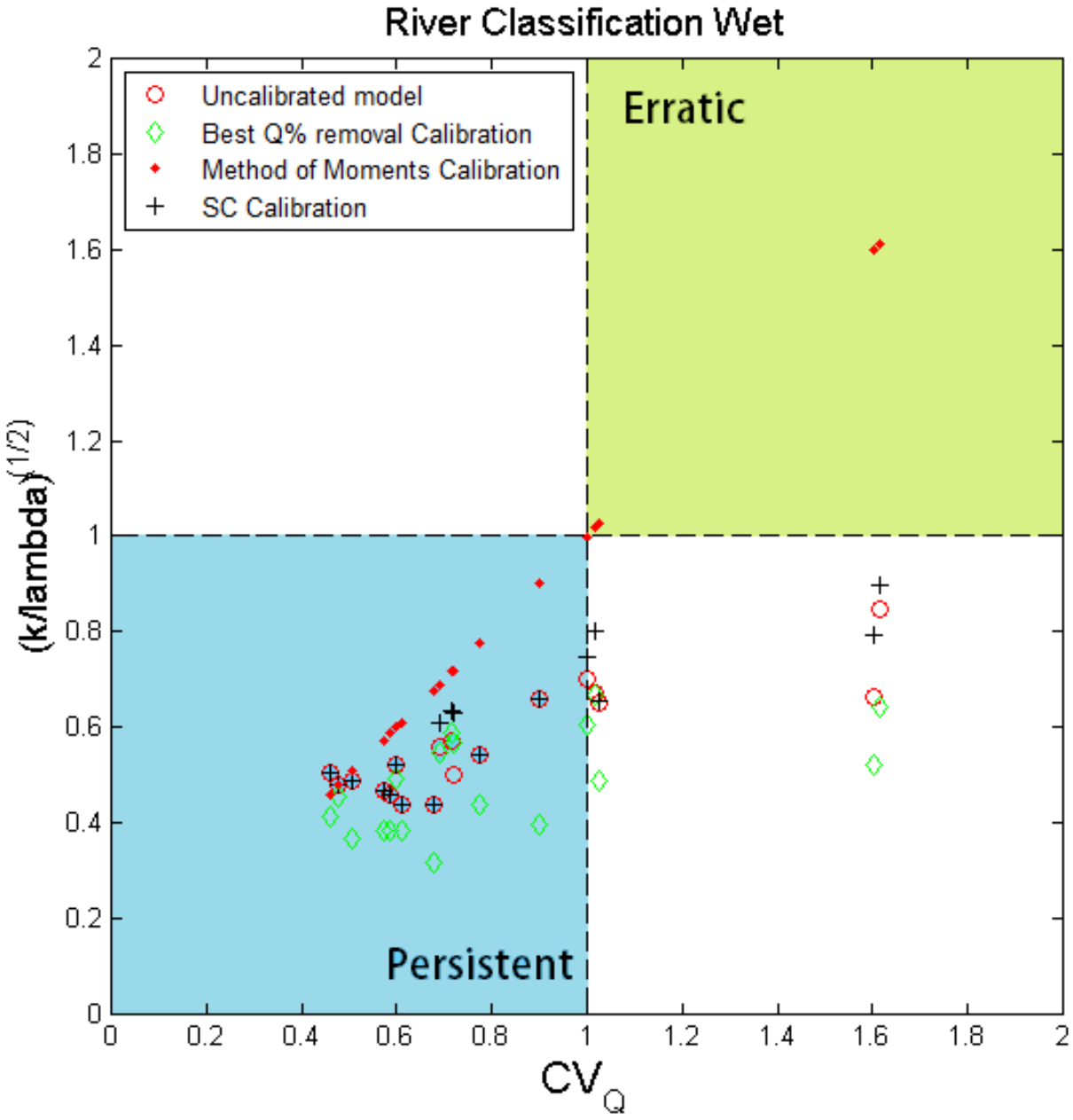

Figure III.71 – Wet season streamflow characterization through CV_Q *Vs* $(k/\lambda)^{1/2}$ plots for non-calibrated model and for different calibration options.

A qualitative and graphical Costa Rican dry-season streamflow regime characterization can be done looking at the previous plots while, to make an analytical one, is sufficient to observe the difference between the values expressed in the columns "*Dataset information – CV_Q*" and "*CV calibrated model – SC/Q%*". The SC calibration is not able to "fix" the correspondence required by equation I.17 in order to obtain a perfect

streamflow regime definition and the theoretical model lacks accuracy as well. With or without SC calibration all the rivers show analytically a *persistent* regime, even if the empirical data CV_Q define some of them as *erratic*. Moreover, as for the dry season study, the best Q% removal shows the negative aspect of a reduced-streamflow analysis: the discard of high values discharge causes an underestimation of the k over λ ratio which leads, as consequence, to a worst correspondence with the observed CV_Q. The only calibrated pdfs able to show a perfect link between an analytical characterization of the streamflow regime and empirical one are the one deduced using the method of moments, even if the related pdf and SSD shows the worst performances.

Chapter 4 – Discussion

This thesis work was able to show different application of the stochastic model introduced by Botter et al. [2007a, 2007b, 2008, 2009] in 18 catchments in Costa Rica in different climatic regions and considering an annual/seasonal subdivision. Thanks to a stochastic analysis on daily streamflow datasets and to the assumption that every streamflow increase can be assumed as a response triggered by an effective precipitation, it was possible to deduce the main frequency of effective precipitation events, λ, setting it equal to the main frequency of the streamflow jumps, calculated for every basin at annual and seasons time scales. Thus, the main rainfall intensity, α, could be deduced thanks to the equation I.18. In this way it was possible to bypass the lack of rainfall data series. The last parameter of the model, the hydrograph recession rate k, for a linear storage-discharge relationship, or K and a, for a non-linear storage-discharge assumption, were then deduced according to the methods described in sections 1.3.1 and 1.3.2. according to the analytical results obtained from the application of the model it is possible to say that the linear regression studied with the M3a method was able to give, for the annual study of the pdf, the better results and it can be considered as the most performing method in absence of a seasonal subdivision of the dataset. When the seasonal characterization is studied the M3a method is no more the only best-performing method and the non-linear approach is able to give better performances around 50% of the times during dry and wet season study.

It's important to underline how, passing from an annual time interval to a seasonal catheterization or the streamflow, allows the analytical pdf to reproduce better the empirical pdf curve improve the fitting and, therefore, give a more accurate representation of the streamflow regime and its properties.

The analytical pdfs were then built and their capacity to fit to the empirical pdf was estimated using, as performance method, a *sum of squared difference* calculation. Successively the most performing linear model was calibrated according to the methods in section 1.5 and the new-calibrated pdf was a-posteriori compared with the observed data pdf in order to evaluate the increment of performance. The model allowed a streamflow regime classification subdivision into *erratic* and *persistent* [Botter et al., 2013] basing this definition on the correspondence between the coefficient of variation, CVq, directly deduced by the streamflow dataset and the ratio $(k/\lambda)^{0.5}$ in which k and λ are, respectively, the hydrograph recession rate and the frequency of effective precipitation events of the pure-theoretical model or the calibrated one.

A summary of the streamflow regime characterization can be obtained in the following table, able to display and reassume the kind of regime according to empirical dataset, uncalibrated model and different calibrated models.

According to different calibration method it is possible to obtain different $(k/\lambda)^{0.5}$ ratios and the characterization of the 18 basins can be reassumed in the following table in which the streamflow regime is defined for not-calibrated and calibrated models and for every time interval considered (annual and seasonal). It's evident to see how the only calibration method able to find a direct correspondence with the regime define by empirically defined *CVq* was the method of moments one. The SC calibration is able to return an increment in term of regime definition being the $(k/\lambda)^{0.5}$ factor deduced after this calibration more coherent than the not-calibrated theoretical model one. The best Q% removal is, on the other hand, the worse methods in terms of streamflow regime characterization: the relative $(k/\lambda)^{0.5}$ factors deduced for every basin are less coherent than the initial one performed by the theoretical model.

		Classification of streamflow regime according to											
River	**Time interval**	**Empirical data**		**Pre-calibration best-fitting linear model**			**Post-calibration**						
							SC		*Q%*		*Moments*		
		CVq	*Regime*	*Method*	$(k/\lambda)^{0.5}$	*Regime*	$(k/\lambda)^{0.5}$	*Regime*	$(k/\lambda)^{0.5}$	*Regime*	$(k/\lambda)^{0.5}$	*Regime*
Rio Frio (Guatuso)	Annual	0.931	Persistent	M3a	0.6986	Persistent	0.7585	Persistent	0.6974	Persistent	0.9317	Persistent
	Dry season	0.948	Persistent	M3a	0.6423	Persistent	0.653	Persistent	0.4642	Persistent	0.9488	Persistent
	Wet season	0.774	Persistent	M1b	0.5421	Persistent	0.5421	Persistent	0.4384	Persistent	0.7741	Persistent
Rio San Carlos (Terron Colorado)	Annual	0.716	Persistent	M3a	0.6161	Persistent	0.6481	Persistent	0.6101	Persistent	0.7167	Persistent
	Dry season	0.659	Persistent	M3a	0.5971	Persistent	0.5971	Persistent	0.4174	Persistent	0.6593	Persistent
	Wet season	0.587	Persistent	M1a	0.4576	Persistent	0.4576	Persistent	0.384	Persistent	0.5871	Persistent
Rio Sarapiqui (Cariblanco)	Annual	0.798	Persistent	M3a	0.5854	Persistent	0.5854	Persistent	0.5111	Persistent	0.7984	Persistent
	Dry season	0.835	Persistent	M3a	0.5791	Persistent	0.5791	Persistent	0.4268	Persistent	0.8357	Persistent
	Wet season	0.675	Persistent	M1a	0.4357	Persistent	0.4357	Persistent	0.3164	Persistent	0.6757	Persistent
Rio Tempisque (Guardia)	Annual	1.83	Erratic	M3a	0.6463	Persistent	0.9301	Persistent	0.6172	Persistent	1.8361	Erratic
	Dry season	1.753	Erratic	M2	0.4147	Persistent	0.6327	Persistent	0.5115	Persistent	1.7535	Erratic
	Wet season	1.60	Erratic	M3a	0.664	Persistent	0.792	Persistent	0.5188	Persistent	1.6008	Erratic
Rio Tenorio (Rancho Rey)	Annual	0.95	Persistent	M3a	0.6595	Persistent	0.6595	Persistent	0.4536	Persistent	0.9539	Persistent
	Dry season	0.681	Persistent	M2	0.439	Persistent	0.4658	Persistent	0.3542	Persistent	0.6816	Persistent
	Wet season	0.899	Persistent	M3a	0.6575	Persistent	0.6576	Persistent	0.3954	Persistent	0.8999	Persistent
Rio Barranca (Guapinol)	Annual	1.256	Erratic	M3a	0.6817	Persistent	0.9999	Persistent	0.8845	Persistent	1.2561	Erratic
	Dry season	1.044	Erratic	M3a	0.6306	Persistent	0.6572	Persistent	0.3838	Persistent	1.0447	Erratic
	Wet season	0.999	Persistent	M3a	0.7001	Persistent	0.7452	Persistent	0.6046	Persistent	0.9998	Persistent

Rio Poas (Tacares)	Annual	0.625	Persistent	M3a	0.4693	Persistent	0.5937	Persistent	0.4994	Persistent	0.6253	Persistent
	Dry season	0.328	Persistent	M1a	0.2706	Persistent	0.2766	Persistent	0.2353	Persistent	0.3284	Persistent
	Wet season	0.477	Persistent	M3a	0.4794	Persistent	0.4794	Persistent	0.4519	Persistent	0.4775	Persistent
Rio G.Candelaria (El Rey)	Annual	1.323	Erratic	M3a	0.6543	Persistent	0.9999	Persistent	0.9796	Persistent	1.3233	Erratic
	Dry season	1.082	Erratic	M3a	0.524	Persistent	0.5935	Persistent	0.4235	Persistent	1.0823	Erratic
	Wet season	1.018	Erratic	M3a	0.6721	Persistent	0.8032	Persistent	0.6661	Persistent	1.0188	Erratic
Rio Naranjo (Londres)	Annual	0.821	Persistent	M3a	0.5432	Persistent	0.876	Persistent	0.7656	Persistent	0.8218	Persistent
	Dry season	0.620	Persistent	M3a	0.5423	Persistent	0.5423	Persistent	0.3634	Persistent	0.6201	Persistent
	Wet season	0.600	Persistent	M3a	0.5227	Persistent	0.5227	Persistent	0.4902	Persistent	0.6001	Persistent
Rio Savegre (Providencia)	Annual	0.934	Persistent	M3a	0.5129	Persistent	0.7933	Persistent	0.6567	Persistent	0.9343	Persistent
	Dry season	0.577	Persistent	M3a	0.4127	Persistent	0.4244	Persistent	0.3373	Persistent	0.5777	Persistent
	Wet season	0.718	Persistent	M3a	0.4982	Persistent	0.6302	Persistent	0.5663	Persistent	0.7188	Persistent
G. de Terraba (Palmar)	Annual	0.981	Persistent	M3a	0.5807	Persistent	0.999	Persistent	0.8596	Persistent	0.9812	Persistent
	Dry season	0.999	Persistent	M3a	0.5361	Persistent	0.672	Persistent	0.4152	Persistent	0.9993	Persistent
	Wet season	0.716	Persistent	M1a	0.571	Persistent	0.6333	Persistent	0.5895	Persistent	0.7149	Persistent
Rio Coto Brus (Caracucho)	Annual	0.922	Persistent	M3a	0.5418	Persistent	0.9066	Persistent	0.7938	Persistent	0.9224	Persistent
	Dry season	0.810	Persistent	M3a	0.4909	Persistent	0.5432	Persistent	0.357	Persistent	0.8107	Persistent
	Wet season	0.68	Persistent	M1a	0.5576	Persistent	0.6067	Persistent	0.5469	Persistent	0.689	Persistent
Rio Reventazon (Palomo)	Annual	0.696	Persistent	M1b	0.6294	Persistent	0.6644	Persistent	0.625	Persistent	0.6962	Persistent
	Dry season	0.886	Persistent	M3a	0.617	Persistent	0.617	Persistent	0.4335	Persistent	0.8862	Persistent
	Wet season	0.508	Persistent	M1b	0.489	Persistent	0.489	Persistent	0.3651	Persistent	0.508	Persistent
Rio Pejibaye (Oriente)	Annual	0.626	Persistent	M3a	0.6304	Persistent	0.6392	Persistent	0.5841	Persistent	0.6261	Persistent
	Dry season	0.794	Persistent	M3a	0.6299	Persistent	0.63	Persistent	0.4306	Persistent	0.7945	Persistent
	Wet season	0.459	Persistent	M3a	0.505	Persistent	0.5051	Persistent	0.4135	Persistent	0.4591	Persistent
Rio Pacuare (Dos Montanas)	Annual	0.744	Persistent	M3a	0.6438	Persistent	0.6439	Persistent	0.6122	Persistent	0.7439	Persistent
	Dry season	0.964	Persistent	M3a	0.6673	Persistent	0.6673	Persistent	0.4507	Persistent	0.9644	Persistent
	Wet season	0.571	Persistent	M1a	0.4676	Persistent	0.4676	Persistent	0.3815	Persistent	0.5713	Persistent
Rio Banano (Asunciòn)	Annual	1,0462	Erratico	M1b	0.5887	Persistent	0,6493	Persistent	0,4981	Persistent	1,0461	Erratic
	Dry season	1,0678	Erratic	M3a	0.6914	Persistent	0,6914	Persistent	0,4987	Persistent	1,0677	Erratic
	Wet season	1,0252	Erratic	M1b	0.6518	Persistent	0,6527	Persistent	0,4885	Persistent	1,0252	Erratic
Rio Estrella (Pandosa)	Annual	1,485	Erratic	M3a	0.8249	Persistent	0,8546	Persistent	0,6273	Persistent	1,4849	Erratic
	Dry season	1,3078	Erratic	M3a	0.8104	Persistent	0,7674	Persistent	0,5798	Persistent	1,3077	Erratic
	Wet season	1,6145	Erratic	M3a	0.8461	Persistent	0,8954	Persistent	0,6425	Persistent	1,6145	Erratic
Rio Telire (Bratsi)	Annual	0,6856	Persistent	M3a	0.5749	Persistent	0,5749	Persistent	0,5286	Persistent	0,6855	Persistent
	Dry season	0,7254	Persistent	M3a	0.5891	Persistent	0,5892	Persistent	0,5018	Persistent	0,7254	Persistent
	Wet season	0,6105	Persistent	M1a	0.4389	Persistent	0,4390	Persistent	0,3839	Persistent	0,6104	Persistent

Table III.42 – Streamflow regime characterization for all the catchment analyzed according to empirical data, theoretical uncalibrated pdf and calibrated pdf.

It’s possible to reassume the calibration characteristics in the following list:

- MLE and Fitdist calibration methods are able to return, most of the time, an increment in terms of SSD starting from the theoretically-based pdf. These methods can be considered as “safe calibrations” and, being already performed by MATLAB, they even don’t need long further study or computation. On the other hand, if compared with the other methods used, they are not able to best-fit the observed pdf and the related SSD is always higher than the one deduced by SC or best Q% removal methods.
- SC method resulted to be the best one in the annual calibration for many of the catchments and its performances are often better than the MLE method being able to return a SSD always lower, or at least equal, than the initial one defined by the theoretical model. Moreover, SC calibration is able to return new calibrated pdf parameters able to give a better result for the streamflow regime characterization defined by equation I.17. On the other hand this method shows lower results in term of SSD when it’s compared with the Best Q% removal calibration for a seasonal study. Moreover this method allowed to display how the magnitude of the correction parameter Δ is strictly dependent on the seasonality index of the catchments and, both for annual characterization and a seasonal one, all the river studied requires a stronger modification of the initial theoretical model when a stronger seasonality, displayed by high values of SI. The theoretical uncalibrated model can be considered, therefore, more reliable for those catchment with a SI lower than 1.5, for an annual characterization, and lower than 2.0 for a seasonality study;

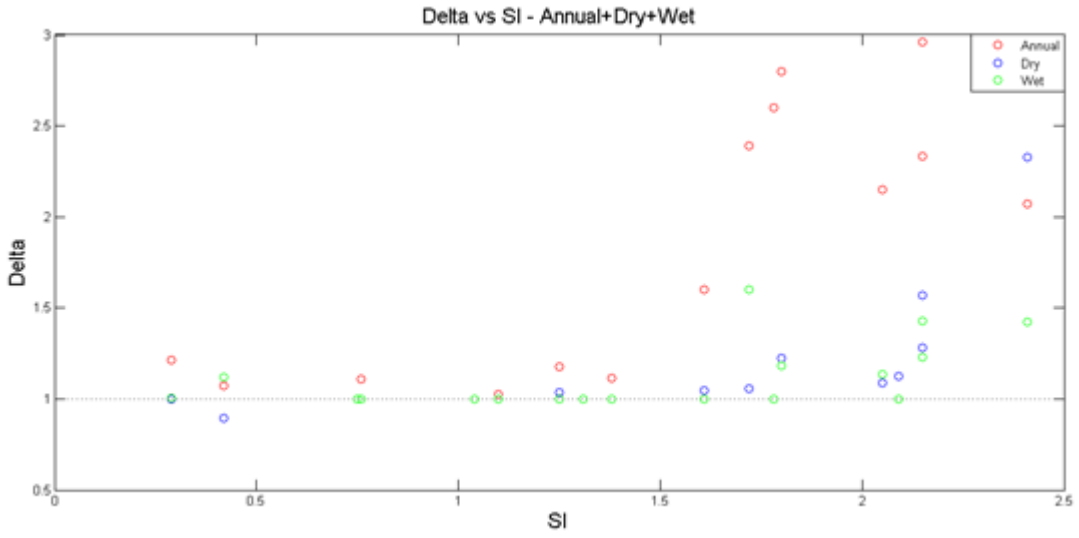

Figure IV.72 - *SI vs* Δ after SC calibration for different time intervals

This property can be underlined studying the pdf of the different Δ deduced in every application. It’s possible to spot, another time, a gamma behavior pdf in which the most probable value of the correction factor is given by the 1. This results underlines the reliability of the theoretical uncalibrated model, but doesn’t consider the best-fitting correction parameters for a seasonality study

which are, on the contrary, obtained with the best Q% removal calibration method.

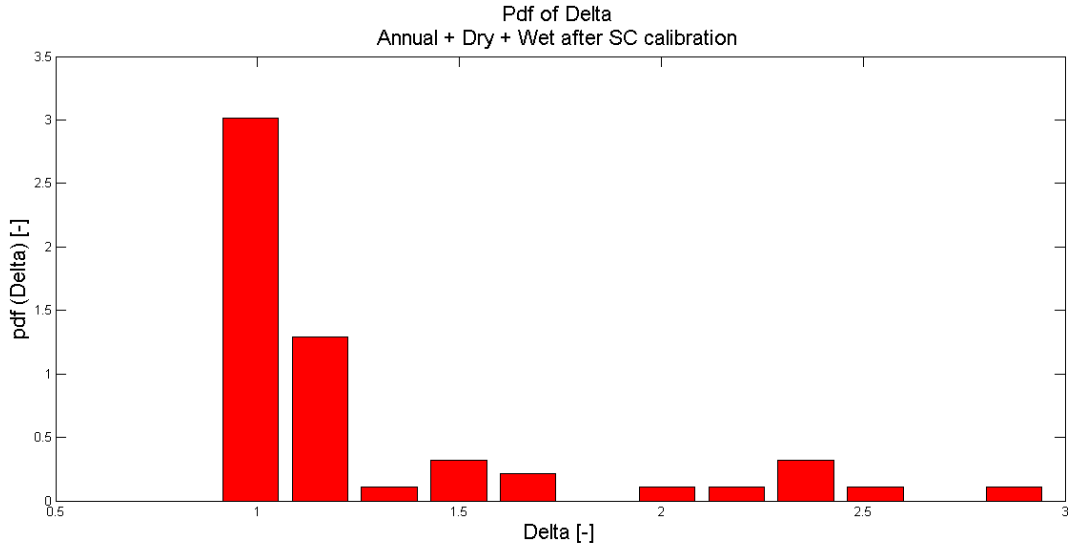

Figure IV.73 – *pdf(Δ)* after SC calibration considering every calibrated model (18 catchments for annual, dry season and wet season time interval)

- Best Q% removal calibration is able to return the best fit with the empirical pdf in terms of SSD for almost every catchment studied during the seasonality characterization. On the other hand this method represent the worst one when the relative $(k/\lambda)^{0.5}$ factors deduced for every basin are compared to the corresponding *CVq* coefficients: the result is a less effective linkage and a bad streamflow regime coherence, a result that can be appreciated both analytically (in the previous table) and graphically in the figures III.33, III.52 and III.71 in which the couples (*CVq*, $(k/\lambda)^{0.5}$) in the third plot are more away from the best result possible, which is represented by the bisector. The magnitude of the correction parameters Δ_1 and Δ_2 was correlated on the magnitude of the seasonality index and it's possible to spot how their value follow a slightly different behavior from the one deduced after SC calibration. The correction parameters tend to be more frequent on the $\Delta=0.5$ value when seasonality study are performed and their magnitude increases when the SI is higher than 1.5 and 2. The annual time step, on the contrary, shows a similar trend to the one underlined in figure IV.72: the average correction is 1 for SI<1.5, the dispersion increases as far the SI increases as well, a consequence that can be graphically observe in the following figure III.74.

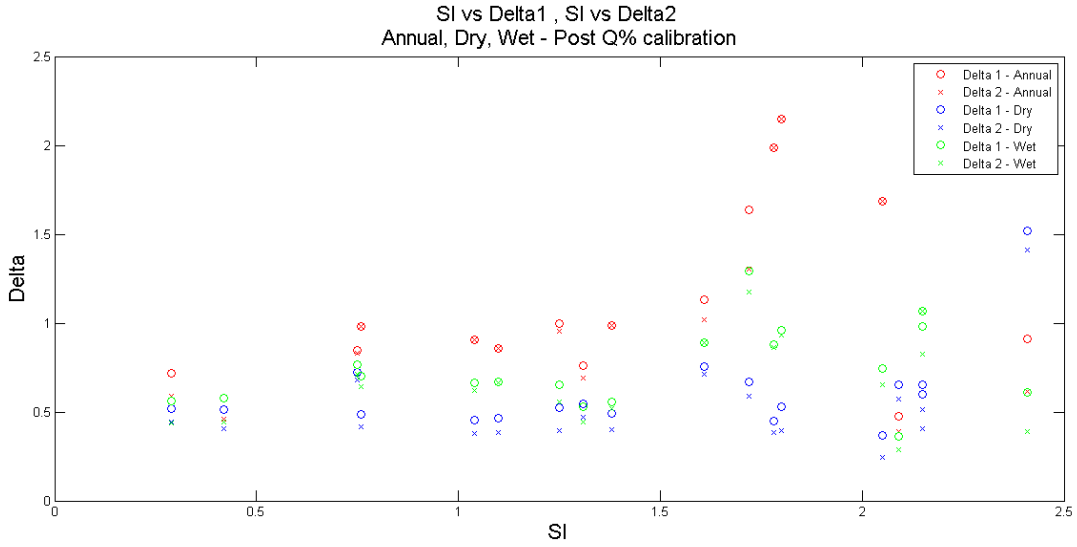

Figure IV.74 - *SI vs* Δ_1 and Δ_2 after Best Q% calibration for different time intervals

Moreover, the Pdf associated to the all Δ_1 and Δ_2 deduced after the Best Q% removal calibration is represented in the following figure:

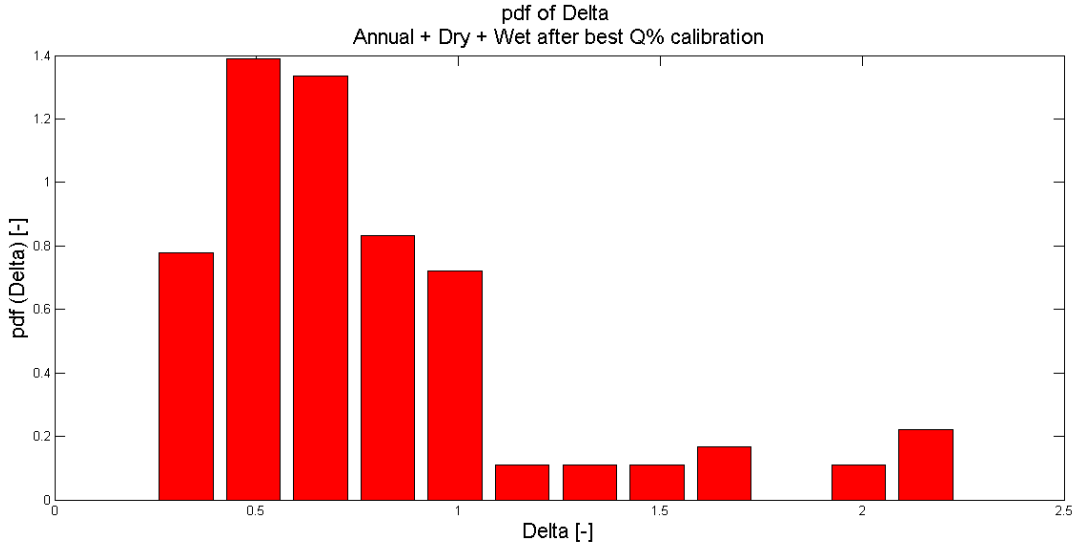

Figure IV.75 – *pdf(*Δ*)* after Best Q% removal calibration considering every calibrated model (18 catchments for annual, dry season and wet season time interval)

- The method of moments has the diametrically opposite problems and advantages of Best Q% removal calibration. It's indeed able to give the best correspondence in terms of flow regime characterization and the deduced parameters lead to a univocal link among *CVq* and $(k/\lambda)^{0.5}$, a result that can be appreciated both analytically using the table displayed in this section and the graphs showed in figure III.33, III.52 and III.71 in which all the points are able to display on the bisector. On the other hand this method shows the worst calibration, being its pdf not able to represent the observed data pdf and the

related SSD values deduced for every basin have a value higher than the non-calibrated model one.

It's interesting to spot another property of the model used: every calibration methods, except the Best Q% removal one, is able to return exactly the same value for every correction parameters (Δ_1 and Δ_2). What does it mean? The consequence to have a $\Delta_1=\Delta_2$ leads to an important property that can be showed recalling what was said in section 1.5.1. Remembering that r_1 and s_1 are, respectively rate and shape parameters of the calibrated model and that r and s are rate and shape parameter of the best-fitting uncalibrated model, if $\Delta_1=\Delta_2$ it's possible to write the following statement considering the equations in I.22:

$$\frac{s_1}{s} = \frac{r}{r_1}$$

Which leads to the following equation:

$$s_1 \cdot r_1 = r \cdot s$$

$$\frac{\lambda}{k} \cdot \alpha \cdot k = r \cdot s$$

Which leads to this property already introduced in previous equation I.29

$$\langle Q \rangle = r \cdot s \qquad \text{(I. 29)}$$

Now, the advantage of this consideration is that, if it exists a graphical trend between the calibrated rate parameter or shape parameter deduced by the observed basins it's possible to deduce automatically respectively the shape or the rate parameter as well: therefore an already-calibrated pdf of an unknown streamflow can be deduced solely knowing its mean discharge value, $<Q>$.

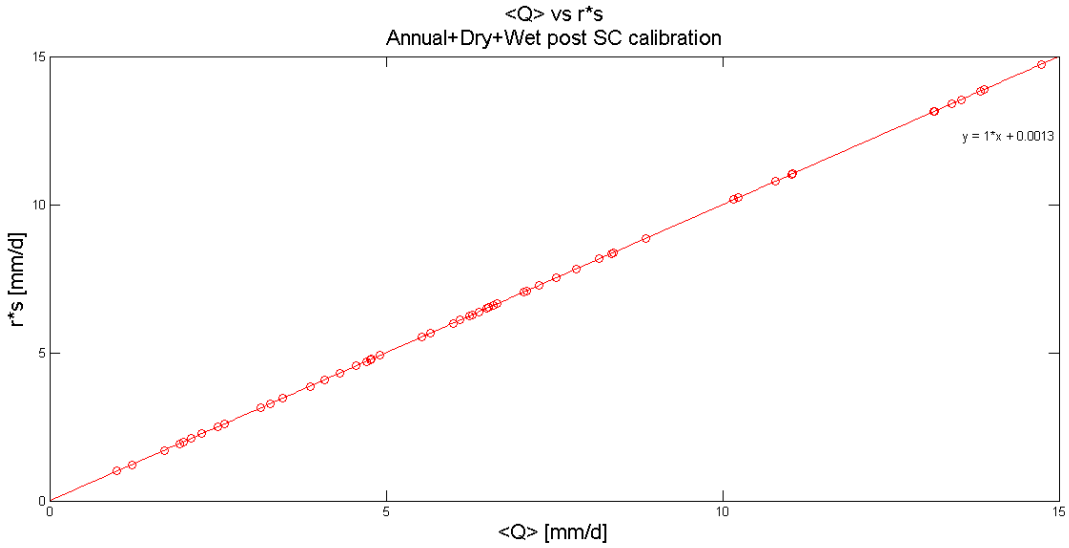

Figure IV.76 - $<Q>$ *vs* $r \cdot s$ relationship after SC calibration for different time intervals

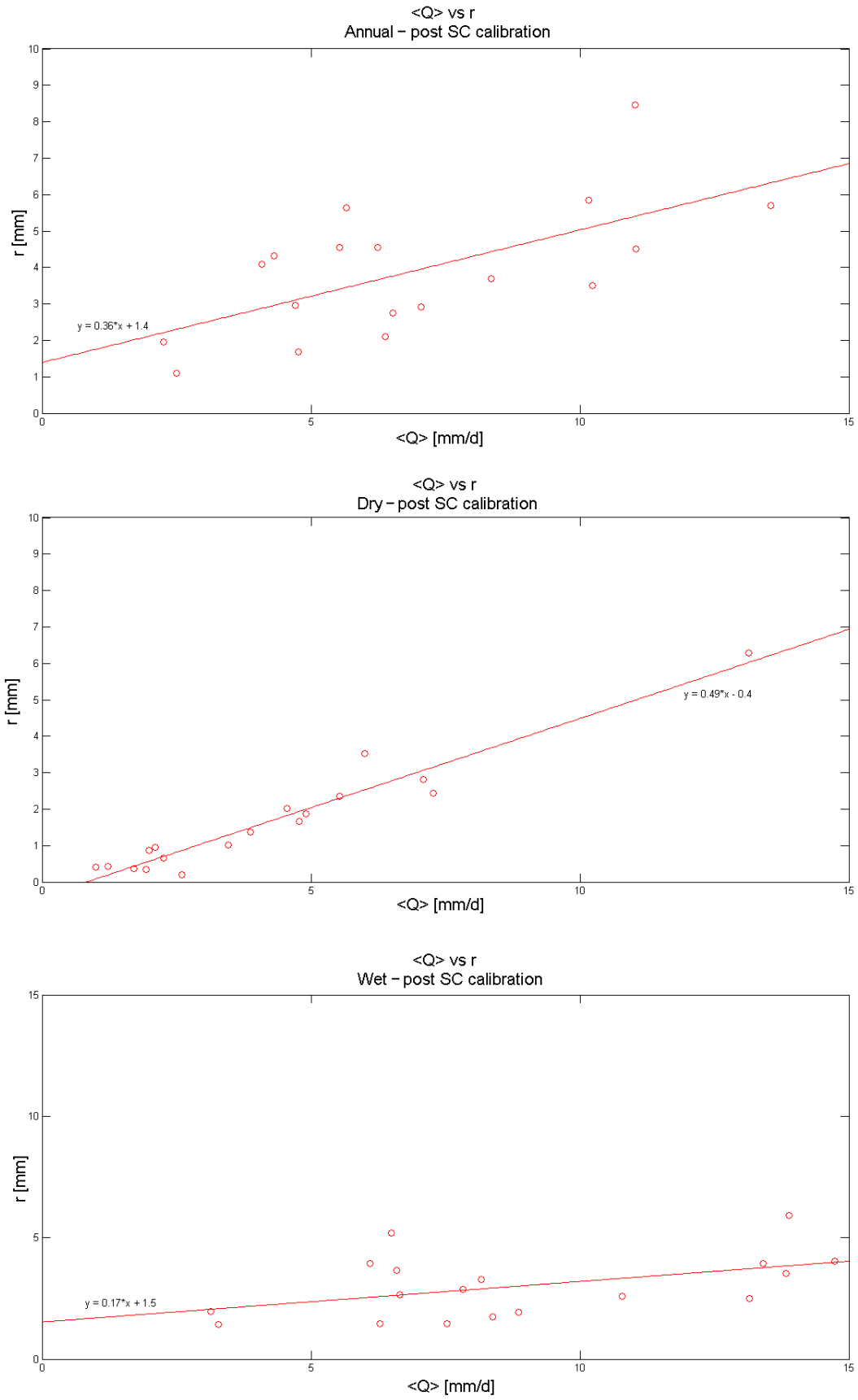

Figure IV.77 - <*Q*> *vs r* relationship after SC calibration for different time intervals

The <*Q*> *vs r·s* relationship was immediate and gives points in a <*Q*> *vs rs* which are almost not scattered at all around the bisector line. Therefore, regardless the time interval analyzed (annual, dry and wet) the final plots shows a perfect correspondence, as showed by the plot in figure IV.76.

As it is possible to observe from the plots in figure IV.77, <*Q*> *vs r* relationship is strictly dependent on the time series analyzed: for annual time interval the plot presents more scattered values than the plot obtained through a seasonal characterization, with the best correspondence obtained considering solely the dry season.

Therefore, if a certain deduced <*Q*> *vs r* plot for a certain hydroclimatic region can be considered reliable, it's possible to use it and, knowing the <*Q*> of another unknown nearby pristine catchment, deduce the relative rate parameter. Then, using a <*Q*> *vs rs* relationship (or plot, like the one in figure IV.76) the shape parameter can be deduced as well. In this way it's possible to roughly estimate for practical hydrological purposes the analytical (and already calibrated) pdf of a unknown catchment.

Collecting all the <*Q*> *vs r* for every time interval in a unique plot:

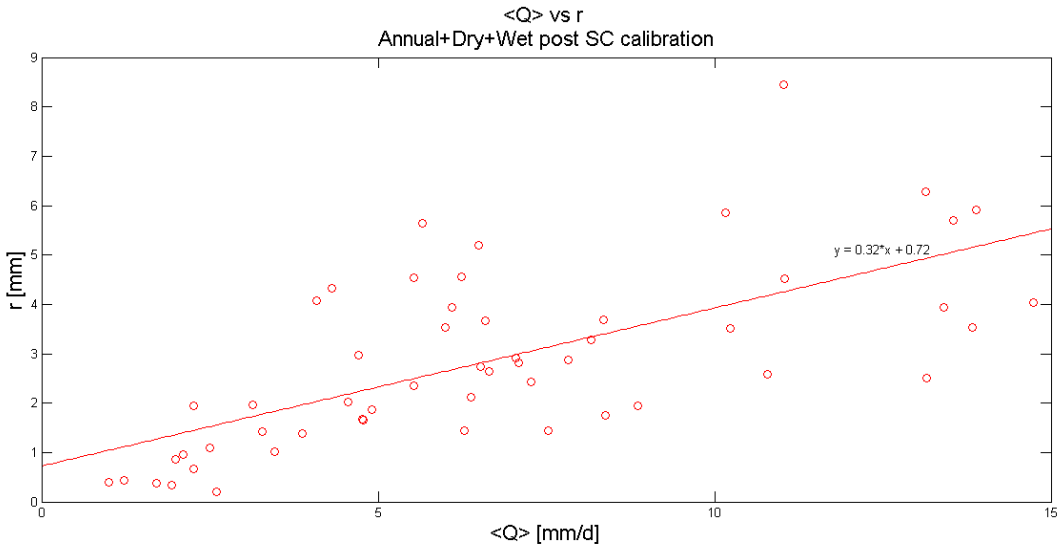

Figure IV.78 - <*Q*> *vs r* relationship after SC calibration for every time intervals

In which it's possible to observe how the relationship is not free of uncertainties and how these increases as the mean streamflow value increases as well. Therefore this method is not really reliable for big catchment or for streamflow with big discharge values, but it can be helpful to define the pdf related to the sub-catchments.

What happens when the Best Q% removal calibration is considered? This kind of calibration is able to change both shape and rate parameters being the deduced correction factors different from each other ($\Delta_1 \neq \Delta_2$). This consideration makes the I.29 equation not univocally defined and <*Q*> *vs r·s* relationship presents slightly scattered values:

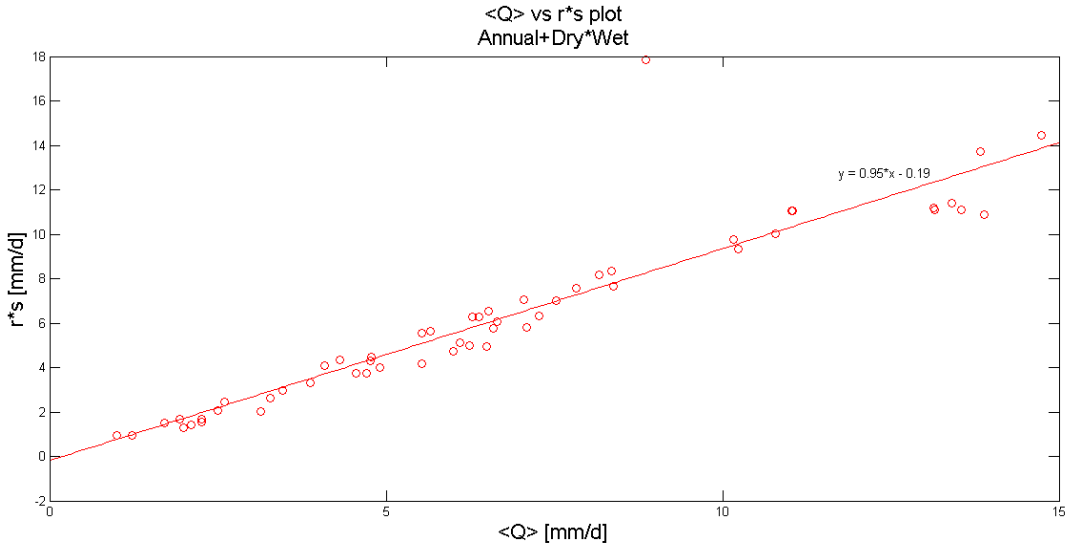

Figure IV.79 - <*Q*> *vs r·s* relationship after Best Q% removal calibration for different time intervals

And collecting all the <*Q*> *vs r* for every time interval in a unique plot :

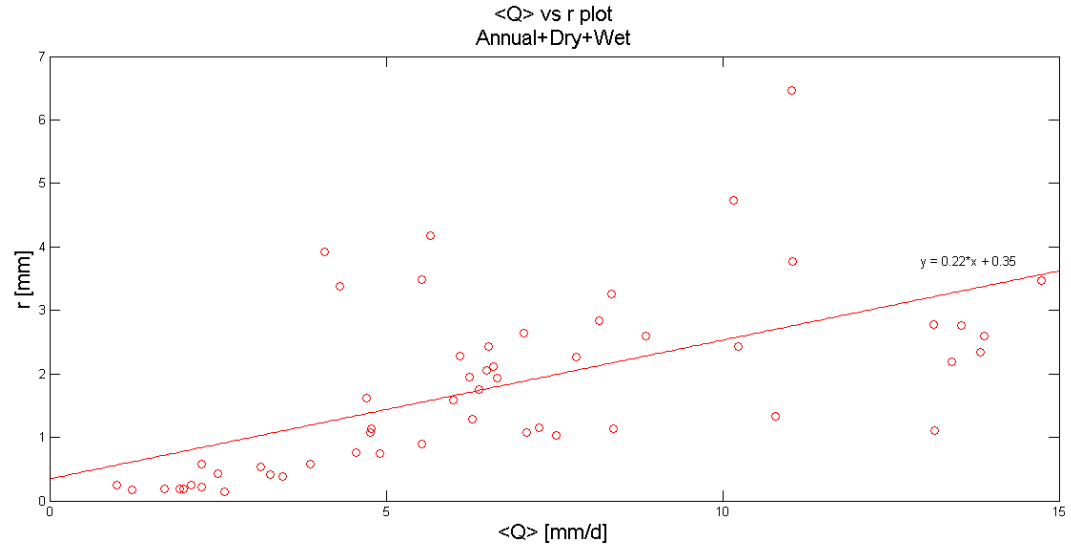

Figure IV.80 - <*Q*> *vs r·* relationship after Best Q% removal calibration for different time intervals

In which the most scattered value are related to the annual time interval. In fact, discarding the (<*Q*>, *r*) couples related to an annual study the line is able to give a better representation of the relationship in which a good representation can be observed especially for main discharge values lower than 7 mm/d, confirming how this method can be considered a reliable instrument especially for small catchments or sub-catchments:

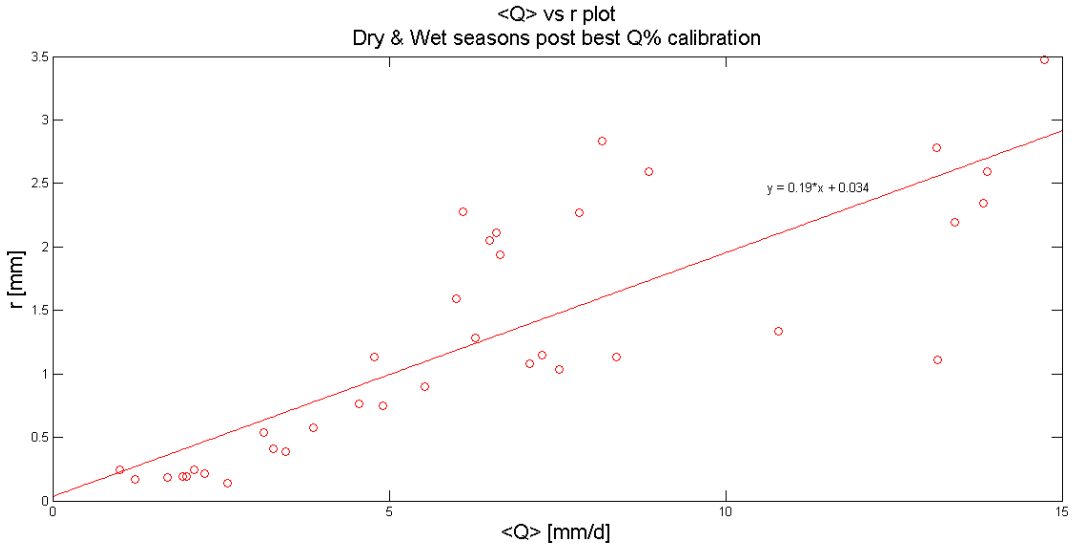

Figure IV.81 - <*Q*> *vs r*· relationship after Best Q% removal calibration for only dry and wet season

Regardless these considerations, which can lead to further theoretical studies and applications, the temporal evolution of Costa Rican streamflow studied by Birkel [2005] on the basis of simple pluvial flow regimes defined by Dyck & Peschke [1995] can with this thesis modified and the streamflow analyzed can be categorized on the basis of the streamflow pdf associated. The two different qualitative regimes identified as *The Regular Caribbean Type* and *The Irregular Type* on the basis of precipitation-streamflow pattern and climatic and morphological features can be modified in order to have a description based on the hydroclimatic parameters α, λ and k obtaining a distinction between *erratic* and *persistent streamflow regime*. According to the model described in section 1 and to the qualitative and analytical difference between *erratic* and *persistent streamflow regime* it's possible to give the subsequent streamflow characterization.

River	**Climatic region**	**Time interval**	**Streamflow regime**
Rio Frio (Guatuso)	Northern Zone	Annual	Persistent
		Dry season	Persistent
		Wet season	Persistent
Rio San Carlos (Terron Colorado)	Northern Zone	Annual	Persistent
		Dry season	Persistent
		Wet season	Persistent
Rio Sarapiqui (Cariblanco)	Northern Zone	Annual	Persistent
		Dry season	Persistent
		Wet season	Persistent
Rio Tempisque (Guardia)	North Pacific	Annual	Erratic
		Dry season	Erratic
		Wet season	Erratic

Rio Tenorio (Rancho Rey)	North Pacific	Annual	Persistent
		Dry season	Persistent
		Wet season	Persistent
Rio Barranca (Guapinol)	Central Valley	Annual	Erratic
		Dry season	Erratic
		Wet season	Persistent
Rio Poas (Tacares)	Central Valley	Annual	Persistent
		Dry season	Persistent
		Wet season	Persistent
Rio G.Candelaria (El Rey)	Central Pacific	Annual	Erratic
		Dry season	Erratic
		Wet season	Erratic
Rio Naranjo (Londres)	Central Pacific	Annual	Persistent
		Dry season	Persistent
		Wet season	Persistent
Rio Savegre (Providencia)	Central Pacific	Annual	Persistent
		Dry season	Persistent
		Wet season	Persistent
G. de Terraba (Palmar)	South Pacific	Annual	Persistent
		Dry season	Persistent
		Wet season	Persistent
Rio Coto Brus (Caracucho)	South Pacific	Annual	Persistent
		Dry season	Persistent
		Wet season	Persistent
Rio Reventazon (Palomo)	Caribbean	Annual	Persistent
		Dry season	Persistent
		Wet season	Persistent
Rio Pejibaye (Oriente)	Caribbean	Annual	Persistent
		Dry season	Persistent
		Wet season	Persistent
Rio Pacuare (Dos Montanas)	Caribbean	Annual	Persistent
		Dry season	Persistent
		Wet season	Persistent
Rio Pacuare (Pandora)	Caribbean	Annual	Erratic
		Dry season	Erratic
		Wet season	Erratic
Rio Pacuare (Bratsi)	Caribbean	Annual	Erratic
		Dry season	Erratic
		Wet season	Erratic
Rio Pacuare (Dos Montanas)	Caribbean	Annual	Persistent
		Dry season	Persistent
		Wet season	Persistent
Rio Pacuare (Dos Montanas)	Caribbean	Annual	Persistent
		Dry season	Persistent
		Wet season	Persistent

Table III.43 – Streamflow regime definition underlying how different microclimatic zones have no univocal linkage with the classification proposed. It's possible to have *erratic* streamflow regime in *Regular Caribbean type Catchments* and persistent streamflows in *Irregular Pacific Catchents*.

The understanding of the hydrologic regimes and their evolution under non-stationary climate drivers is a key issue for the management of freshwater ecosystems, the security of human water uses and can help to analyze the capacity of a streamflow to affect the morphology in a catchment. The study in this thesis showed an application of a stochastic mechanistic model on 18 Costa Rican catchment which was able to define the hydrologic

regime for different sub-climatic zones and for different seasons in absence of rainfall precipitation data. The theoretical model was able to represent a proper stochastic fitting with the pdf deduced directly from observed data for every catchment, the performances were furtherly increased through a calibration and the final analysis can give information about frequency of high flows, floods and droughts periods for every catchment. These evidences would give positive implications for water resources management, hydrologic hazard and can suggest development strategies, as changes in hydropower policies in Costa Rican basins. Starting from these considerations it's possible to underline the general flexibility of this hydrologic stochastic model which can lead to important applications for other developing countries in which any hydrological characterization is still lacking as well as a detailed dataset.

Chapter 5 – Conclusions

This work allowed the analysis of catchment flow regimes along a climatic gradient in Costa Rica. Many catchments on the Pacific side are able to show, according to the model, a *persistent regime* and, on the other hand, some catchments on the Caribbean side display an *erratic behavior*. This observation leads to the necessity to integrate, during the hydrologic classification of catchments, a stochastic study in order to deduce the pdf associated to the river. The pdf is able to summarize long-term and catchment-scale hydrologic characteristics and, being based on long-term streamflow and rainfall data, offers a classification more solid than a streamflow regime solely based on streamflow and rainfall monthly patterns.

The absence of rainfall data can be bypassed in a long-term stochastic study with an analysis based solely on the streamflow observation. It is possible, in this way, to approximate the main effective rainfall frequency and intensity.

Characterizing the streamflow pdf using a seasonal timescale allows the model to give an analytical pdf able to reproduce better the empirical pdf if compared to the pdf deduced at annual timescale. Thus, the application of the model is able to improve the performance in terms of SSD using a seasonality timescale and the streamflow is better represented.

The M3a linear recession method enables an improved representation and it is able to return the best hydrograph recession rate and therefore the corresponding pdf has the lowest SSD at annual timescale. On the contrary, after a seasonality timescale subdivision, the nonlinear model outperforms often the linear methods having a SSD often lower the calibrated linear model. For both annual and season timescale the other linear methods (M1a, M1b, M2, M3b) shows not relevant performances.

The calibration is able to improve the performances in order to deduce the shape and rate parameter of the analytical pdf able to return the best fitting with the observed data. The best calibration is the SC one for an annual characterization of the streamflow and best Q% removal for a seasonal study. On the other hand the best Q% removal overestimates shape parameter of the pdf and decrease the accuracy in terms of streamflow regime identification. Moreover, the increase of performance due to calibration is sometimes negligible if compared to the increase of performance obtained using a seasonality timescale.

Ringraziamenti

Un sentito ringraziamento va al mio relatore Gianluca Botter, per aver avuto fiducia nelle mie capacità sin dall'inizio e avermi spronato in questo lavoro di tesi. Poter attingere alla sua conoscenza è stato per me un grande onore. Ringrazio la sua pazienza e, nella speranza di non aver deluso le sue aspettative e la sua fiducia, gli auguro ogni bene.

A Christian Birkel, mio professore, guida e amico durante il soggiorno in Costa Rica. La sua gentilezza, affabilità e disponibilità hanno illuminato le mie giornate, trascorse fra una calibrazione in ufficio e un'immersione nel fango in foresta. Un ringraziamento affettuoso va anche a Joni, Sebastian, Vanessa, Marlon, Andrés, Fernando, Marcelo, John Mark, Sky e i suoi machete, per aver reso questa esperienza ricca, viva e indimenticabile.

Alla mia famiglia. Un abbraccio ai miei meravigliosi genitori, Maya e Francesco, per accompagnarmi con il loro amore in ogni mio traguardo, per la loro onestà e per la capacità che hanno di risollevarmi dopo un fallimento. Se un domani dovessi riuscire a diventare un genitore amorevole, generoso e paziente un quarto di quel che siete stati voi con me potrò dire di essere un uomo fortunato. Un bacio alle mie sorelle, Celeste e Francesca, al loro amore incondizionato e al loro essermi sempre accanto con dedizione, bontà e sincerità. Una carezza ai miei nonni, instancabili esempi di nobiltà d'animo, dedizione e temperanza.

Ai fantastici amici incrociati in questi anni di università: Nico, Fede, Chiara, Ale, Giulia, Max, Martin, Marina, Michele, Stefano, Alberto, Rachele, Tommy, Lucrezia, Enrico, Beppe, Fabio, Rocco, Ramona. Che questa amicizia possa continuare a lungo, nonostante la mia sociopatia, anche fuori dalla facoltà.

A Jacopo, una delle persone migliori che conosca, per esserci sempre.

And, last but not least, a sweet kiss to my Janka. Thank you for your patience, for your strength and the tender love you are able to bring into my life every day. Milujem ta moja laska.

References

Amorocho J. and Orlob G.T., 1961, *Nonlinear analysis of hydrologic systems*. Water Resour. Cent. Contrib. 60. 154 pp., Univ. of Calif., Los Angeles;

Amorocho J., 1963, *Measures of the linearity of hydrologic systems*. J. Geophys. Res.,. 68(8). 2237–2249;

Basso S. 2016., 2016, *A physically-based analytical model of flood-frequency curves.* Geophysical Research Letters. doi:10.1002/2016GL.6915;

Beven K., 2001, *Rainfall-Runoff Modelling*: The Primer. John Wiley. Chichester. U. K.;

Birkel C., 2005, *Temporal and Spatial Variability of Drought Indices in Costa Rica.* Institut fur Hydrologie der Albert-Ludwigs-Universitat Freiburg i. Br. Diplomarbeit unter Leitung von Prof. Dr. S. Demuth. Freiburg i. Br., Juli 2005;

Birkel C., Soulsby C., Tetzlaff D., 2012, *Modelling the impacts of land-cover change on streamflow dynamics of a tropical rainforest headwater catchment*. Hydrological Science Journal. DOI: 10.1080/02626667.2012.728707;

Birkel C., Soulsby C., 2015. *Advancing tracer-aided rainfall-runoff modelling: a review of progress. problems and unrealized potential*. Hydrological Processes DOI:10.1002/hyp.10594;

Birkel C., Soulsby C., 2016. *Linking tracers. water age and conceptual models to identify dominant runoff processes in a sparsely monitored humid tropical catchment*. Hydrological Processes DOI:10.1002/hyp.10941;

Botter G., Porporato A., Daly E., Rodriguez-Iturbe I., Rinaldo A., 2007a, *Probabilistic characterization of base flows in river basins: Roles of soil. vegetation. and geomorphology*. Water Resour Res 43(6):W06404;

Botter G., Porporato A., Rodriguez-Iturbe I., Rinaldo A., 2007b, *Basin-scale soil moisture dynamics and the probabilistic characterization of carrier hydrologic flows: Slow. leaching-prone components of the hydrologic response*. Water Resour Res 43(2): W02417;

Botter G., Porporato A., Rodriguez-Iturbe I., Rinaldo A., 2009, *Nonlinear storage-discharge relations and catchment streamflow regimes*. Water Resour Res 45(10):W10427;

Botter G., Basso S., Rodriguez-Iturbe I., Rinaldo A., 2013, *Resilience of river flow regimes.* PNAS. 110. 32. 12925-12930. doi:10.1073/pnas.1311920110;

Botter G., 2014, *Flow regime shifts in the Little Piney Creek (US).* Advances in Water Resources 71. 44-54. 2014M;

Brutsaert W., and Nieber J.L., 1977, *Regionalized drought flow hydrographs from a mature glaciated plateau*. Water Resour. Res., 13(3). 637–648;

Brutsaert W., 2005, *Hydrology: An Introduction*. Cambridge Univ. Press. New York;

Ceola S., Hodl I., Adlboller M., Singer G., Bertuzzo E., Mari L., Botter G., Waringer J., Battin T.J., Rinaldo A., 2013, *Hydrologic variability affects invertebrate grazing on phototrophic biofilms in stream microcosms*. PLoS ONE 2013;8(4): e60629. dx.doi.org/10.1371/journal.pone.0060629;

Chow. V.T., Maidment D.R., and Mays L.W., 1988, *Applied Hydrology*. McGraw-Hill. New York;

Daniels A.E., Bagstad K., Esposito V., Moulaert A., Rodriguez C.M., 2011, *Understanding the impacts of Costa Rica's PES: are we asking the tight question's?* Ecological Economics. 69 2116-2126. 2011;

Enfield D.B., and Alfaro E.J., 1999, *The dependence of Caribbean rainfall on the interaction of the Tropical Atlantic and Pacific Oceans*. Journal of Climate. 12. 2093-2012;

Farmer D., Sivapalan M., and Jothityangkoon C., 2003, *Climate. soil. and vegetation controls upon the variability of water balance in temperate and semiarid landscapes: Downward approach to water balance analysis*. Water Resour. Res., 39(2). 1035. doi:10.1029/2001WR000328;

Hastenrath S., 1967, *Rainfall distribution and regime in Central America*. Theoretical and Applied Climatology. 15 (3). 201-241. doi:10.1007/ BF02243853;

Kirchner J.W., 2009, *Catchments as simple dynamical systems: Catchment characterization. rainfall-runoff modeling. and doing hydrology backward*. Water Resour. Res.,45. W02429. doi:10.1029/2008WR006912;

Lawton R.O., Nair U.S., Pielke S.A. Sr., Welch R.M., 2001, *Climatic impact of tropical lowland deforestation on nearby montane cloud forests.* Science. 2001 Oct 19;294(5542):584-7;

Milly P.C.D., Dunne K.A., Vecchia A.V., 2005, *Global pattern of trends in streamflow and water availability in a changing climate*. Nature. 438. pp. 347–350;

Poff N.L., Olden J.D., Merritt D.M., Pepin D.M., 2007, *Homogenization of regional riverdynamics by dams and global biodiversity implications*. Proc Natl Acad Sci2007;104(14):5732–7. http://dx.doi.org/10.1073/pnas.0609812104;

Poff N.L., Allan J.D., Bain M.B., Karr J.R., Prestegaard K.L., Richter B.D., Sparks R.E., Stromberg J.C., Dec 1997, *The Natural Flow Regime*. Bioscience; 47. 11; Research Library pg. 769;

Ray. D. K., U. S. Nair. R. O. Lawton. R. M. Welch. and R. A. Pielke Sr., 2006, *Impact of land use on Costa Rican tropical montane cloud forests: Sensitivity of orographic cloud formation to deforestation in the plains*. J. Geophys. Res., 111. D02108. doi:10.1029/2005JD006096;

Richter B.D., Baumgartner J.V., Powell J., Braun D.P., 1996, *A Method for Assessing Hydrologic Alteration within Ecosystems.* Conservation Biology, Pages 1163-1174 Volume 10, No. 4, August 1996;

Rodriguez-Iturbe. I., and Rinaldo A., 1997, *Fractal River Basins: Chance and Self-Organization*. Cambridge Univ. Press. New York;

Rodriguez-Iturbe I., Porporato A., Ridolfi L., Isham V., 1999, *Probabilistic modelling of water balance at a point: The role of climate. soil and vegetation*. Proc R Soc Lond A Math Phys Sci 455(1990):3789–3805. Cox DR;

Rodriguez-Iturbe I., Porporato A., 2004, *Eco-Hydrology of Water Controlled Ecosystems*. Cambridge Univ Press. Cambridge. UK;

Sader S.A., Joyce A.T. *Deforestation rates and trends in Cosa Rica 1940 to 1983*. Biotropica. 20(1). 11-19;

Van de Griend A.A., De Vries J.J., and Seyhan E., 2002, *Groundwater discharge from areas with a variable specific drainage resistance*. J. Hydrol., 259. 203– 220;

Veldkamp A., Fresco L.O., 1996, *CLUE-CR: an integrated multiscale model to simulate land use change scenarios in Costa Rica*. Ecological Modelling. 91. 231-248;

Waylen P., Caviedes C., Mesa G.P.O., Quesada M., 1998, *Rainfall Distribution and Regime in Costa Rica and its Response to the El Niño-Southern Oscillation*. Yearbook (Conference of Latin Americanist Geographers) 24 January 1998;